The Stability of a Stripe for the Gierer-Meinhardt Model and the Effect of Saturation

T. KOLOKOLNIKOV, W. S U N, M. J. WARD, and J. W E I

Theodore Kolokolnikov; Optique Nonlinéaire Théorique, Free University of Brussels
Wentao Sun, Dept. of Mathematics, University of British Columbia, and School of Mathematics and Systems Science, Shandong University, China
Michael Ward; Dept. of Mathematics, University of British Columbia, Vancouver, Canada V6T 1Z2 (corresponding author)
Juncheng Wei; Dept. of Mathematics, Chinese University of Hong Kong, New Territories, Hong Kong.

(*Received 31 May 2005*)

The stability of two different types of stripe solutions that occur for two different forms of the Gierer-Meinhardt (GM) activator-inhibitor model is analyzed in a rectangular domain. For the basic GM model with exponent set (p, q, r, s), representing the powers of certain nonlinear terms in the reaction kinetics, a homoclinic stripe is constructed whereby the activator concentration localizes along the mid-line of the rectangular domain. In the semi-strong regime, characterized by a global variation of the inhibitor concentration across the domain, instability bands with respect to transverse zigzag instabilities and spot-generating breakup instabilities of the homoclinic stripe are determined analytically. In the weak interaction regime, where both the inhibitor and activator concentrations are localized, the spectrum of the linearization of the homoclinic stripe is studied numerically with respect to both breakup and zigzag instabilities. For certain exponent sets near the existence threshold of this homoclinic stripe, where stripe self-replicating behavior is observed, it is shown numerically that a stripe can be stable with respect to a breakup instability, but is unstable with respect to a transverse zigzag instability. The zigzag instability is found numerically to be the precursor to a space-filling curve. For a GM model in the semi-strong regime that is modified to include a small level of saturation of the activator production, it is shown that a homoclinic stripe solution still exists but, in contrast to the unsaturated GM model, can be stable with respect to breakup instabilities. For larger levels of the saturation, the homoclinic stripe ceases to exist and is replaced by a mesa-stripe, which is composed of two front-back heteroclinic transition layers joined together by an asymptotically flat plateau. In the near-shadow limit of an asymptotically large inhibitor diffusivity, and in a rectangular domain, it is shown analytically that a mesa-stripe is stable to spot-generating breakup instabilities, but can be unstable to either slow zigzag or breather-type instabilities. Finally, the asymptotic and numerical stability results for both homoclinic and mesa-stripes are favorably compared with results obtained from full numerical simulations of the GM model.

1 Introduction

In a two-dimensional domain, intricate spatially localized patterns consisting of either spots, stripes, mixed spot-stripe patterns, or space-filling curves, have been observed in numerical simulations of certain classes of singularly perturbed reaction-diffusion systems. For activator-inhibitor systems, such as the well-known Gierer-Meinhardt (GM) model of biological morphogenesis, spot and stripe patterns are ubiquitous (cf. [**6**], [**13**], [**21**], [**22**], [**46**], Chapter 15 of [**11**]). For the Gray-Scott (GS) model of theoretical chemistry, an even greater diversity of spatio-temporal patterns occur including, temporally oscillating spots, spot-replication behavior, spatio-temporal chaos of spot patterns, and labyrinthine patterns of stripes (cf. [**32**], [**26**], [**27**], [**37**]). In other settings, localized stripe and spot patterns occur for certain hybrid chemotaxis reaction-diffusion models of bacterial pattern formation (cf. [**36**], [**45**], Chapter 5 of [**24**]) and of fish skin patterns on growing domains (cf. [**18**], [**30**], [**31**]). Localized patterns also arise in the reaction-diffusion modeling of vegetation patterns in arid environments (cf. [**9**], [**12**], [**19**]).

Most of the previous analyzes of the stability of stripe patterns have been based on a weakly nonlinear theory where

the solution is assumed to be close to some spatially uniform state across the cross-section of the stripe. However, for singularly perturbed two-component reaction-diffusion systems, this assumption of near-uniform spatial dependence in the stripe cross-section is generally not valid. For such systems in a two-dimensional domain, there are two main types of spatially heterogeneous stripes; homoclinic stripes and mesa-stripes.

A homoclinic stripe results when either one or both of the two solution components becomes localized, or concentrates, on a planar curve in the domain. There are two distinct parameter regimes for homoclinic stripes. The semi-strong interaction regime occurs when the ratio of the two diffusivities is asymptotically large, so that only one of the two solution components (the fast component) is localized to form a stripe. In this case, the cross-section of the stripe is closely approximated by a homoclinic orbit of a certain scalar ODE problem for the fast subsystem. Although the fast solution component has a negligible interaction with the boundaries of the domain, the slow (global) solution component has a significant interaction with the domain boundary and, possibly, with adjacent stripes. In contrast, in the weak interaction regime, where both diffusivities are asymptotically small and of the same order, both solution components are localized to form a stripe. In this case, the cross-section of the stripe is closely approximated by a homoclinic orbit of a coupled ODE system for the two fast components. The term "weak" interaction here refers to the negligible interaction of these two fast components with the boundaries of the domain and with any adjacent stripes. Homoclinic stripes in both the weak and semi-strong regimes arise in the basic GM model (cf. [**4**]), and in certain parameter ranges of the Gray-Scott model (cf. [**15**], [**16**], [**23**]).

A different type of stripe can occur for bistable singularly perturbed reaction-diffusion systems such as the Fitzhugh-Nagumo model. For such systems, the stripe cross-section typically consists of two transition layers, each closely approximated by a heteroclinic solution of the equilibrium problem, that are joined together by an asymptotically flat plateau region. We refer to such a stripe solution as a mesa-stripe[1]. The stability of such stripe solutions was analyzed rigorously in [**34**] and [**35**] for certain classes of bistable reaction-diffusion systems. The analyses of [**34**] and [**35**] were based on the SLEP (singular limit eigenvalue problem) method developed in [**28**] and [**29**] to analyze the stability of mesa-pulses in one-spatial dimension. For a generalized Fitzhugh-Nagumo model, the stability and dynamics of mesa-stripes were analyzed in [**7**] by a contour dynamics approach. The existence and stability of mesa-stripes for a Brusselator model was studied in [**17**]. Mesa-stripe solutions can also occur for a modification of the GM model where activator saturation effects are included.

There are two main types of linearized instabilities associated with a homoclinic stripe; varicose (breakup) instabilities, and transverse (zigzag) instabilities. For a varicose instability of a homoclinic stripe, the eigenfunction for the perturbation of any fast component is an even function across the stripe cross-section, and has a normal-mode modulation tangential to the stripe. This has the effect of inducing a ripple on the amplitude of any fast component along the length of the stripe. Since an instability of this type typically leads to the disintegration of the stripe into a sequence of spots, we refer to it here as a breakup instability. Alternatively, for a zigzag instability of a homoclinic stripe, the eigenfunction for the perturbation of any fast component is an odd function across the stripe cross-section, and has a normal mode modulation in the direction tangent to the stripe. This has the effect of inducing a ripple on the location of the centerline of the stripe.

For the GM and GS models in the semi-strong regime, a homoclinic stripe is typically unstable to a spot-generating breakup instability (cf. [**4**], [**15**], [**16**], [**23**]). For the GS model in the weak interaction regime, a homoclinic stripe

[1] Mesa means table in Spanish. This term was suggested by P. Fife as referenced in [**17**]

can be de-stabilized solely by a transverse zigzag instability, which seems to be the precursor to a complicated space-filling curve (cf. [**16**]). Zigzag and breakup instabilities have also been studied in [**8**] for a reaction-diffusion system on an unbounded domain with piecewise linear kinetics. Breakup instabilities of localized rings of bacteria, leading to spot formation, have been observed in numerical simulations of certain hybrid chemotaxis reaction-diffusion systems (cf. [**36**], [**45**], Chapter 5 of [**24**]).

Based on numerical experiments and a Turing-type linearized stability analysis, the inclusion of saturation effects into the basic GM model is, qualitatively, a well-known way to obtain stable stripe patterns (cf. [**13**], [**21**], [**22**]). Breakup instabilities do not, in general, occur for a mesa-stripe solution and the instability of this solution typically occurs by two types of transverse instabilities that develop over long time-scales; zigzag instabilities where the edges of the mesa-stripe are in phase, and breather instabilities where these edges are 90° out of phase.

The primary goal of this paper is to give detailed analytical and numerical results for breakup and transverse instability bands of homoclinic and mesa stripes for the basic GM model, and for the modified GM model where saturation effects are included. Our analysis addresses several key qualitative features observed in numerical simulations of stripe behavior. It determines explicit parameter ranges in these GM models where a homoclinic stripe exists and is stable with respect to spot-generating breakup instabilities. It suggests a common qualitative mechanism responsible for the disappearance of a breakup instability band. It identifies parameter ranges where a transverse instability is the dominant instability mechanism, and where labyrinthine patterns are likely to occur.

The basic GM model, where saturation effects are neglected, can be written in the dimensionless form (cf. [**10**])

$$a_t = \varepsilon_0^2 \Delta a - a + \frac{a^p}{h^q}\,, \quad \tau h_t = D\Delta h - h + \frac{a^r}{\varepsilon_0 h^s}\,, \quad X = (X_1, X_2) \in \Omega\,,\ t > 0\,; \quad \partial_n a = \partial_n h = 0\,, \quad x \in \partial\Omega\,, \tag{1.1}$$

where the exponent set (p, q, r, s) is assumed to satisfy

$$p > 1\,, \qquad q > 0\,, \qquad r > 1\,, \qquad s \geq 0\,, \qquad \text{with} \qquad \zeta \equiv \frac{qr}{(p-1)} - (s+1) > 0\,. \tag{1.2}$$

The classical GM model corresponds to the exponent set $(2, 1, 2, 0)$. We consider (1.1) in the rectangular domain

$$\Omega:\ -1 < X_1 < 1\,, \quad 0 < X_2 < d_0\,. \tag{1.3}$$

By re-scaling a and h, and introducing $X = x/l$ where $l = 1/\sqrt{D}$, (1.1) can be re-cast into the equivalent form

$$a_t = \varepsilon^2 \Delta a - a + \frac{a^p}{h^q}\,, \quad \tau h_t = \Delta h - h + \frac{a^r}{\varepsilon h^s}\,, \quad x = (x_1, x_2) \in \Omega_l\,,\ t > 0\,; \quad \partial_n a = \partial_n h = 0\,, \quad x \in \partial\Omega_l\,, \tag{1.4}$$

where

$$\Omega_l:\ -l < x_1 < l\,, \quad 0 < x_2 < d; \qquad d \equiv d_0 l\,; \qquad \varepsilon \equiv \varepsilon_0 l\,; \qquad l \equiv 1/\sqrt{D}\,. \tag{1.5}$$

In (1.1), the semi-strong regime is characterized by $\varepsilon_0 \ll 1$ and $D = O(1)$, while the weak interaction regime corresponds to $\varepsilon_0 \ll 1$ and $D = O(\varepsilon_0^2) \ll 1$. In terms of (1.4), the weak interaction regime corresponds to the limit $l \to \infty$ with $\varepsilon = \varepsilon_0 l = O(1)$. For the basic GM model (1.4), we will study the stability of a homoclinic stripe of zero curvature that is obtained when a concentrates along the mid-line $x_1 = 0$ of Ω_l.

Alternatively, the classical GM model (1.1), which is modified to include the effect of saturation of the activator production, can be written in the dimensionless form (cf. [**13**], [**21**], [**22**])

$$a_t = \varepsilon_0^2 \Delta a - a + g(a, h)\,, \qquad g(a, h) \equiv \frac{a^2}{h\,(1 + \kappa a^2)}\,; \qquad \tau h_t = D\Delta h - h + a^2\,. \tag{1.6}$$

Here $\kappa > 0$ is the saturation parameter. For the weak saturation case $\kappa = O(\varepsilon_0^2)$, (1.6) has a homoclinic stripe

solution as for the basic GM model (1.1). However, for $\kappa = O(1)$, the numerical simulations of (1.6) in [**13**], [**21**], [**22**], and [**46**], have suggested the existence of a mesa-stripe solution for (1.6) that is stable to the formation of spots.

The stability of a homoclinic stripe for the basic GM model (1.4) was studied in [**4**]. In the semi-strong interaction regime, the existence of a homoclinic stripe solution for (1.4) on the infinite strip domain $\mathbb{R}^1 \times (0, d)$ was analyzed in [**4**] using geometric singular perturbation techniques. In addition, by reducing the study of a certain nonlocal eigenvalue problem (NLEP) to computations involving hypergeometric functions, the stability of this stripe with respect to breakup instabilities was analyzed in [**4**]. In [**4**], explicit results for the breakup instability bands were obtained for certain exponent sets (p, q, r, s), and it was shown that a homoclinic stripe for (1.4) is stable to breakup instabilities only for asymptotically thin domains of order $d = O(\varepsilon_0)$.

For the semi-strong regime of (1.4), we extend this previous work of [**4**] on breakup instabilities to the finite rectangular domain $[-l, l] \times [0, d]$, and to more general exponent sets (p, q, r, s). Our analysis, which is related to the rigorous analysis of the NLEP in [**39**] and [**40**], gives explicit upper and lower bounds for the breakup instability bands for various ranges of the exponents (p, q, r, s) in (1.4). For various exponent sets and domain lengths $l = 1/\sqrt{D}$, the most unstable mode from the NLEP is calculated numerically. Our main result that breakup instabilities always occur unless the domain is $O(\varepsilon_0)$ thin is given in Proposition 2.3 below. It is an extension of Theorem 4.5 of [**4**]. Full numerical computations of (1.4) are performed to validate the asymptotic theory.

In the semi-strong regime of (1.4), we also analyze the transverse zigzag instabilities of a homoclinic stripe by calculating an explicit formula for the small eigenvalue of order $\lambda = O(\varepsilon_0^2)$ in the spectrum of the linearization. In Principal Result 2.4, we show that there are no unstable zigzag modes in the semi-strong regime for exponent sets that satisfy $\gamma \equiv q/(p-1) \leq 1$. This range includes the classical GM model where $(p, q, r, s) = (2, 1, 2, 0)$. For $\gamma > 1$, we show that an unstable band of zigzag modes with wave number $m = O(1)$ as $\varepsilon_0 \to 0$ exists only when $l = 1/\sqrt{D}$ exceeds some critical threshold l_z, which depends on γ. This threshold is calculated numerically. However, since the time-scale for the development of zigzag instabilities in the semi-strong regime is $O(\varepsilon_0^{-2})$, they are dominated in this regime by spot-generating breakup instabilities that occur on the more rapid $O(1)$ time-scale.

In the weak interaction regime of (1.1), where $D = \varepsilon_0^2 D_0$ with $D_0 = O(1)$, it was proved in [**4**] that there is a minimum value of D_0, labeled by D_{0c}, for which a homoclinic stripe solution exists. As shown in [**14**] (see also [**4**] and Remark 6.2 of [**25**]), this critical value D_{0c} is a saddle-node value of a bifurcation diagram of the norm $|a|_2$ versus D_0. In the one-dimensional case, and for values of D_0 slightly below D_{0c}, a self-replication behavior is observed whereby a localized initial pulse undergoes a repeated edge-splitting process due to ghost effects of the saddle-node bifurcation point (cf. [**4**], [**14**],[**25**], [**26**]). A similar stripe self-replication behavior was observed in [**4**] in the two-dimensional case. For the classical GM model with exponent set $(2, 1, 2, 0)$, and for D_0 slightly above D_{0c}, the full numerical computations in [**4**] suggested that a stripe can be stable with respect to breakup instabilities for *any* domain width.

We extend this previous work by giving a detailed numerical study of the spectrum of the homoclinic pulse in the weak interaction regime of (1.1). In terms of this eigenvalue problem, we numerically calculate the breakup and zigzag instability bands associated with a homoclinic stripe as a function of D_0 for various exponent sets (p, q, r, s). For certain exponent sets, which include the classical GM set $(2, 1, 2, 0)$, we show numerically that there exists a value D_{0b} of D_0, with $D_{0b} > D_{0c}$ for which the instability thresholds of the breakup instability band coalesce. Therefore, there is no spot-generating breakup instability band on the range $D_{0c} < D_0 < D_{0b}$. For the classical GM set this range is $7.17 < D_0 < 8.06$. However, for each of these exponent sets where the breakup band disappears, we show

numerically that there is a nontrivial zigzag instability band on this range of D_0. Therefore, for these exponent sets, a homoclinic stripe is de-stabilized solely by a zigzag instability when D_0 is sufficiently close to D_{0c}. This zigzag instability is found to be the precursor to a space-filling curve. Full numerical simulations of (1.1) are done to confirm the spectral results. Secondary instabilities, such as self-replicating spots, that arise after a spot-generating breakup instability of the stripe are also illustrated.

For the modified classical GM model (1.6) with saturation parameter $\kappa = O(1)$ and for $\varepsilon \to 0$, we construct a mesa-stripe equilibrium solution for (1.6) in the near-shadow limit $D \gg 1$, where $D = \mathcal{D}/\varepsilon_0$ with $\mathcal{D} = O(1)$. The stability of the mesa-stripe is then studied analytically. In contrast to the spectrum for homoclinic stripe solutions of the basic GM model (1.1), the spectrum of the linearization of an equilibrium mesa-stripe solution for (1.6) contains only the small eigenvalues of order $O(\varepsilon_0^2)$ that correspond to transverse instabilities. For $\mathcal{D}$ above some threshold, we show that the mesa-stripe is stable for all domain widths and for all transverse wave numbers m. However, as $\mathcal{D}$ is decreased below some critical value, it is shown analytically that an unstable zigzag instability band emerges at some critical wave number $m = O(1)$. Upon further decreasing $\mathcal{D}$ below some additional threshold, an additional breather instability is triggered. The critical values of $\mathcal{D}$ and the transverse wave number m at the onset of the zigzag and breather instability are determined explicitly as a function of κ. The asymptotic theory is confirmed with full numerical simulations of (1.6). Our case-study analysis of mesa-stripe stability for (1.6) with $\kappa > 0$ and $\kappa = O(1)$ extends the previous studies of [**34**] and [**35**] for generalized Fitzhugh-Nagumo models by providing explicit instability thresholds for zigzag and breather instabilities.

Finally, we consider the modified classical GM model (1.6) with an asymptotically small saturation $\kappa = O(\varepsilon_0^2)$ in the semi-strong regime. The study of stripe stability for this problem provides a bridge between the analysis of breakup instabilities of a homoclinic stripe for (1.4) and the analysis of transverse instabilities of a mesa-stripe for (1.6) with $\kappa = O(1)$. We show that for any $k > 0$, where $\kappa = \varepsilon_0^2 k$, (1.6) admits a homoclinic stripe solution for any $D > 0$ with $D = O(1)$. An NLEP governing breakup instabilities of this homoclinic stripe is then derived analytically. From a numerical computation of the spectrum of this NLEP it is shown that the boundaries of the breakup instability band coalesce at some $k = k_d$, so that this instability band disappears for all $k > k_d$. The reason for the disappearance of this breakup instability band for k sufficiently large is related to the ghost effect of a nearby heteroclinic solution, which has the effect of "fattening" the cross-section of the homoclinic stripe. This suggests that such "fat" homoclinic stripes can share some of the same qualitative stability properties as mesa-stripe solutions. We remark that a qualitatively similar "fattening" of the homoclinic stripe is also likely responsible for the disappearance of breakup instability bands for certain exponent sets of the basic GM model (1.1) in the weak interaction regime sufficiently close to the existence threshold D_{0c} of the homoclinic stripe. The "fattening" of this other homoclinic stripe is related to the existence of nearby multi-bump homoclinic solutions that must necessarily exist close to the existence threshold D_{0c} governing self-replication (cf. [**14**]).

The outline of this paper is as follows. In §2.1 and §2.2 we analyze breakup and zigzag instabilities, respectively, for homoclinic stripe solutions of (1.4) in the semi-strong interaction regime. In §2.3 we show that "fat" homoclinic solutions to (1.6) with $\kappa = O(\varepsilon_0^2)$ can be stable to breakup instabilities. In §3 we numerically study breakup and zigzag instabilities for (1.4) in the weak interaction regime, where both solution components are localized. Finally, in §4 and §5 we analyze the existence and linearized stability, respectively, of a mesa-stripe equilibrium solution to the GM model (1.6) when $\kappa > 0$ and $\kappa = O(1)$.

2 The GM Model Without Saturation: Semi-Strong Regime

In the limit $\varepsilon \to 0$ we now construct an equilibrium stripe solution to (1.4) where the stripe is centered on the mid-line $x_1 = 0$ of the rectangular domain $\Omega := [-l, l] \times [0, d]$, where $d = ld_0$. Since the cross-section of the stripe is a one-dimensional pulse, this solution, with a minor change in notation, was constructed asymptotically in [**10**] using the method of matched asymptotic expansions. The result is as follows.

Principal Result 2.1 (From [**10**]): *For $\varepsilon \to 0$, an equilibrium stripe solution to (1.4), labeled by $a_e(x_1)$ and $h_e(x_1)$, is given asymptotically by*

$$a_e(x_1) \sim \mathcal{H}^{\gamma} w\left(\varepsilon^{-1} x_1\right) ; \qquad h_e(x_1) \sim \mathcal{H} \frac{G_l(x_1)}{G_l(0)} . \tag{2.1}$$

Here $w(y)$ is the unique positive solution to

$$w'' - w + w^p = 0 , \qquad -\infty < y < \infty ; \qquad w \to 0 \quad \text{as} \quad |y| \to \infty ; \qquad w'(0) = 0 , \quad w(0) > 0 . \tag{2.2}$$

The constants $\mathcal{H}$, γ, and $G_l(0)$ in (2.1), for which $h_e(0) = \mathcal{H}$, are defined by

$$\mathcal{H}^{\zeta} \equiv \frac{1}{b_r G_l(0)} ; \qquad b_r \equiv \int_{-\infty}^{\infty} [w(y)]^r \, dy ; \qquad \gamma \equiv \frac{q}{p-1} ; \qquad G_l(0) = \frac{1}{2} \coth l , \tag{2.3}$$

where ζ is defined in (1.2). The Green's function $G_l(x_1)$ in (2.1) satisfies

$$G_{lx_1x_1} - G_l = -\delta(x_1) , \quad -l < x_1 < l ; \qquad G_{lx_1}(\pm l) = 0 ; \qquad G_l(x_1) = \frac{\cosh\left(l - |x_1|\right)}{2 \sinh\left(l\right)} . \tag{2.4}$$

To determine the stability of the stripe solution, we introduce the perturbation

$$a = a_e + e^{\lambda t + i m x_2} \phi , \qquad h = h_e + e^{\lambda t + i m x_2} \eta , \qquad m = \frac{k\pi}{d} , \tag{2.5}$$

where $\phi = \phi(x_1) \ll 1$ and $\eta = \eta(x_1) \ll 1$. The relationship above between m and k results from the Neumann conditions on $x_2 = 0, d$ of $\partial\Omega$. In the analysis below we treat m as a continuous variable. The band of instability with respect to m that is determined below can be mapped to a k-band of instability using (2.5). Substituting (2.5) into (1.4), we obtain the eigenvalue problem

$$\varepsilon^2 \phi_{x_1x_1} - \phi + \frac{p a_e^{p-1}}{h_e^q} \phi - \frac{q a_e^p}{h_e^{q+1}} \eta = \left(\lambda + \varepsilon^2 m^2\right) \phi , \quad -l < x < l ; \qquad \phi_x(\pm l) = 0 , \tag{2.6 a}$$

$$\eta_{x_1x_1} - \left(1 + \tau\lambda + m^2\right) \eta = -\frac{r a_e^{r-1}}{\varepsilon h_e^s} \phi + \frac{s a_e^r}{\varepsilon h_e^{s+1}} \eta , \quad -l < x < l ; \qquad \eta_x(\pm l) = 0 . \tag{2.6 b}$$

There are two classes of eigenvalues and eigenfunctions of (2.6); the large eigenvalues where $\lambda = O(1)$ as $\varepsilon \to 0$, and the small eigenvalues with $\lambda = O(\varepsilon^2)$ as $\varepsilon \to 0$. For the large eigenvalues, which determine the stability of the stripe on an $O(1)$ time-scale, the corresponding eigenfunction has the form

$$\phi(x_1) \sim \Phi\left(\varepsilon^{-1} x_1\right) , \tag{2.7}$$

where $\int_{-\infty}^{\infty} \Phi(y) w^{r-1}(y) \, dy \neq 0$. This stability problem, treated in §2.1, involves the analysis of a nonlocal eigenvalue problem (NLEP). Since unstable eigenfunctions of this type lead to a disintegration of the stripe into spots, we refer to this instability as a breakup instability. Alternatively, the eigenfunction for the small eigenvalues has the form

$$\phi(x_1) \sim w'\left(\varepsilon^{-1} x_1\right) + \varepsilon \phi_1\left(\varepsilon^{-1} x_1\right) + \cdots . \tag{2.8}$$

Since the leading term in (2.8) corresponds to a translation of the spike profile w, unstable modes for this class of eigenvalues lead to zigzag instabilities. This problem is studied below in §2.2.

2.1 Breakup Instabilities: Semi-Strong Regime

We now analyze the spectrum of (2.6) corresponding to breakup instabilities, where $\phi(x_1) \sim \Phi(y)$ with $y = x_1/\varepsilon$ and $\int_{-\infty}^{\infty} \Phi w^{r-1}\, dy \neq 0$. Since the asymptotic derivation of the NLEP for $\Phi(y)$ is similar to that given in §2 of [**39**], we only give an outline of this analysis in Appendix A. The result is as follows:

Principal Result 2.2: *Let $\varepsilon \to 0$, and suppose that $\int_{-\infty}^{\infty} \Phi w^{r-1}\, dy \neq 0$. Then, $\Phi(y)$ satisfies the NLEP*

$$L_0\Phi - \chi_m w^p \frac{\int_{-\infty}^{\infty} w^{r-1}\Phi\, dy}{\int_{-\infty}^{\infty} w^r\, dy} = (\lambda + \varepsilon^2 m^2)\Phi \quad -\infty < y < \infty\,; \quad \Phi \to 0 \quad \text{as} \quad |y| \to \infty\,, \tag{2.9 a}$$

$$L_0\Phi \equiv \Phi'' - \Phi + pw^{p-1}\Phi\,, \qquad C_m(\lambda) \equiv \frac{1}{\chi_m(\lambda)} \equiv \frac{s}{qr} + \frac{\theta_\lambda \tanh(\theta_\lambda l)}{qr \tanh l}\,, \qquad \theta_\lambda \equiv \sqrt{1 + m^2 + \tau\lambda}\,. \tag{2.9 b}$$

*The unique positive eigenvalue ν_0 with eigenfunction Φ_{l0} of the local operator L_0 is (cf. [**20**], Proposition 5.6 of [**3**])*

$$\nu_0 = \frac{1}{4}(p-1)(p+3)\,, \qquad \Phi_{l0} = [w(y)]^{(p+1)/2}\,. \tag{2.10}$$

Equivalently, the eigenvalues of (2.9), with $\int_{-\infty}^{\infty} w^{r-1}\Phi\, dy \neq 0$, are the roots of $g(\lambda) = 0$ defined by

$$g(\lambda) \equiv C_m(\lambda) - f(\lambda + \varepsilon^2 m^2)\,; \qquad f(\mu) \equiv \frac{\int_{-\infty}^{\infty} w^{r-1}\psi\, dy}{\int_{-\infty}^{\infty} w^r\, dy}\,, \qquad \psi \equiv (L_0 - \mu)^{-1} w^p\,. \tag{2.11}$$

To analyze the spectrum of the NLEP (2.9) for the stripe, we modify the rigorous approach developed in [**39**] for a related NLEP governing the stability of a pulse solution on a finite interval. This analysis, as outlined in Appendix A, leads to the following rigorous characterization of the instability band for (2.9):

Proposition 2.3: *Let (p, q, r, s) satisfy (1.2), let $l = 1/\sqrt{D} > 0$ be fixed, and assume that $\varepsilon \ll 1$. Let m_{b-} be the root of the transcendental equation*

$$G(m) \equiv \sqrt{1+m^2}\left(\frac{\tanh\left[\sqrt{1+m^2}\,l\right]}{\tanh l}\right) = \zeta + 1\,, \qquad \zeta \equiv \frac{qr}{p-1} - (s+1) > 0\,. \tag{2.12}$$

For the near-shadow limit $l \to 0$, we get $m_{b-} \sim \sqrt{\zeta}$, and for $l \to \infty$ we obtain $m_{b-} \sim \sqrt{\zeta^2 + 2\zeta}$. In addition, let m_{b+} be given by

$$m_{b+} = \frac{\sqrt{\nu_0}}{\varepsilon} + O(1)\,, \qquad \nu_0 = \frac{1}{4}(p-1)(p+3)\,. \tag{2.13}$$

Then, when either $r = p = 2$, or $r = p+1$ with $1 < p \leq 5$, there is exactly one real positive eigenvalue of (2.9) in $0 < \lambda < \nu_0 - \varepsilon^2 m^2$ for any $\tau \geq 0$ when m is inside the instability band $m_{b-} < m < m_{b+}$. For $r = 2$, this is the only eigenvalue in $Re(\lambda) > 0$. For $m > m_{b+}$, then $Re(\lambda) < 0$ for any $\tau \geq 0$. For $m = m_{b-}$, and if either $r = p = 2$, or $r = p+1$ and $1 < p \leq 5$, then there is a unique real positive eigenvalue $\lambda > 0$ when $\tau > \tau_{m-}$, and $Re(\lambda) \leq 0$ when $0 \leq \tau \leq \tau_{m-}$. Here τ_{m-} is defined by

$$\tau_{m-} = \frac{2qr}{p-1}\left(\frac{1}{p-1} - \frac{1}{2r}\right)\tanh l\left[\frac{\tanh(\theta_- l)}{\theta_-} + l\,\mathrm{sech}^2(\theta_- l)\right]^{-1}\,, \qquad \theta_- \equiv \sqrt{1 + m_{b-}^2}\,. \tag{2.14}$$

Finally, suppose that $0 \leq m < m_{b-}$. Then, for either $r = p = 2$, or $r = p+1$ and $1 < p \leq 5$, there are exactly two real unstable eigenvalues of (2.9) when τ is sufficiently large. In addition, as τ is increased from zero there is a Hopf bifurcation at some point $\tau_H = \tau_H(m)$ (possibly non-unique).

(p,q,r,s)	ε	l	$m_{b-}(n)$	$m_{b-}(a)$	$m_{b+}(n)$	$m_{b+}(a1)$	$m_{b+}(a2)$
(2,1,2,0)	0.100	1.0	1.3241	1.3022	10.351	11.180	10.437
(2,1,2,0)	0.050	1.0	1.3073	1.3022	21.580	22.361	21.618
(2,1,2,0)	0.025	1.0	1.3033	1.3022	43.964	44.721	43.978
(2,1,2,0)	0.010	1.0	1.3022	1.3022	111.07	111.80	111.06
(2,1,2,0)	0.025	$1/\sqrt{10}$	1.0336	1.0332	44.425	44.721	44.423
(2,1,2,0)	0.025	$\sqrt{10}$	1.7267	1.7238	43.721	44.721	43.749
(2,1,3,0)	0.025	1.0	2.1087	2.1029	43.517	44.721	43.560
(2,2,3,3)	0.025	1.0	2.1146	2.1029	42.337	44.721	42.399
(3,2,2,0)	0.025	1.0	1.3024	1.3022	68.589	69.282	68.578
(3,2,3,1)	0.025	1.0	1.3040	1.3022	68.146	69.282	68.139
(4,2,2,0)	0.025	1.0	0.6852	0.6858	91.265	91.652	91.208

Table 1. The lower bound m_{b-} and the upper bound m_{b+} for the breakup instability band for different exponent sets and parameters. Here $m_{b\pm}(n)$ are the full numerical results from the NLEP (2.9), $m_{b-}(a)$ is the asymptotic result from (2.12), and $m_{b+}(a1)$, $m_{b+}(a2)$ are the one- and two-term asymptotic results from (2.17).

Proof The proof of this result is given in Appendix A. ■

To calculate an improved approximation for the upper bound m_{b+} of the instability band we write $m = m_0/\varepsilon$, for $m_0 = O(1)$, and we expand

$$\Phi = \Phi_{l0} + \varepsilon\Phi_1 + \cdots, \qquad m_0^2 = \nu_0 + \varepsilon m_1 + \cdots. \tag{2.15}$$

Substituting (2.15) into (2.9 a), and using $\chi \sim \left(\frac{qr}{m}\right)\tanh l$ for $m \gg 1$, we obtain that Φ_1 satisfies

$$L_0\Phi_1 - \nu_0\Phi_1 = \frac{qr}{\sqrt{\nu_0}} w^p \tanh l \left(\frac{\int_{-\infty}^{\infty} w^{r-1}\Phi_{l0}\, dy}{\int_{-\infty}^{\infty} w^r\, dy} \right) + m_1\Phi_{l0}\,. \tag{2.16}$$

Since L_0 is self-adjoint, m_1 is determined from the solvability condition that the right-hand side of (2.16) is orthogonal to Φ_{l0}. Then, using $m_0 \sim \sqrt{\nu_0} + \frac{\varepsilon m_1}{(2\sqrt{\nu_0})}$, the upper stability bound m_{b+} is given in terms of Φ_{l0} by

$$m_{b+} \sim \frac{\sqrt{\nu_0}}{\varepsilon} - \left(\frac{qr\tanh l}{2\nu_0}\right)\beta\,, \qquad \beta \equiv \frac{\left(\int_{-\infty}^{\infty} w^{r-1}\Phi_{l0}\, dy\right)\left(\int_{-\infty}^{\infty} w^p\Phi_{l0}\, dy\right)}{\left(\int_{-\infty}^{\infty} w^r\, dy\right)\left(\int_{-\infty}^{\infty} \Phi_{l0}^2\, dy\right)}\,. \tag{2.17}$$

For the classical GM model with exponent set $(p,q,r,s) = (2,1,2,0)$, we use $\Phi_{l0} = \mathrm{sech}^3(y/2)$ from (2.10) to calculate β in (2.17) as $\beta = 3I_5I_7/[2I_4I_6]$, where $I_n \equiv \int_0^\infty \mathrm{sech}^n y\, dy$. By using the recursion relation $I_n = (n-2)I_{n-2}/(n-1)$, together with $I_2 = 1$ and $I_1 = \pi/2$, we readily calculate that $\beta = \frac{\pi^2}{64}(45/16)^2$. Therefore, for the classical GM model where $(p,q,r,s) = (2,1,2,0)$ and $\nu_0 = 5/4$, we have for $\varepsilon \to 0$ that

$$m_{b+} \sim \frac{\sqrt{5}}{2\varepsilon} - \frac{\pi^2\tanh l}{80}\left(\frac{45}{16}\right)^2 + \cdots. \tag{2.18}$$

For various exponent sets (p,q,r,s) and values of l and ε, in Table 1 we compare the asymptotic results for the stability thresholds from (2.12) and (2.17) with corresponding results computed numerically from the NLEP (2.9) using finite-difference methods and a discrete eigenvalue solver from LAPACK (cf. [1]). The asymptotic values are found to be very close to the corresponding full numerical results even when $\varepsilon = 0.1$. For $l = 1$, in Fig. 1(a) we compare the full numerical result for the upper threshold m_{b+} with the corresponding asymptotic result (2.17) for

a range of values of ε. For $\varepsilon = 0.025$, in Fig. 1(b) we compare the full numerical result for the lower threshold m_{b-} with the corresponding asymptotic result computed from (2.12) for a range of l values.

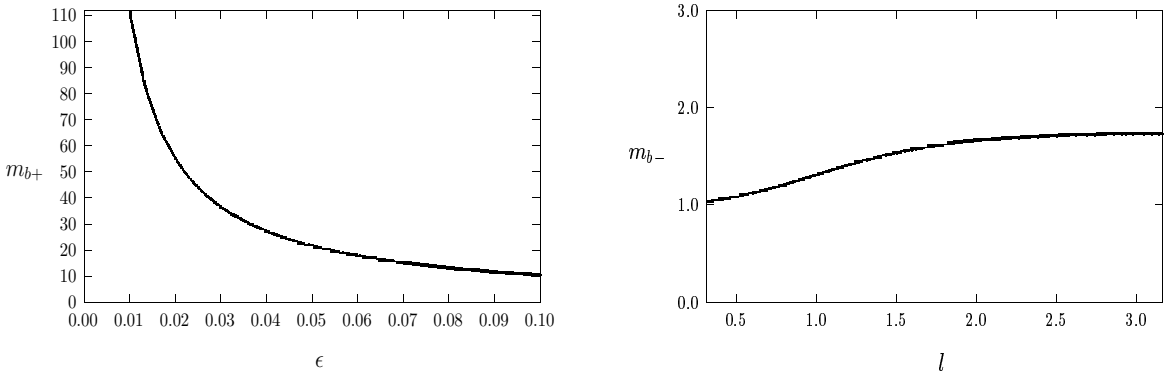

(a) m_{b+} versus ε for $l = 1$ (b) m_{b-} versus l for $\varepsilon = 0.025$

FIGURE 1. Instability thresholds for $(p, q, r, s) = (2, 1, 2, 0)$. Left figure: plot of the upper threshold m_{b+} versus ε for $l = 1$. The heavy solid curve is the full numerical result and the dashed curve is the asymptotic result (2.17). They are essentially indistinguishable in this plot. Right figure: plot of the lower threshold m_{b-} versus l for $\varepsilon = 0.025$. The heavy solid curve is the full numerical result and the dashed curve is the asymptotic result from (2.12). They are again indistinguishable.

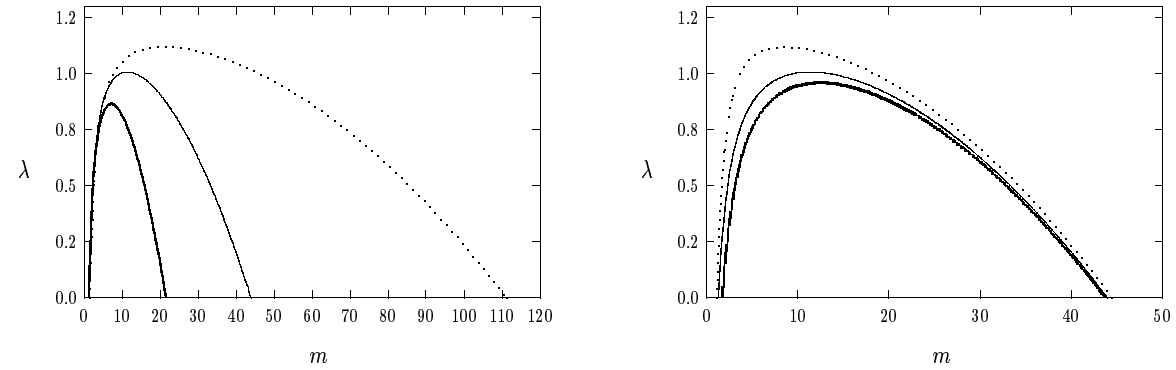

(a) λ versus m for $l = 1$ (b) λ versus m for $\varepsilon = 0.025$

FIGURE 2. Unstable eigenvalue λ in the instability band when $(p, q, r, s) = (2, 1, 2, 0)$ and $\tau = 0$. Left figure: plot of λ versus m when $l = 1$ for $\varepsilon = 0.05$ (heavy solid curve), $\varepsilon = 0.025$ (solid curve), and $\varepsilon = 0.01$ (dashed curve). Right figure: λ versus m when $\varepsilon = 0.025$ for $l = \sqrt{10}$ (heavy solid curve), $l = 1$ (solid curve), and $l = 1/\sqrt{10}$ (dashed curve).

For $l = 1$, $\tau = 0$, and for the classical GM exponent set $(p, q, r, s) = (2, 1, 2, 0)$, in Fig. 2(a) we plot the unique unstable eigenvalue λ in the instability band $m_{b-} < m < m_{b+}$ computed numerically from the NLEP (2.9) for three values of ε. From Proposition 2.3, this eigenvalue is necessarily real. In Fig. 2(b) we show a similar plot of the unique unstable eigenvalue λ for $\varepsilon = 0.025$ for several values of l. Finally, in Fig. 3, we plot the numerically computed unique real positive eigenvalue for $\tau = 0$ within the instability band $m_{b-} < m < m_{b+}$ for various exponent sets (p, q, r, s).

Notice that some of these sets do not satisfy the conditions on the exponents in Proposition 2.3. Therefore, we expect that the conclusions in Propositions 2.3 will hold for a wider range of exponent sets than listed there.

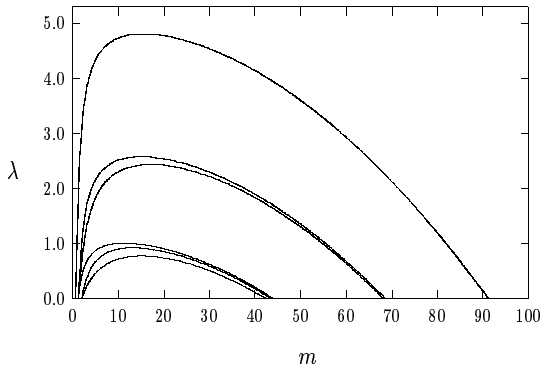

FIGURE 3. The unique unstable eigenvalue in the instability band for different exponent sets (p, q, r, s) when $\varepsilon = 0.025$, $l = 1$, and $\tau = 0$. From top to bottom the curves are for $(4, 2, 2, 0)$, $(3, 2, 2, 0)$, $(3, 2, 3, 1)$, $(3, 1, 2, 0)$, $(2, 1, 3, 0)$, and $(2, 2, 3, 3)$.

We now make a few remarks. In [**4**] breakup instabilities of a stripe for the GM model (1.1) were analyzed using geometric singular perturbation theory for the infinite strip domain $\mathbb{R}^1 \times [0, d_0]$. This problem is equivalent to studying (1.4) in the limit $l = 1/\sqrt{D} \to \infty$, but with $\varepsilon \ll 1$. For the classical GM model with exponent set $(p, q, r, s) = (2, 1, 2, 0)$, a detailed stability result for a stripe in such a domain is given in Theorem 4.5 of [**4**]. Proposition 2.3, given above, generalizes this previous result to allow for a finite rectangular domain and for other exponent sets (p, q, r, s). For $l \to \infty$ and for $(p, q, r, s) = (2, 1, 2, 0)$, the resulting instability band $\sqrt{3} < m < \sqrt{5}/(2\varepsilon)$ is equivalent to that given in Theorem 4.5 of [**4**]. For other exponent sets (p, q, r, s) some partial stability results for the infinite strip domain were given in [**4**]. Specifically, the lower threshold $m_{b-} = \sqrt{\zeta^2 + 2\zeta}$ of the breakup band for the limit $l \gg 1$, where ζ is defined in (1.2), is equivalent to that given in (4.17) of Corollary 4.4 of [**4**]. In addition, the limiting result obtained from (2.14) for τ_{m-} in the limit $l \to \infty$ is readily seen to be equivalent to that given in the unlabeled formula above Remark 4.7 of [**4**]. For the exponent set $(2, 1, 2, 0)$, we calculate that $\tau_{m-} \to 6$ as $l \to \infty$. An important remark is that a stripe is stable with respect to breakup instabilities only when the inequality $m = k\pi/d < \sqrt{\nu_0}/\varepsilon$ holds for all positive integers k. By using $\varepsilon = \varepsilon_0 l$ and $d = l d_0$, this shows that a stripe for (1.1) is stable only when the domain width d_0 for (1.1) is $O(\varepsilon_0)$ thin and satisfies $d_0 < d_{0b} \equiv \pi\varepsilon_0/\sqrt{\nu_0}$. The same critical domain width was found in Corollary 5.1 of [**4**] for a stripe solution in the infinite strip $\mathbb{R}^1 \times [0, d]$. Therefore, the effect of lateral boundaries does not influence the critical domain width. However, both the lower threshold m_{b-} for the breakup instability band and the unstable eigenvalue within the band do depend on $l = 1/\sqrt{D}$.

We now test the theoretical predictions for breakup instabilities with full numerical simulations of (1.1) in the square domain $[-1, 1] \times [0, 2]$. The numerical computations are done using a finite-element method with sufficient resolution to accurately compute thin stripes or localized spots.

Experiments 1-2: For Experiment 1, we take $(p, q, r, s) = (2, 1, 2, 0)$, $\varepsilon_0 = 0.025$, $D = 1$, and $\tau = 0.1$. For $\tau = 0.1$ there are no Hopf bifurcations for modes with $m < m_{b-}$. From the solid curve in Fig. 2(a) with $l = 1/\sqrt{D} = 1$ the most unstable mode is $m \approx 12$ where $\lambda \approx 1.0$. In addition, $\lambda \geq 0.9$ for $5.5 < m < 21.0$. The predicted number N of spots, which corresponds to the number of maxima of the eigenfunction $\cos(my)$ on $0 < y < d_0 = 2$, is

$N = md_0/(2\pi) = m/\pi$. The initial condition for (1.1) is taken to be a perturbation of (2.1) of the form

$$a = \frac{3\mathcal{H}}{2}\mathrm{sech}^2\left(\frac{x_1}{2\varepsilon_0}\right)(1+\delta v)\ , \quad v = \sum_{k=1}^{20}\cos\left(\frac{k\pi x_2}{2}\right)\ ; \qquad h = \frac{\mathcal{H}\cosh[l(1-|x_1|)]}{\cosh l}\,, \tag{2.19}$$

where $\mathcal{H} = \frac{1}{3l}\tanh 1$, $l = 1$, and $\delta = 0.001$. The initial perturbation v covers the entire unstable band in Fig. 2(a). In the numerical results shown in the first row of Fig. 4 the initial stripe is seen to break up into seven spots on an $O(1)$ time-scale. This corresponds to $m \approx 21.5$ which is near the most unstable mode. In Experiment 2 we choose the same parameter values except that D is now decreased to $D = 0.1$, so that $l = \sqrt{10}$. From the heavy solid curve in Fig. 2(b) where $l = \sqrt{10}$ the most unstable mode is $m \approx 12.3$ with $\lambda = 0.96$, and that $\lambda \geq 0.9$ for $8.1 < m < 18.7$. The predicted number N of spots is $N = m/\pi \approx 4$. With the initial condition as given in (2.19) with $l = \sqrt{10}$, the resulting numerical solution of (1.1) is shown in the second row of Fig. 4. The initial stripe is seen to break up into five spots (a boundary spot is counted as half of a spot).

Experiment 3: Next, we take $(p, q, r, s) = (3, 2, 2, 0)$, $\varepsilon_0 = 0.025$, $D = 1$, and $\tau = 0.1$. The initial condition is

$$a = \sqrt{2}\mathcal{H}\mathrm{sech}\left(\frac{x_1}{\varepsilon_0}\right)(1+\delta v)\ , \quad v = \sum_{k=1}^{20}\cos\left(\frac{k\pi x_2}{2}\right)\ ; \qquad h = \frac{\mathcal{H}\cosh(1-|x_1|)}{\cosh 1}\,, \tag{2.20}$$

with $\mathcal{H} = \frac{1}{2}\tanh 1$ and $\delta = 0.001$. The most unstable mode from Fig. 3 is $m \approx 14.9$ with $\lambda \approx 2.6$. Near this maximum, $\lambda \geq 2.3$ when $6.74 < m < 29.85$. We predict $N = m/\pi$ spots. In the bottom row of Fig. 4 we show that the stripe breaks into nine spots at $t = 1.0$, which corresponds to $m \approx 28$. Since the unstable eigenvalue for the exponent set $(3, 2, 2, 0)$ is larger than for $(2, 1, 2, 0)$ (see Fig. 4), the time-scale for breakup is quicker than in Experiments 1 and 2.

Although the stability theory is able to predict the initial number of spots that are generated from the break up of a stripe, it does not account for secondary instabilities relating to a spot competition process that leads to the ultimate annihilation of some of these spots. This secondary instability, which we do not study here, is seen in Fig. 4(f) for the exponent set $(3, 2, 2, 0)$ with $D = 1$. A spot competition process (not shown) also occurs in Experiment 1 on the range $t > 5$, where only two spots ultimately remain. However, for the smaller value $D = 0.1$, the five spots that are initially generated from the stripe in Experiment 2 are found to persist for $t \gg 1$. In [**10**] and [**39**] a related competition instability was studied analytically for a k-spike solution to the one-dimensional GM model. This analysis showed that for $\tau \ll 1$ there is a threshold value D_k of D for which k-spikes will be stable only when $D < D_k$. Similar thresholds occur for spots, as was shown rigorously in [**43**].

2.2 Zigzag Instabilities: Semi-Strong Regime

Next, we analyze zigzag instabilities of a stripe that are associated with unstable eigenfunctions of the form (2.8). Since this analysis is similar to that for a spike given in §4 of [**10**], we only outline the key steps of the derivation in Appendix B. In this way, we obtain the following result for the critical eigenvalue $\lambda = O(\varepsilon^2)$:

Principal Result 2.4: *For $\varepsilon \to 0$ and $\tau \ll O(\varepsilon^{-2})$, the small eigenvalue governing translational instabilities satisfies*

$$\lambda \sim \varepsilon^2\left[2\gamma\theta_\lambda \tanh l \tanh(\theta_\lambda l) - 2\gamma - m^2\right]\ , \qquad \theta_\lambda \equiv \sqrt{1+m^2+\tau\lambda}\,, \qquad \gamma \equiv \frac{q}{p-1}\,. \tag{2.21}$$

Suppose that $\tau \ll O(\varepsilon^{-2})$. Then, there are no unstable zigzag modes when $\gamma \leq 1$, which includes the classical GM exponents $(p, q, r, s) = (2, 1, 2, 0)$. Alternatively, when $\gamma > 1$ there is a band $m_{z-} < m < m_{z+}$ of unstable zigzag

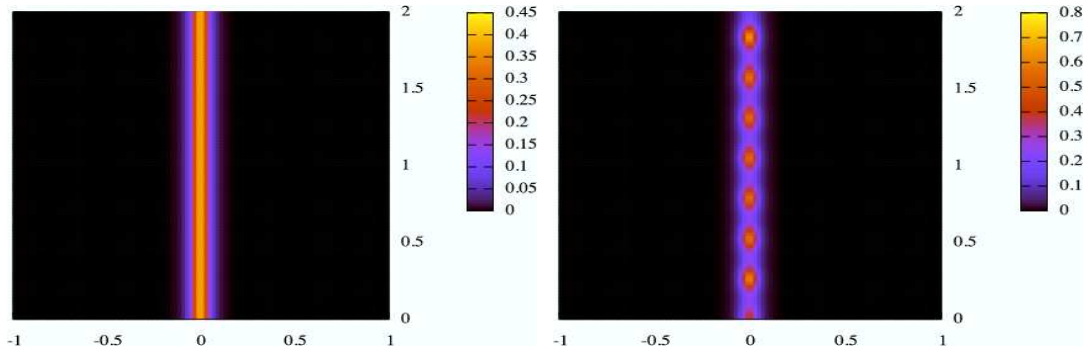

(a) Experiment 1: $t = 0$

(b) Experiment 1: $t = 9$

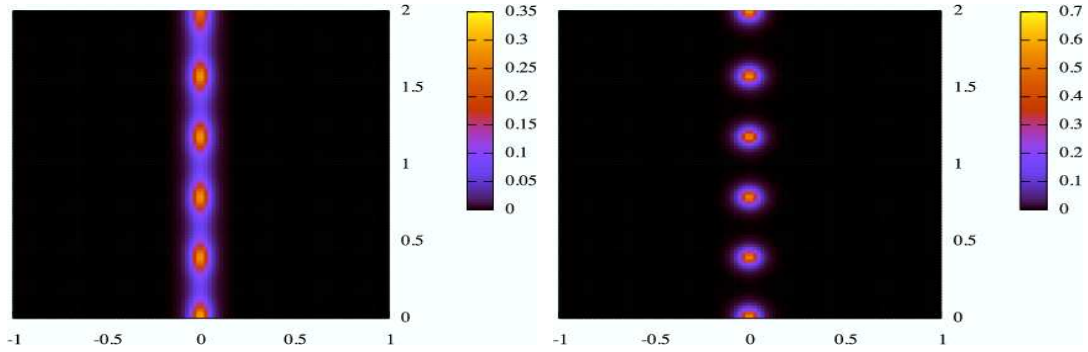

(c) Experiment 2: $t = 12$

(d) Experiment 2: $t = 20$

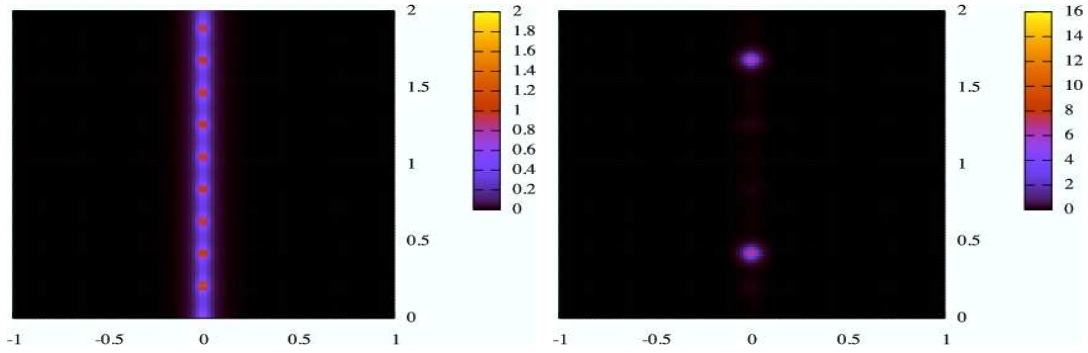

(e) Experiment 3: $t = 1.0$

(f) Experiment 3: $t = 2.4$

FIGURE 4. Breakup instability of a stripe for (1.1) with $\varepsilon_0 = 0.025$, $\tau = 0.1$, and $\Omega = [-1, 1] \times [0, 2]$. **Top Row: Experiment 1:** $(p, q, r, s) = (2, 1, 2, 0)$, and $D = 1.0$. The stripe initially breaks into seven spots, which corresponds to a growth rate that is near that of the most unstable mode. However, there is a secondary instability and eventually only two spots remain (not shown). **Middle Row: Experiment 2:** $(p, q, r, s) = (2, 1, 2, 0)$ and $D = 0.1$. The stripe breaks up into a five-spot pattern, which corresponds closely to the most unstable mode. There is no secondary instability. **Bottom Row: Experiment 3:** $(p, q, r, s) = (3, 2, 2, 0)$ and $D = 1.0$. The stripe initially breaks up into a nine-spot pattern. There is a secondary instability and only two spots remain. The time-scale for spot formation is faster than in Experiment 1.

modes only when the domain half-length l exceeds some critical value l_z, or equivalently when $D < D_z = l_z^{-2}$. For $l \to \infty$, $m_{z+} \sim 2\sqrt{\gamma(\gamma-1)}$ and $m_{z-} \sim \sqrt{\frac{8\gamma}{\gamma-1}}e^{-l} \ll 1$.

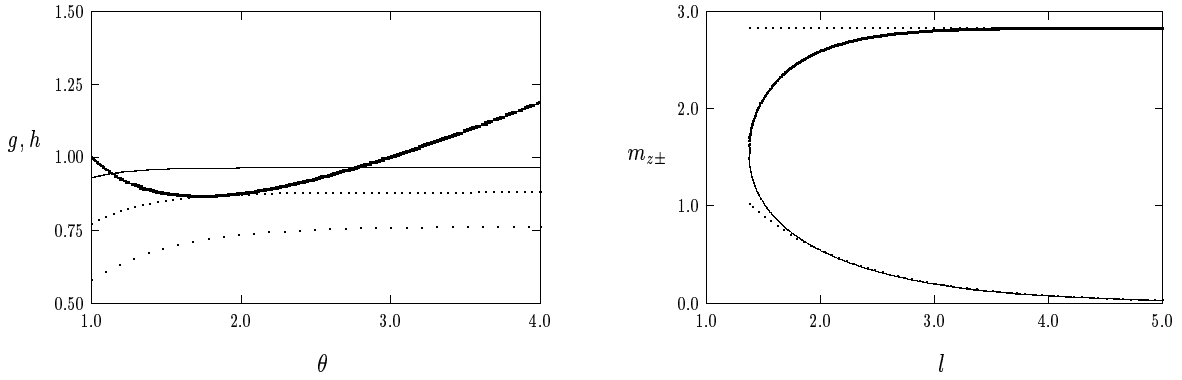

(a) graphical determination of unstable zigzag band

(b) zigzag stability thresholds for $\gamma = 2$

FIGURE 5. Left figure: plot of $h(\theta)$ for $\gamma = 2$ (heavy solid curve) together with $g(\theta)$ for $l = 1$ (widely spaced dots), $l = l_z \approx 1.37$ (dashed curve), and $l = 2$ (solid curve). Here $g(\theta)$ and $h(\theta)$ are defined in (2.22). The unstable zigzag modes correspond to where $g(\theta) > h(\theta)$. Right figure: the upper and lower zigzag stability thresholds m_{z-} (solid curve) and m_{z+} (heavy solid curve) for $\gamma = 2$ as a function of l when $l > l_z \approx 1.37$. The band disappears when $m \approx 1.55$.

We now derive this result. In Appendix B, (2.21) for λ is obtained by modifying the analysis in §4 of [**10**]. To derive the stability result in Principal Result 2.4, we assume $\tau \ll O(\varepsilon^{-2})$ so that $\theta_\lambda \sim \sqrt{1+m^2}$. Then, the stability threshold $\lambda = 0$ in (2.21) corresponds to intersection of the two functions $h(\theta)$ and $g(\theta)$ for $\theta \geq 1$, defined by

$$g(\theta) = h(\theta)\,, \qquad g(\theta) = \tanh(\theta l)\tanh l\,, \qquad h(\theta) = \frac{\theta^2 + (2\gamma - 1)}{2\gamma\theta}\,, \qquad \theta \equiv \sqrt{1+m^2}\,. \tag{2.22}$$

Notice that $\lambda > 0$ whenever $g(\theta) > h(\theta)$. Since $h(1) = 1$ and $g(1) < 1$, the stripe is translationally stable for $m \geq 0$ sufficiently small. Next, we calculate that $h(\theta)$ has a unique minimum at $\theta = \theta_z \equiv \sqrt{2\gamma - 1}$ when $\gamma > 1/2$, where $h(\theta_z) = \gamma^{-1}\sqrt{2\gamma - 1}$. First, suppose that $0 < \gamma \leq 1$. Then, since $\theta_z \leq 1$ when $\frac{1}{2} < \gamma \leq 1$, and θ_z is undefined when $0 < \gamma < \frac{1}{2}$, we conclude that $h'(\theta) > 0$ for all $\theta \geq 1$. Since $h(1) = 1$, and $g(\theta) < 1$, it follows that there are no roots to (2.22) in $\theta > 1$ when $0 < \gamma \leq 1$. Therefore, there are no zigzag instabilities when $0 < \gamma \leq 1$. Alternatively, for $\gamma > 1$, we obtain that $\theta_z > 1$ and $h(\theta_z) < 1$. Since for each $\theta > 1$, $g(\theta)$ is an increasing function of l, we conclude that there exists a band of unstable zigzag modes only when $l > l_z$, where l_z is the critical value where $g(\theta)$ and $h(\theta)$ intersect tangentially. Since $l = 1/\sqrt{D}$, this implies that there is an unstable band of zigzag modes only when $D < D_z = l_z^{-2}$. We illustrate this result graphically in Fig. 5(a) where we plot $h(\theta)$ for $\gamma = 2$ together with $g(\theta)$ for different values of l. For $\gamma = 2$, in Fig. 5(b) we plot the upper and lower zigzag thresholds m_{z+} and m_{z-}, respectively, versus l for $l > l_z$. The dashed lines in this figure are the asymptotic approximations $m_{z+} \sim 2\sqrt{\gamma(\gamma-1)}$ and $m_{z-} \sim \sqrt{\frac{8\gamma}{\gamma-1}}e^{-l}$ for $l \gg 1$, which are readily derived from (2.22). In Fig. 6 we plot the critical domain half-length l_z versus γ.

Since $m = k\pi/d$, and $d = ld_0$ with $l = 1/\sqrt{D}$, we conclude from the upper bound $m = m_{z+}$ that a stripe for (1.1) with $\gamma = q/(p-1) > 1$ is stable to zigzag instabilities only when the domain width d_0 for (1.1) satisfies $d_0 < d_{0z} \equiv \pi\sqrt{D}/m_{z+} = O(1)$. For $0 < \gamma < 1$, there are no zigzag instabilities for any domain width.

From the results here and in §2.1, we conclude that a stripe for (1.1) in the semi-strong regime is stable with

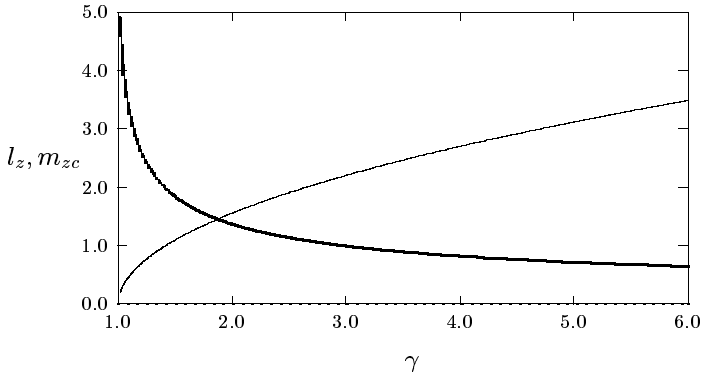

FIGURE 6. Plots of the critical domain half-length l_z (heavy solid curve) and the mode m where the zigzag band disappears (solid curve) versus $\gamma = \frac{q}{p-1}$ for $\gamma > 1$. For $l > l_z$, there is a band of unstable zigzag modes.

respect to both breakup and zigzag instabilities only for thin domains satisfying $d_0 < \pi\varepsilon_0/\sqrt{\nu_0}$, where ν_0, given in (2.10), is the positive eigenvalue of L_0. Since zigzag instabilities develop on a long time $O(\varepsilon^{-2})$ time-scale, they are dominated by any breakup instability that occurs. Finally, we remark that although we have presented only a formal derivation of (2.21), it can be derived rigorously by using a similar Lyapunov-Schmidt reduction analysis as in [**44**].

2.3 GM Model With Small Saturation: Fat Homoclinics

In the semi-strong regime, where $D = O(1)$, we now show that the inclusion of a small amount of saturation in the activator production for the classical GM model can lead to the disappearance of the breakup instability band. The resulting modified classical GM model in a rectangular domain is

$$a_t = \varepsilon_0^2 \Delta a - a + \frac{a^2}{h(1+ka^2)}, \quad \tau h_t = D\Delta h - h + \frac{a^2}{\varepsilon_0}, \quad X = (X_1, X_2) \in \Omega = \{-1 < X_1 < 1, 0 < X_2 < d_0\}, \tag{2.23}$$

with $\partial_n a = \partial_n h = 0$ on $\partial\Omega$. We refer to (2.23) as the small saturation limit of (1.6), since if we replace a and h in (2.23) with $\varepsilon_0 a$ and $\varepsilon_0 h$, we obtain (1.6) with $\kappa = \varepsilon_0^2 k$. Thus, $k = O(1)$ in (2.23) corresponds to $\kappa = O(\varepsilon_0^2)$ in (1.6).

For $\varepsilon \to 0$ we now asymptotically construct an equilibrium homoclinic stripe solution. In the inner region, we let $y = X_1/\varepsilon$ to obtain that $h \sim \mathcal{H}$ and $a \sim \mathcal{H} w(y)$, where $w(y)$ satisfies

$$w'' + f(w) = 0, \quad f(w) \equiv -w + \frac{w^2}{1+bw^2} \qquad -\infty < y < \infty; \qquad b = k\mathcal{H}^2. \tag{2.24}$$

For $0 \le b < \frac{1}{4}$ it follows that $w = 0$ and $w = w_\pm$, with $0 < w_- < w_+$, are the rest points of (2.24), where

$$w_\pm = \frac{1}{2}\left[1 \pm \sqrt{1-4b}\right]. \tag{2.25}$$

Both $w = 0$ and $w = w_+$ are saddle points, while w_- is a center. It is readily shown that (2.24) has a homoclinic pulse solution with $w(0) > 0$ and $w(\pm\infty) = 0$ provided that there exists a value $w_m \in (w_-, w_+)$ for which $\mathcal{F}(w_m) = 0$, where $\mathcal{F}(w) \equiv -\int_0^w f(s)\,ds$. Such a value of w_m exists for $0 < b < b_0 < \frac{1}{4}$. However, when $b = b_0$, then (2.24) has a heteroclinic solution with asymptotic end-states $w = 0$ and $w = w_+$. To determine this critical value b_0 of b we set $\mathcal{F}(w_+) = 0$. Upon integrating $f(w)$, we find that w_+ and b_0 are determined uniquely by

$$b_0 = \frac{w_+ - 1}{w_+^2}, \qquad 2w_+ \tan^{-1}\left(\sqrt{w_+ - 1}\right) = (w_+ + 1)\sqrt{w_+ - 1}. \tag{2.26}$$

By solving (2.26) numerically, we obtain

$$b_0 \approx 0.211376\,, \qquad w_+ \approx 3.295209\,. \tag{2.27}$$

In summary, (2.24) has a unique homoclinic solution with $w(0) > 0$ and $w(\pm\infty) = 0$ provided that $0 < b < b_0$.

In the outer region, we calculate a^2/ε_0 in (2.23) in terms of a Dirac mass. In this way, we obtain

$$h_{X_1X_1} - \theta_0^2 h = -\frac{\beta\mathcal{H}^2}{D}\delta(X_1)\,, \quad -1 < X_1 < 1\,; \quad h_{X_1}(\pm 1) = 0\,, \tag{2.28}$$

where $\beta \equiv \int_{-\infty}^{\infty} w^2\,dy$ and $\theta_0 \equiv D^{-1/2}$. We solve (2.28) in terms of a Green's function, and we impose the matching condition $h(0) = \mathcal{H}$, which determines $\mathcal{H}$. Finally, we recall that $b = k\mathcal{H}^2$. This leads to the following formal result:

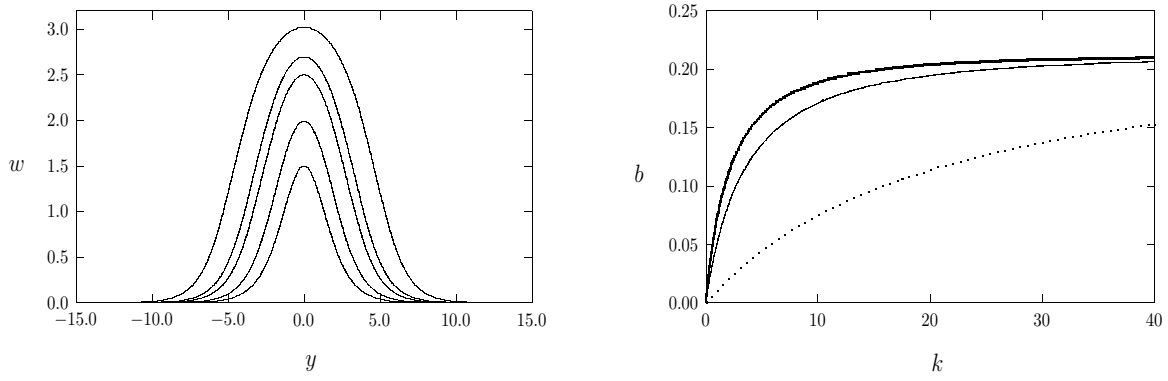

(a) w versus y for various b (b) b versus k

FIGURE 7. Left figure: plots of the homoclinic solution $w(y)$ to (2.24). From top to bottom the curves are for $b = 0.211$, $b = 0.2034$, $b = 0.195$, $b = 0.145$, and $b = 0.0$. Right figure: b versus k for $D = 10$ (heavy solid curve), $D = 1$ (solid curve), and $D = 0.1$ (dotted curve).

Principal Result 2.5 *For $\varepsilon \to 0$, and for any $k > 0$, there is a unique homoclinic stripe solution to (2.23) given by*

$$a_e(X_1) \sim \mathcal{H} w\left(\varepsilon^{-1}X_1\right)\,, \qquad h_e(X_1) \sim \mathcal{H}\frac{G(X_1)}{G(0)}\,; \qquad G(X_1) \equiv \frac{\cosh\left[\theta_0(1-|X_1|)\right]}{2\theta_0\sinh\theta_0}\,. \tag{2.29}$$

Here, for a fixed value of b in $0 \le b < b_0 \approx 0.2114$, $w(y)$ is the unique positive homoclinic solution to (2.24). The saturation constant k and $h(0) \equiv \mathcal{H}$ are related to b and D by

$$\mathcal{G}(b) \equiv b\beta^2 = 4kD\tanh^2\left(1/\sqrt{D}\right)\,, \quad \mathcal{H} = \frac{2\sqrt{D}}{\beta}\tanh\left(1/\sqrt{D}\right)\,, \quad \beta \equiv \int_{-\infty}^{\infty} w^2\,dy\,. \tag{2.30}$$

In (2.30), the integral β, which is readily computed numerically, depends only on b and satisfies $\beta(b) \to +\infty$ as $b \to b_0^-$. Since $\beta > 0$ and $d\beta/db > 0$ (see Appendix B of [**42**]), it follows that $\mathcal{G}(b)$ is a monotone increasing in b with $\mathcal{G}(0) = 0$ and $\mathcal{G}(b) \to +\infty$ as $b \to b_0^-$. Therefore, from (2.30), there is a unique value of k for each fixed D and b in $0 \le b < b_0$, and that $k \to \infty$ as $b \to b_0^-$. Therefore, as $k \to \infty$, we have $b \to b_0^-$, and the fattened homoclinic w approaches a mesa pattern that is comprised of a front-back heteroclinic structure connected by an asymptotically flat plateau. In Fig. 7(b) we use (2.30) to plot b versus k for several values of D, showing that $k \to \infty$ as $b \to b_0^-$. In Fig. 7(a) we plot the solution $w(y)$ to (2.24) for several values of b. Notice that for b slightly below b_0, $w(y)$ becomes rather fat as a result of the ghost effect of the heteroclinic connection that exists when $b = b_0$.

Next, we study breakup instabilities of the homoclinic stripe by deriving an NLEP. Since this derivation is similar to that given in Appendix A, we only highlight its key steps. We introduce a perturbation of the form (2.5). Then, in place of (A.1) and (A.2), we obtain that $\Phi(y)$, with $y = X_1/\varepsilon$, satisfies

$$\Phi'' - \Phi + \frac{2w}{(1+bw^2)^2}\Phi - \frac{\eta(0)w^2}{1+bw^2} = \left(\lambda + \varepsilon^2 m^2\right)\Phi\,, \quad -\infty < y < \infty\,; \quad \Phi \to 0 \quad \text{as} \quad |y| \to \infty\,. \tag{2.31}$$

Assuming that $\int_{-\infty}^{\infty} \Phi w\, dy \neq 0$, then $\eta(0)$ in (2.31) is to be calculated from

$$\eta_{X_1X_1} - \theta_\lambda^2 \eta = 0\,, \quad -1 < X_1 < 1\,; \qquad \eta_{X_1}(\pm 1) = 0\,; \qquad \theta_\lambda \equiv \sqrt{m^2 + \frac{(1+\tau\lambda)}{D}}\,, \tag{2.32 a}$$

$$[\eta] = 0\,; \qquad [\eta_{X_1}] = -\frac{2\mathcal{H}}{D}\int_{-\infty}^{\infty} w\Phi\, dy\,. \tag{2.32 b}$$

We solve (2.32) in terms of a Green's function, which yields $\eta(0)$ in (2.31). This leads to the following NLEP:

Principal Result 2.6: *Let $\varepsilon \to 0$, and suppose $\int_{-\infty}^{\infty} \Phi w\, dy \neq 0$. Then, for $0 \le b < b_0$, the stability of the homoclinic stripe for the modified GM model (2.23) on an $O(1)$ time-scale is determined by the spectrum of the NLEP*

$$L_{0b}\Phi - \frac{\chi_m w^2}{(1+bw^2)}\frac{\int_{-\infty}^{\infty} w\Phi\, dy}{\int_{-\infty}^{\infty} w^2\, dy} = (\lambda + \varepsilon^2 m^2)\Phi \quad -\infty < y < \infty\,; \quad \Phi \to 0 \quad \text{as} \quad |y| \to \infty\,, \tag{2.33 a}$$

$$L_{0b}\Phi \equiv \Phi'' - \Phi + \frac{2w}{(1+bw^2)^2}\Phi\,, \quad \chi_m \equiv \frac{2\theta_0 \tanh\theta_0}{\theta_\lambda \tanh\theta_\lambda}\,, \quad \theta_0 \equiv D^{-1/2}\,, \quad \theta_\lambda \equiv \sqrt{m^2 + \frac{(1+\tau\lambda)}{D}} \tag{2.33 b}$$

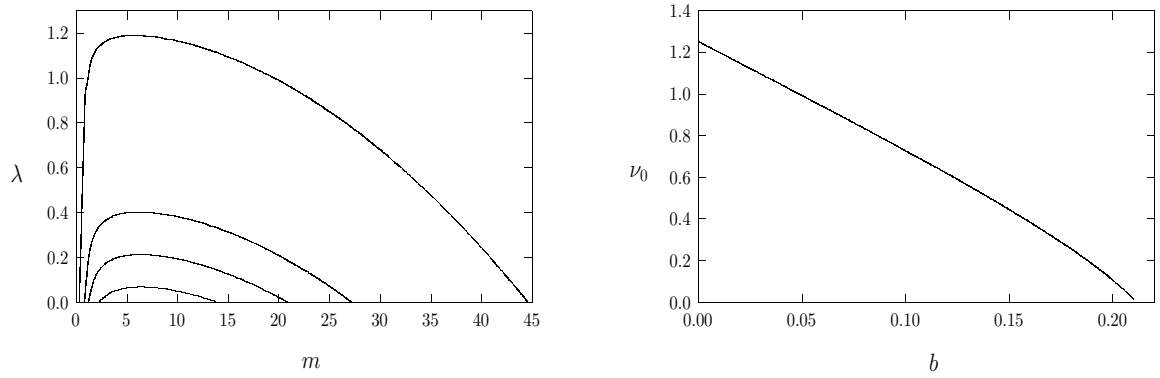

(a) λ versus m (b) ν_0 versus b

FIGURE 8. Left figure: the unstable eigenvalue λ versus m within an instability band when $D = 10$ and $\varepsilon_0 = 0.025$. From top to bottom the curves are for $k = 0$, $k = 3.663$, $k = 6.802$, and $k = 12.519$. Right figure: the principal eigenvalue ν_0 of the local operator L_{0b} versus b, with $\nu_0 \to 0$ as $b \to 0.2114$.

For $\varepsilon \ll 1$, and in the absence of saturation effects (i. e. $b = 0$), it was shown in §2.1 that there is always a breakup instability band for any $D > 0$. We now study numerically whether this instability band can disappear for some range of b on the homoclinic existence interval $0 \le b < b_0$. For simplicity we will only consider the case where $\tau = 0$. Although we are unable to give a rigorous analysis of the spectrum of (2.33) as a function of b, we can readily identify the mechanism for the possible coalescence of the upper and lower breakup instability thresholds. Since $\chi_m \to 0$

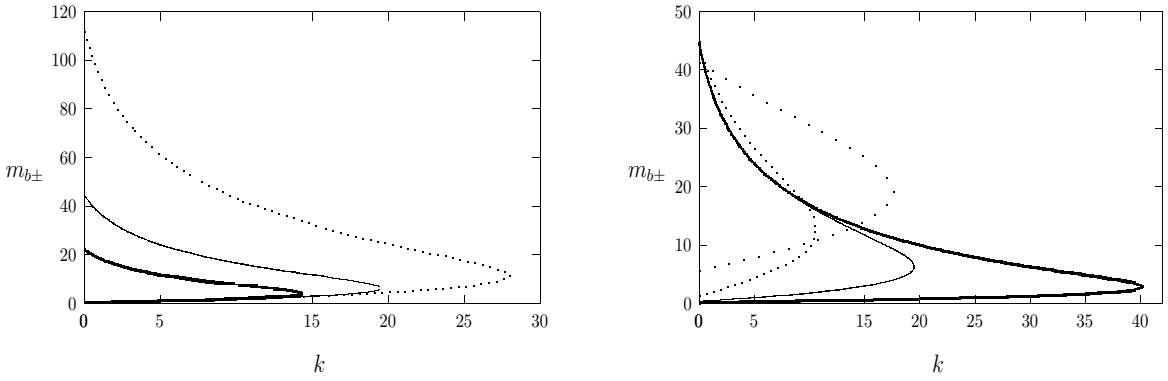

(a) $m_{b\pm}$ versus k for $D = 10$

(b) $m_{b\pm}$ versus k for $\varepsilon_0 = 0.025$

FIGURE 9. Left figure: plots of $m_{b\pm}$ versus k when $D = 10$ for $\varepsilon_0 = 0.05$ (heavy solid curve), $\varepsilon_0 = 0.025$ (solid curve), and $\varepsilon_0 = 0.01$ (dotted curve). Right figure: plots of $m_{b\pm}$ versus k when $\varepsilon_0 = 0.025$ for $D = 100$ (heavy solid curve), $D = 10$ (solid curve), $D = 1$ (dotted curve), and $D = 0.1$ (widely spaced dots).

as $m \to \infty$ in (2.33), it follows by the same reasoning as in §2.1 that the upper stability boundary, m_{b+}, satisfies $m_{b+} \sim \sqrt{\nu_0}/\varepsilon_0$ for $\varepsilon_0 \ll 1$, where $\nu_0 = \nu_0(b) > 0$ is the unique positive eigenvalue of the local operator $L_{0b}\Psi = \nu\Psi$. However, ν_0 must tend to zero as $b \to b_0^- \approx 0.2114$, or equivalently as $k \to \infty$, since we necessarily must have $\nu_0 = 0$ for the heteroclinic orbit where $b = b_0$. This behavior of ν_0 is confirmed in Fig. 8(b) where we plot the numerically computed curve $\nu_0 = \nu_0(b)$. Therefore, for any fixed ε small, it follows that $m_{b+} \to 0$ as $b \to b_0^-$. In addition, since a homoclinic pulse with $m = 0$ for (2.33) is always stable when $\tau = 0$ (cf. [**42**]), it follows that if the lower instability boundary exists, it will satisfy $m_{b-} > 0$. Hence, the instability band $m_{b-} < m < \sqrt{\nu_0}/\varepsilon_0$ must become narrower as b increases towards b_0, or equivalently as $k \to \infty$.

To numerically calculate breakup instability bands, we first solve (2.24) numerically and then discretize (2.33) using centered differences and the trapezoidal rule. The eigenvalues of the resulting matrix eigenvalue problem are found using LAPACK [**1**], and a quasi-Newton method is used to locate the edges of any instability band. Continuation in b is then used starting from $b = 0$, where the instability band is known from Proposition 2.3. Finally, the relation (2.30) between b and k determines the instability band with respect to the saturation parameter k in (2.23).

For $D = 10$ and $\varepsilon_0 = 0.025$, in Fig. 8(a) we plot the unique positive eigenvalue within the instability band for four values of k. As k increases the band becomes narrower, until it finally pinches off at the critical value $k \approx 19.4$. This coalescence of the edges of the breakup instability band for k sufficiently large occurs for other values of D and ε_0. In particular, when $D = 10$, in Fig. 9(a) we show the merging of the upper and lower thresholds $m_{b\pm}$ at some value of k for three values of ε_0. In Fig. 9(b) we show a similar merging behavior when $\varepsilon_0 = 0.025$ for four values of D.

Qualitatively, these numerical results show that the breakup instability disappears on some range $k > k_{0d}$ (or equivalently $b_{0d} < b < b_0 \approx 0.2114$) when the homoclinic solution w to (2.24) is sufficiently broad (see Fig. 7(a)). This widening of the homoclinic is a result of the ghost effect of the heteroclinic connection that exists when $b = b_0$. Therefore, we suggest that the stability properties of "fat" homoclinic stripes can be similar to those of mesa-stripe solutions, such as those that occur for the Fitzhugh-Nagumo model (cf. [**34**], [**35**]) and the modified GM model of §4–5 with large saturation, where spot-generating breakup instabilities do not occur.

[htb]

(p,q,m,s)	D_{0c}	α_c	D_{0b}	D_{0z}	D_{0m}	D_{0s}
$(2,1,2,0)$	7.17	1.58	8.06	24.0	8.92	9.82
$(2,1,3,0)$	10.35	1.42	19.14	30.0	12.36	16.31
$(3,2,2,0)$	3.91	1.62	$--$	32.3	5.08	5.23
$(3,2,3,1)$	4.41	1.53	5.13	28.0	5.36	5.97
$(2,2,3,3)$	33.7	2.28	$--$	$--$	41.80	85.52
$(4,2,2,0)$	0.89	1.36	1.00	27.9	1.06	0.89

Table 2. The second and third columns are the saddle-node bifurcation values D_{0c} and $\alpha_c \equiv a(0)$ for the existence of a stripe. The fourth column are the values D_{0b} of D_0 for the lower bound of the breakup instability band. A stripe is stable to breakup instabilities when $D_{0c} < D_0 < D_{0b}$. For $(3,2,2,0)$ and $(2,2,3,3)$ the band does not terminate before D_{0c} and so D_{0b} is undefined. The fifth column are the values D_{0z} of D_0 for the upper bound of the zigzag instability band in the weak-interaction regime. For $(2,2,3,3)$, where $\gamma = q/(p-1) = 2$, the band continues into the semi-strong regime. The sixth column are the smallest values D_{0m} of D_0 where $a(y)$ has a multi-bump structure on the lower branch of the $a(0)$ versus D_0 bifurcation diagram. The seventh column are the saddle-node values D_{0s}, computed in [**33**], representing the smallest value of D_0 where a radially symmetric spot solution exists in $\mathbb{R}^2$.

3 The GM Model Without Saturation: Weak Interaction Regime

In the weak interaction regime we now show numerically that, depending on the exponent set (p,q,r,s), a stripe for (1.1) can be stable with respect to breakup instabilities for any domain width d_0, but is unstable to zigzag instabilities unless $d_0 = O(\varepsilon_0)$ thin. As in §2.3, this disappearance of the breakup instability band is again related to the "fattening" of a homoclinic solution as a parameter is varied. In (1.4) the weak interaction regime corresponds to the limit $l = 1/\sqrt{D} \gg 1$ with $\varepsilon = \varepsilon_0 l = O(1)$. Equivalently, in (1.1) we write $D = D_0\varepsilon_0^2$ for some $D_0 = O(1)$ and we let $\varepsilon_0 \to 0$. In terms of $y = x_1/\varepsilon_0$, and upon re-scaling a and h in (1.1), the resulting equilibrium problem for (1.1) is to look for even homoclinic solutions to the coupled system

$$a_{yy} - a + \frac{a^p}{h^q} = 0\,, \quad D_0 h_{yy} - h + \frac{a^r}{h^s} = 0\,, \quad \infty < y < \infty\,; \qquad a \to 0\,, \quad h_y \to 0\,, \quad |y| \to \infty\,. \tag{3.1}$$

In [**14**] numerical solutions to (3.1) are computed by using the boundary-value solver COLSYS [**2**] together with path-following in D_0. As D_0 is decreased from some initially large value it was shown for various exponent sets in [**14**] that the bifurcation diagram of $a(0)$ versus D_0 for (3.1) has a saddle-node bifurcation at some critical value D_{0c} and that there are no homoclinic solutions to (3.1) when $0 < D_0 < D_{0c}$. The existence of such a fold-point value D_{0c} was proved in [**4**] using geometric singular perturbation theory. For the classical GM model, where $(p,q,r,s) = (2,1,2,0)$, a plot of $a(0)$ versus D_0 is shown in Fig. 10(a). When viewed as a pulse solution in one-dimension, the upper branch of this bifurcation diagram is stable when τ is below some $O(1)$ Hopf bifurcation threshold $\tau_H = \tau_H(D_0)$, and the lower branch is unstable for any $\tau \geq 0$ (cf. [**14**]). The dashed portion along the lower solution branch of Fig. 10(a) is where $a(y)$ has two distinct local maxima, with one on either side of the symmetry point $y = 0$. This two-bump structure begins at the point where $a_y(0) = 0$, which we label by $D_0 = D_{0m}$.

A stripe solution a_e, h_e for the two-dimensional GM model (1.1) is obtained by taking the homoclinic solution of (3.1) as the cross-sectional profile of the stripe. The stripe, with a width $O(\varepsilon_0)$, is then localized along the mid-line $x_1 = 0$ of the rectangular domain. For various exponent sets we then determine the stability of this stripe solution

along each point on the upper branch of the $a(0)$ versus D_0 bifurcation diagram by writing

$$a = a_e\left(\varepsilon_0^{-1}x_1\right) + \Phi\left(\varepsilon_0^{-1}x_1\right)e^{\lambda t}\cos(mx_2)\,, \qquad h = h_e\left(\varepsilon_0^{-1}x_1\right) + N\left(\varepsilon_0^{-1}x_1\right)e^{\lambda t}\cos(mx_2)\,. \tag{3.2}$$

By substituting (3.2) into (1.1) we obtain the following eigenvalue problem for $\Phi(y)$ and $N(y)$ on $0 \le y < \infty$:

$$\Phi_{yy} - (1+\mu)\Phi + \frac{pa_e^{p-1}}{h_e^q}\Phi - \frac{qa_e^p}{h_e^{q+1}}N = \lambda\Phi\,, \qquad D_0N_{yy} - (1+D_0\mu)\,N + \frac{ra_e^{r-1}}{h_e^s}\Phi - \frac{sa_e^r}{h_e^{s+1}}N = \tau\lambda N\,. \tag{3.3}$$

Here $\mu \equiv \varepsilon_0^2 m^2$, where m is either the breakup mode or the zigzag mode transverse to the stripe.

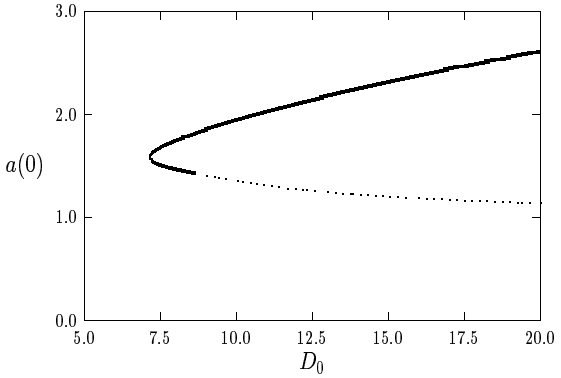

(a) $a(0)$ versus D_0 for $(2,1,2,0)$

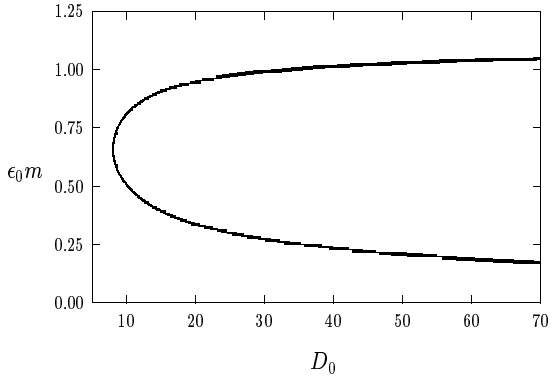

(b) Breakup instability band for $(2,1,2,0)$

FIGURE 10. Left figure: bifurcation diagram of $a(0)$ versus D_0 for (3.1) for $(p,q,r,s) = (2,1,2,0)$. On the dashed portion of the lower branch $a(y)$ has a multi-bump structure. Right figure: the breakup instability band versus D_0 for $(p,q,r,s) = (2,1,2,0)$. For modes $\varepsilon_0 m$ within the band the stripe is unstable. The band terminates before the saddle-node value $D_{0c} = 7.17$.

To study breakup instabilities we compute the spectrum of (3.3) for even eigenfunctions Φ and N so that $\Phi_y(0) = N_y(0) = 0$. We first compute the homoclinic solution of (3.1) on a long interval $0 < y < L$, where $L \gg 1$. We then discretize (3.3) on the same interval $[0,L]$ by using centered differences, and we label $\boldsymbol{\Phi_0} = (\Phi_0(y_1),\ldots,\Phi_0(y_n))^t$ and $\boldsymbol{N_0} = (N_0(y_1),\ldots,N_0(y_n))^t$, where $y_j = jh$ for $j = 0,\ldots,n$ with $h = L/n$. We also impose that $\Phi_y(L) = N_y(L) = 0$. In this way, we obtain the block matrix eigenvalue problem

$$\begin{pmatrix} \mathcal{M} - (1+\mu)I + \Lambda_1 & -\Lambda_2 \\ \Lambda_3 & D_0\mathcal{M} - (1+D_0\mu)I - \Lambda_4 \end{pmatrix}\begin{pmatrix} \boldsymbol{\Phi_0} \\ \boldsymbol{N_0} \end{pmatrix} = \lambda\begin{pmatrix} I & 0 \\ 0 & \tau I \end{pmatrix}\begin{pmatrix} \boldsymbol{\Phi_0} \\ \boldsymbol{N_0} \end{pmatrix}. \tag{3.4}$$

Here Λ_j for $j = 1,\ldots,4$ are $n \times n$ diagonal matrices, and $\mathcal{M}$ is a tridiagonal matrix defined by

$$\Lambda_{1jj} = \frac{pa_e^p(y_j)}{h_e^q(y_j)}\,, \qquad \Lambda_{2jj} = \frac{qa_e^p(y_j)}{h_e^{q+1}(y_j)}\,,$$

$$\Lambda_{3jj} = \frac{ra_e^{r-1}(y_j)}{h_e^s(y_j)}\,, \qquad \Lambda_{4jj} = \frac{sa_e^r(y_j)}{h_e^{s+1}(y_j)}\,,$$

$$\mathcal{M} \equiv \frac{1}{h^2}\begin{pmatrix} -2 & 2 & 0 & \cdots & 0 & 0 & 0 \\ 1 & -2 & 1 & \ddots & \ddots & 0 & 0 \\ 0 & \ddots & \ddots & \ddots & \ddots & \ddots & 0 \\ \vdots & \ddots & \ddots & \ddots & \ddots & \ddots & \vdots \\ 0 & \ddots & \ddots & \ddots & \ddots & \ddots & 0 \\ 0 & 0 & \ddots & \ddots & 1 & -2 & 1 \\ 0 & 0 & 0 & \cdots & 0 & 2 & -2 \end{pmatrix}. \tag{3.5}$$

For $\tau = 0.01$, we numerically determine the range of values of μ where (3.4) has unstable eigenvalues. For D_0

sufficiently large, and for all of the exponent sets in Table 2, our computational results from LAPACK [1] with $n = 250$ meshpoints and $L = 15$ show that there are threshold values μ_1 and μ_2 for which there is a unique real positive eigenvalue λ_0 in the breakup instability band $\sqrt{\mu_1} < \varepsilon_0 m < \sqrt{\mu_2}$, and that $\mathrm{Re}(\lambda) < 0$ for $0 \le \varepsilon_0 m < \sqrt{\mu_1}$ and $\varepsilon_0 m > \sqrt{\mu_2}$. However, as D_0 is decreased towards the existence threshold D_{0c}, our results show that the instability band disappears for some of these exponent sets at some critical value $D_{0b} > D_{0c}$ on the upper branch. Numerical values for D_{0b} are given in Table 2. Increasing n and L did not change the results in Table 2 significantly.

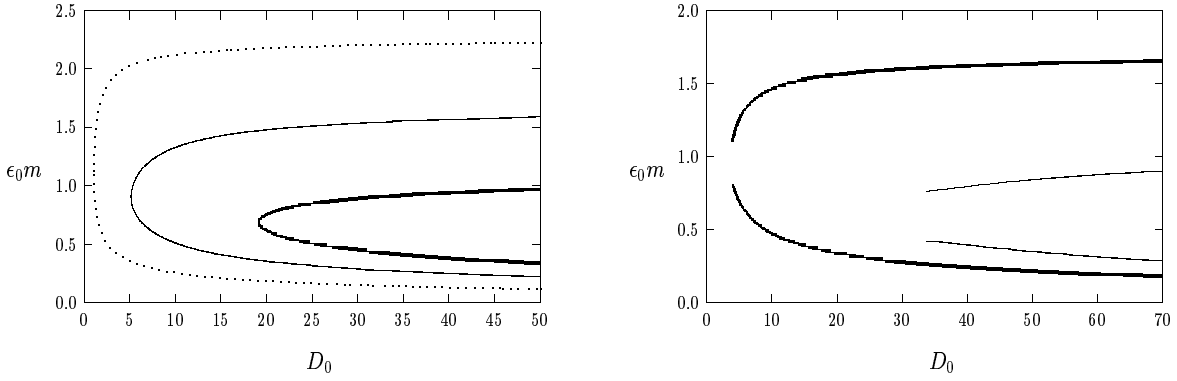

(a) breakup bands: $(4,2,2,0)$, $(3,2,3,1)$, $(2,1,3,0)$ (b) breakup bands: $(3,2,2,0)$, $(2,2,3,3)$

FIGURE 11. Left figure: breakup instability bands that terminate before the saddle-node value D_{0c}. The heavy solid curve is for $(p,q,r,s) = (2,1,3,0)$, the solid curve is for $(3,2,3,1)$, and the dashed curve is for $(4,2,2,0)$. Right figure: breakup bands that do not terminate before D_{0c}. The heavy solid and solid curves are for $(3,2,2,0)$ and $(2,2,3,3)$, respectively.

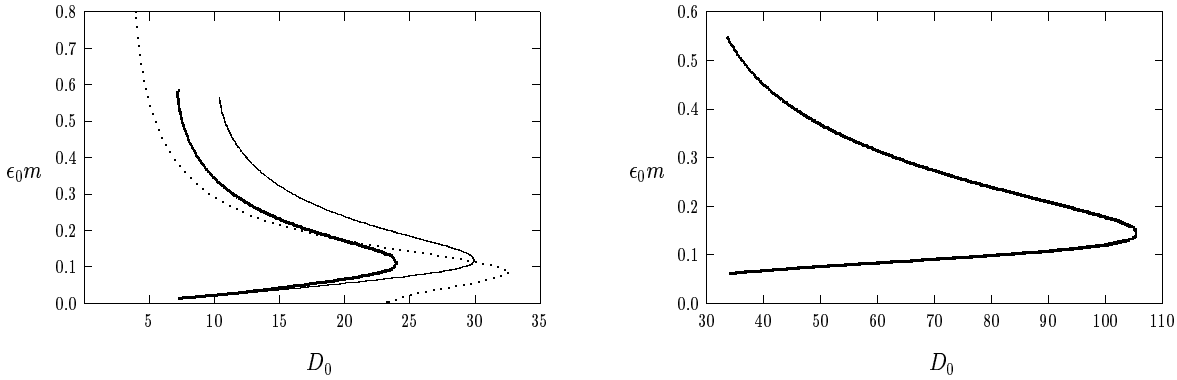

(a) zigzag bands: $(2,1,2,0)$, $(2,1,3,0)$, $(3,2,2,0)$ (b) zigzag band: $(2,2,3,3)$

FIGURE 12. Left figure: the zigzag instability band for $(2,1,2,0)$ (heavy solid curve), for $(2,1,3,0)$ (solid curve), and for $(3,2,2,0)$ (dashed curve), plotted for $D_0 > D_{0c}$. For these exponent sets there is a value D_{0z} of D_0 for which there is an unstable band for $D_{0c} < D_0 < D_{0z}$. Within the band there is a unique and real unstable eigenvalue. Right figure: the unstable zigzag band for $(2,2,3,3)$. Since $\gamma = q/(p-1) = 2 > 1$, this band continues into the semi-strong interaction regime and terminates there (see §2.2).

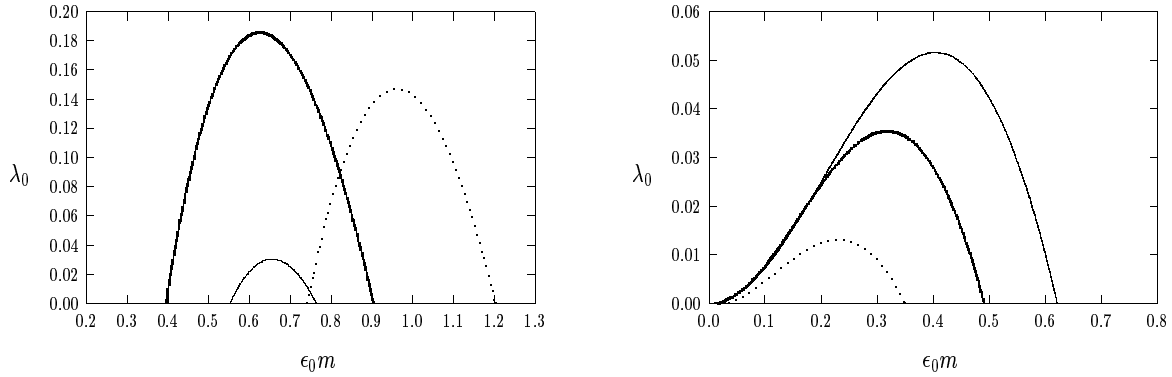

(a) unstable breakup eigenvalue

(b) unstable zigzag eigenvalue

FIGURE 13. Left figure: the unstable breakup eigenvalue λ_0 within an instability band. The heavy solid curve is for $(2,1,2,0)$ with $D_0 = 15.0$, the solid curve is for $(2,1,2,0)$ with $D_0 = 9.01$, and the dashed curve is for $(3,2,2,0)$ with $D_0 = 4.5$. Right figure: the unstable zigzag eigenvalue λ_0 within an instability band. The heavy solid curve is for $(2,1,2,0)$ with $D_0 = 7.60$, the solid curve is for $(3,2,2,0)$ with $D_0 = 4.5$, and the dashed curve is for $(2,1,3,0)$ with $D_0 = 14.0$.

In Fig. 10(b) we plot the upper and lower thresholds for the breakup instability band for the exponent set $(p,q,r,s) = (2,1,2,0)$ showing the coalescence of the thresholds when $D_0 = D_{0b} = 8.06$. This critical value compares reasonably well with the corresponding critical value $D_0 \approx 1/(.12) = 8.33$ estimated in [**4**] (see page 99 of [**4**]) based on full numerical computations and on an extrapolation of stability results from the semi-strong regime into the weak interaction regime (see Fig. 5.2 of [**4**]). Therefore, for the classical GM model, a stripe solution for (1.1) exists and is stable with respect to breakup instabilities when $7.17 < D_0 < 8.06$. In Fig. 11(a) we plot similar upper and lower stability thresholds of the breakup instability band for the exponent sets $(4,2,2,0)$, $(3,2,3,1)$, and $(2,1,3,0)$. For these exponent sets the breakup instability band disappears below some threshold value D_{0b} larger than D_{0c}, so that a stripe solution for (1.1) is stable with respect to breakup on the range $D_{0c} < D_0 < D_{0b}$. For three parameter sets, in Fig. 13(a) we plot the unique unstable real eigenvalue within an instability band. As seen from this figure, the most unstable mode occurs roughly in the middle of this band.

However, as shown in Fig. 11(b), the breakup instability band does not disappear at some D_0 value greater than the existence threshold D_{0c} for the exponent sets $(3,2,2,0)$ and $(2,2,3,3)$. Consequently, for these exponent sets, a stripe solution to (1.1) will always be unstable to breakup instabilities when the domain width d_0 is $O(1)$.

Next, we study zigzag instabilities by calculating the spectrum of (3.3) for odd eigenfunctions Φ and N so that $\Phi(0) = N(0) = 0$. The discrete eigenvalue problem has the same form as in (3.4) and (3.5) except that now $y_j = jh$ for $j = 1,\ldots,n$ with $h = L/n$, and where $\mathcal{M}_{12} = 1$ replaces the corresponding entry in the matrix $\mathcal{M}$ in (3.5). The spectrum of the resulting discrete eigenvalue problem is then computed numerically for $\tau = 0.01$, $L = 15$, and with $n = 250$. In Fig. 12(a) we show the unstable zigzag band for three exponent sets for which $\gamma = \frac{q}{p-1} = 1$. Recall that for $\gamma = 1$ the theory of §2.2 showed that there is no unstable zigzag band in the semi-strong interaction regime. Our computational results show that as D_0 is decreased towards the existence threshold D_{0c}, an unstable zigzag band first emerges at some critical value D_{0z} with $D_{0z} > D_{0c}$. Numerical values for D_{0z} are given in Table 2. Within the zigzag band there is a unique unstable real eigenvalue when $\tau = 0.01$. For three parameter sets, this eigenvalue is

plotted in Fig. 13(b) within an instability band. From §2.2 we recall that there is an unstable zigzag band in the semi-strong regime $D = O(1)$ when $\gamma = \frac{q}{p-1} > 1$. For the exponent set $(2, 2, 3, 3)$, where $\gamma = 2$, in Fig. 12(b) we show the continuation of this band into the weak interaction regime. For a domain length $L = 15$, or equivalently $\varepsilon_0 = 1/15$, we obtain from Fig. 12(b) that the zigzag band exists for $D_0 < D_{0z} \approx 107$. This value corresponds to $D = D_0\varepsilon_0^2 \approx 0.4755$, or equivalently $l = 1/\sqrt{D} = 1.45$. This critical value of l for $\gamma = 2$ agrees well with the critical value $l_z \approx 1.4$ obtained from Fig. 6 for when the zigzag band first forms in the semi-strong interaction regime.

We now qualitatively summarize our conclusions regarding the stability of the stripe. An important conclusion is that for the exponent sets (p, q, m, s) where the breakup instability disappears at some value above the existence threshold as D_0 is decreased, the stripe will always be unstable with respect to zigzag instabilities for domain widths d_0 that are $O(1)$ as $\varepsilon_0 \to 0$. Since the upper zigzag threshold m_{z+} satisfies $m_{z+} = O(\varepsilon_0^{-1})$, the zigzag instability can only be suppressed near the existence threshold D_{0c} by taking the domain width d_0 to be $O(\varepsilon_0)$ thin. We also observe from Fig. 13 that the time-scale for breakup instabilities is generally faster than for zigzag instabilities. However, both time-scales are independent of ε_0. By comparing Fig. 10(b) and Fig. 11 with Fig. 12, we observe that whenever a breakup instability band exists the breakup and zigzag bands overlap in such a way that there are no domain widths d_0 where a zigzag instability is not accompanied by a breakup instability.

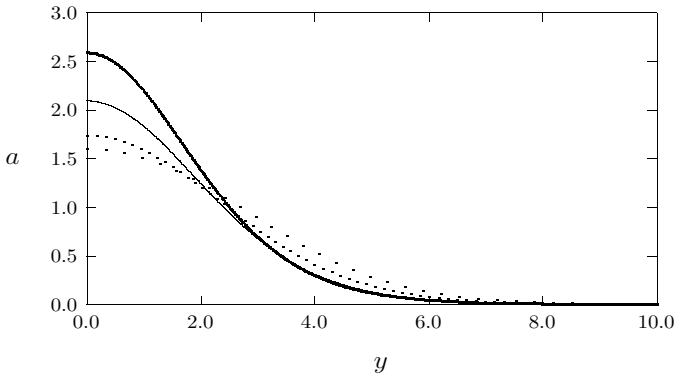

FIGURE 14. Plots of $a(y)$ for various D_0 computed from (3.1) for the exponent set $(2, 1, 2, 0)$. The heavy solid, solid, dotted, and widely-spaced dotted curves are for $D_0 = 19.6$, $D_0 = 11.9$, $D_0 = 7.9$, and $D_0 = 7.2$, respectively. Notice that the homoclinic becomes broader as D_0 is decreased.

Remark 3.1: It appears to be difficult to provide a rigorous study of the eigenvalue problem (3.3) to theoretically confirm the possible coalescence of the breakup instability band and the emergence of the zigzag band near the existence threshold D_{0c}. However, the shape of the homoclinic $a(y)$ near the existence threshold gives some indication on the reason for the change in the dominant instability mechanism. For D near D_{0c}, the region near the maximum of $a(y)$ is generally wider than it is for larger values of D_0. This is shown numerically in Fig. 14 for the exponent set $(2, 1, 2, 0)$. In fact, on the unstable branch, but near D_{0c}, the cross-section of the "fattened" homoclinic stripe develops a multi-bump structure at some value D_{0m} (see Table 2). In addition to the general pulse-splitting criteria of [**5**], this multi-bump structure also appears to be an essential factor for self-replication behavior (cf. [**14**]). Therefore, near the existence threshold, the cross-section of the homoclinic stripe becomes fatter in a similar way as was studied in §2.3 for the small-saturation GM model (2.23) in the semi-strong regime. This suggests that the stability problem near

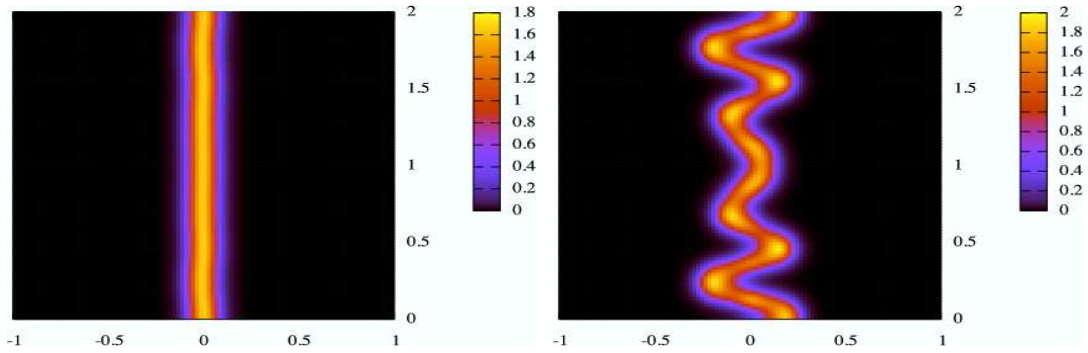

(a) Experiment 1: $t = 200$ (b) Experiment 1: $t = 300$

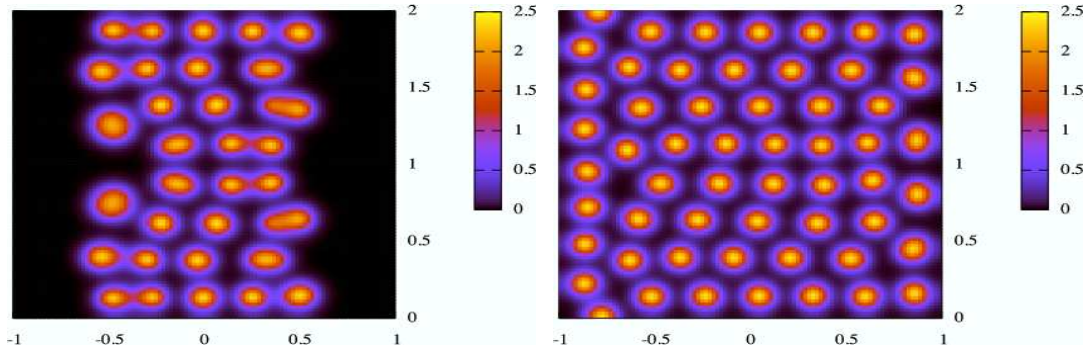

(c) Experiment 1: $t = 400$ (d) Experiment 1: $t = 1000$

FIGURE 15. **Experiment 1:** The numerical solution to (1.1) for $(p, q, r, s) = (2, 1, 2, 0)$ with $\varepsilon_0 = 0.025$, $D_0 = 7.6$, $\tau = 0.01$, and in a square domain $\Omega = [-1, 1] \times [0, 2]$. The initially straight stripe develops a zigzag instability. Spots are formed near the region of maximum curvature of the wriggled stripe. These spots then undergo a repeated self-replication process leading to a Turing-type pattern.

the existence threshold D_{0c} can be similar to that of a bistable system where zigzag instabilities are the dominant instability mechanism (cf. [**34**]) and where breakup instabilities do not occur. ■

We now perform a few numerical experiments on (1.1) to illustrate and validate the spectral results for breakup and zigzag instabilities. For each of the experiments below, we solve (1.1) for $\tau = 0.01$ in the square domain $\Omega = [-1, 1] \times [0, 2]$, with an initial condition of the form

$$a(x_1, x_2, 0) = A\text{sech}^2\left(\frac{x_1}{\varepsilon_0}\right), \qquad h(x_1, x_2, 0) = H\text{sech}^2\left(\frac{x_1}{2\varepsilon_0}\right). \tag{3.6}$$

Whenever the equilibrium stripe exists, in the experiments below we have taken $A = a(0)$ and $H = h(0)$ where a and h are the numerical solution of (3.1) for the specified value of D_0.

Experiments 1 and 2: In Experiment 1 we take $(p, q, r, s) = (2, 1, 2, 0)$, $\varepsilon_0 = 0.025$, and $D_0 = 7.6$. The initial condition for (1.1) is (3.6) with $A = 1.69$ and $H = 1.45$. Since $D_{0c} < D_0 < D_{0b}$ there is no breakup instability band, and we predict that the initially straight stripe will not break up into spots. From the heavy solid curve in Fig. 13(b) the most unstable zigzag mode is $\varepsilon_0 m \approx 0.315$ with a corresponding growth rate $\lambda_0 \approx 0.035$. Therefore, the number of zigzag crests is theoretically predicted to be $N = \frac{m}{\pi} = \frac{0.315}{\pi\varepsilon_0} \approx 4$. The full numerical results from

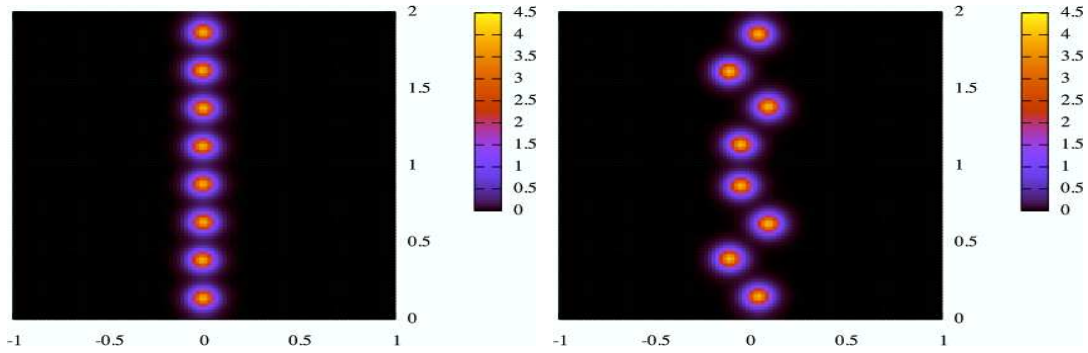

(a) Experiment 2: $t = 500$ (b) Experiment 2: $t = 800$

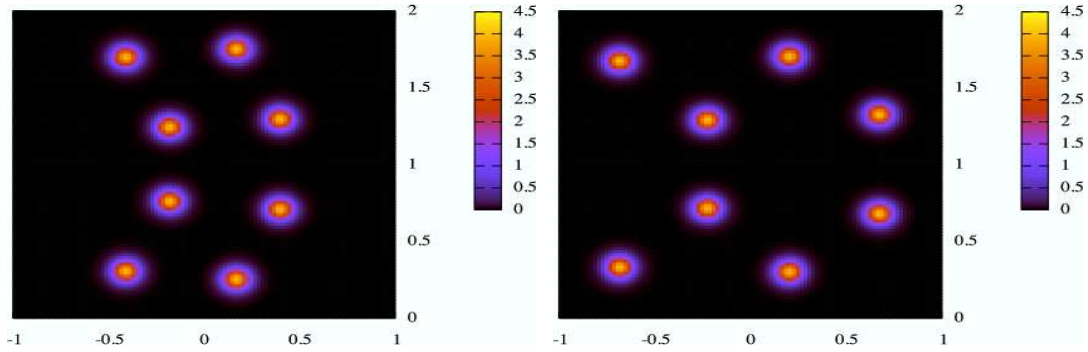

(c) Experiment 2: $t = 3000$ (d) Experiment 2: $t = 30000$

FIGURE 16. **Experiment 2:** The numerical solution to (1.1) for $(p, q, r, s) = (2, 1, 2, 0)$ with $\varepsilon_0 = 0.025$, $D_0 = 15.0$, $\tau = 0.01$, and in a square domain $\Omega = [-1, 1] \times [0, 2]$. The stripe initially breaks up into eight spots that are not in perfect vertical alignment owing to the zigzag instability of the initial stripe. There is no self-replication behavior and there is an exponentially slow, or metastable, evolution of the eight spots towards a stable equilibrium configuration consisting of a hexagonal structure.

(1.1) are shown in Fig. 15. We observe that, initially, there is indeed no breakup instability and that when $t = 300$ the stripe develops a noticeable zigzag instability with four crests. However, the wriggled stripe then undergoes a breakup instability near the points of its maximum curvature leading to spot formation. Since $D_0 = 7.6$ is below the existence threshold $D_{0s} = 9.82$ for a locally radially symmetric spot solution (see Table 2), these spots then undergo a repeated self-replication process which fill the entire domain. The solution at time $t = 1000$, shown in Fig. 15(d), is near an equilibrium state and more closely resembles a Turing-type pattern than a pattern with isolated spots.

In Experiment 2 we take $(p, q, r, s) = (2, 1, 2, 0)$, $\varepsilon_0 = 0.025$, and we increase D_0 to $D_0 = 15.0$. The initial condition for (1.1) is (3.6) with $A = 2.3$ and $H = 1.8$. Since $D_0 > D_{0b} = 8.06$ and $D_0 < D_{0z} = 24.0$ the initially straight stripe is unstable to a breakup and a zigzag instability. From the heavy solid curve in Fig. 13(a) the most unstable breakup mode is $\varepsilon_0 m \approx 0.623$ with a growth rate of $\lambda_0 \approx 0.186$. Therefore, the theoretically predicted number of spots is $N = \frac{m}{\pi} = \frac{0.623}{\pi\varepsilon_0} \approx 8$. From the full numerical results shown in Fig. 16(a) it is observed that the stripe initially breaks up into eight spots. The eight spots in Fig. 16(a) are not in perfect vertical alignment owing to the zigzag instability of the initial stripe. Then, as shown in Fig. 16(b), the repulsive spot interactions accentuate the broken vertical symmetry. Since $D_0 = 15$ is well above the spot-existence threshold of $D_{0s} = 9.82$ given in Table 2, there is

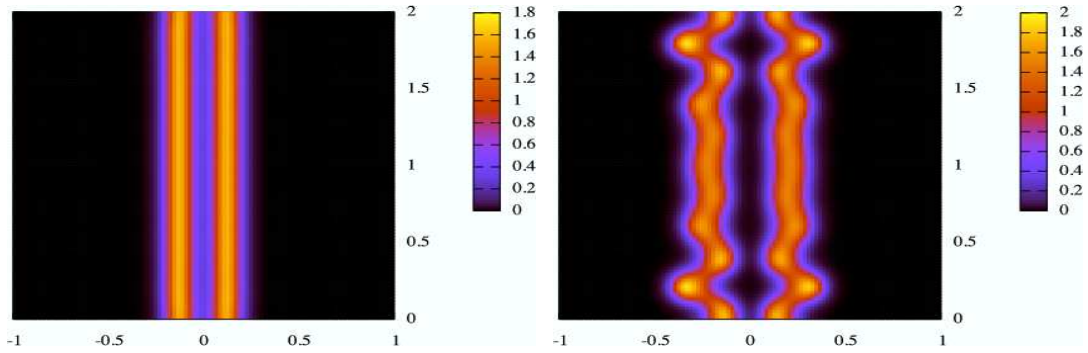

(a) Experiment 3: $t = 75$

(b) Experiment 3: $t = 175$

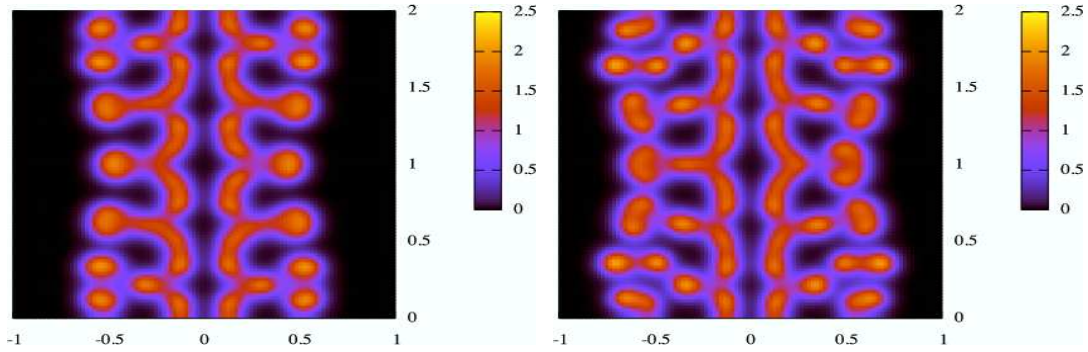

(c) Experiment 3: $t = 225$

(d) Experiment 3: $t = 250$

FIGURE 17. **Experiment 3:** The numerical solution to (1.1) for $(p, q, r, s) = (2, 1, 2, 0)$ with $\varepsilon_0 = 0.025$, $D_0 = 6.8$, $\tau = 0.01$, and in a square domain $\Omega = [-1, 1] \times [0, 2]$. Since $D_0 < D_{0c}$, the initially straight stripe splits into two. The two stripes become wriggled as a result of a zigzag instability. Spots are formed near the region of maximum curvature of the wriggled stripes. These spots then undergo a self-replication process.

no spot self-replication behavior. Instead there is an exponentially slow, or metastable, drift of the spots towards a stable hexagonal equilibrium configuration (cf. Fig. 16(c) and Fig. 16(d)).

Experiment 3: Next, we take $(p, q, r, s) = (2, 1, 2, 0)$, $\varepsilon_0 = 0.025$, and $D_0 = 6.8$. The initial condition for (1.1) is (3.6) with $A = 1.6$ and $H = 1.4$. Since $D_0 < D_{0c}$, there is no equilibrium stripe solution. For the related problem of a pulse on a one-dimensional interval with $D_0 < D_{0c}$, an initial one-pulse profile undergoes a edge-splitting pulse-replication process leading to a Turing-type pattern (cf. [**4**], [**14**], Remark 6.2 of [**25**]). The numerical results for the two-dimensional GM model are shown in Fig. 17. We observe that the stripe first splits into two and then develops a zigzag instability. The wriggled stripes undergo a breakup instability near their points of maximal curvature. Since $D_0 < D_{0s}$ the emerging spots then undergo a spot-splitting process. For short times, stripe-replication behavior was computed in Fig. 5.3 of [**4**] for $D_0 = 1/(.14) \approx 7.14$ before any zigzag instabilities occur.

Experiment 4: We now take $(p, q, r, s) = (3, 2, 2, 0)$, $\varepsilon_0 = 0.025$, and $D_0 = 4.5$. The initial condition for (1.1) is (3.6) with $A = 1.82$ and $H = 0.74$. For this exponent set, in addition to the zigzag instability, a breakup instability is guaranteed since the breakup band does not terminate in the weak interaction regime. From the dashed curve in Fig. 13(a) the most unstable breakup mode is $\varepsilon_0 m \approx 0.96$ with a growth rate of $\lambda_0 \approx 0.147$. With this most

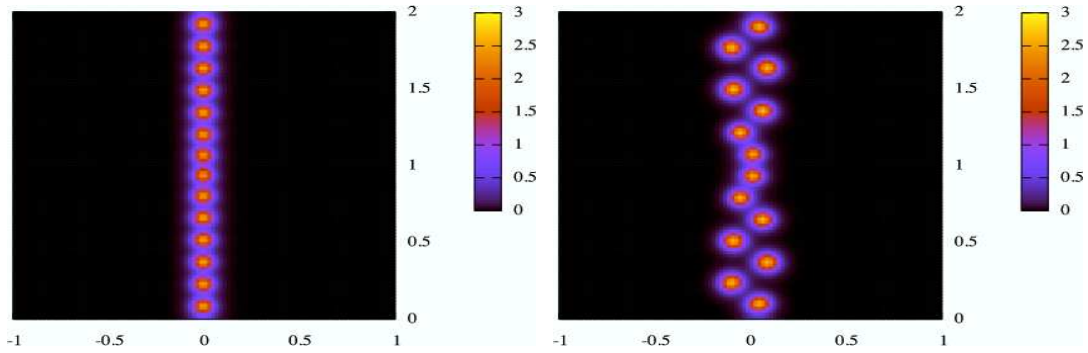

(a) Experiment 4: $t = 100$ (b) Experiment 4: $t = 200$

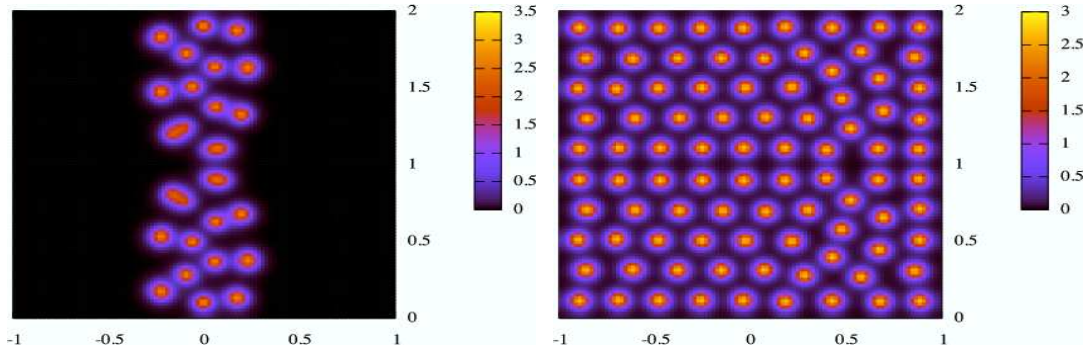

(c) Experiment 4: $t = 250$ (d) Experiment 4: $t = 1000$

FIGURE 18. **Experiment 4:** The numerical solution to (1.1) for $(p, q, r, s) = (3, 2, 2, 0)$ with $\varepsilon_0 = 0.025$, $D_0 = 4.5$, $\tau = 0.01$, and in a square domain $\Omega = [-1, 1] \times [0, 2]$. Since the breakup instability band exists up to D_{0c}, the initially straight stripe breaks up into spots. It then develops a twist as a result of a zigzag instability. Since $D_0 < D_{0s} = 5.23$, the spots then undergo a repeated self-replication process leading to a Turing-type pattern.

unstable mode, we predict that the stripe will break up into $N = \frac{m}{\pi} = \frac{0.96}{\pi\varepsilon_0} \approx 12$ spots. Alternatively, from the solid curve in Fig. 13(b), the most unstable zigzag mode is $\varepsilon_0 m \approx 0.43$ with a corresponding growth rate $\lambda_0 \approx 0.051$. This corresponds to a most unstable zigzag mode with $N = \frac{m}{\pi} = \frac{0.43}{\pi\varepsilon_0} \approx 5$ crests. In the numerical results shown in Fig. 18 we observe that the initially straight stripe breaks up into fourteen spots (see Fig. 18(a)) and then develops a zigzag instability with six crests, which breaks the vertical symmetry of the array of spots (see Fig. 18(b)). Since $D_0 < D_{0s} = 5.23$ the resulting spots then undergo a spot-splitting process (cf. Fig. 18(c)) leading to a final state that closely resembles a Turing-type pattern (cf. Fig. 18(d)).

Experiment 5: Finally, we consider $(p, q, r, s) = (2, 1, 3, 0)$, $\varepsilon_0 = 0.01$, and $D_0 = 14.0$. The initial condition for (1.1) is (3.6) with $A = 1.6$ and $H = 1.3$. For this exponent set there are no breakup instabilities on the rather wide range $10.35 < D_0 < 19.14$ (see Table 2). Therefore, we expect no breakup instability. From the dashed curve in Fig. 13(b) the most unstable zigzag mode is $\varepsilon_0 m \approx 0.23$, with a corresponding growth rate $\lambda_0 \approx 0.0131$, and the expected number of zigzag crests is $N = \frac{m}{\pi} = \frac{0.23}{\pi\varepsilon_0} \approx 7$. In the numerical results shown in Fig. 19(b) a zigzag instability with exactly seven crests is observed. In contrast to Experiment 1 where D_0 was only slightly below the breakup threshold D_{0b}, for this example D_0 is significantly below the breakup threshold and the wriggled stripe in

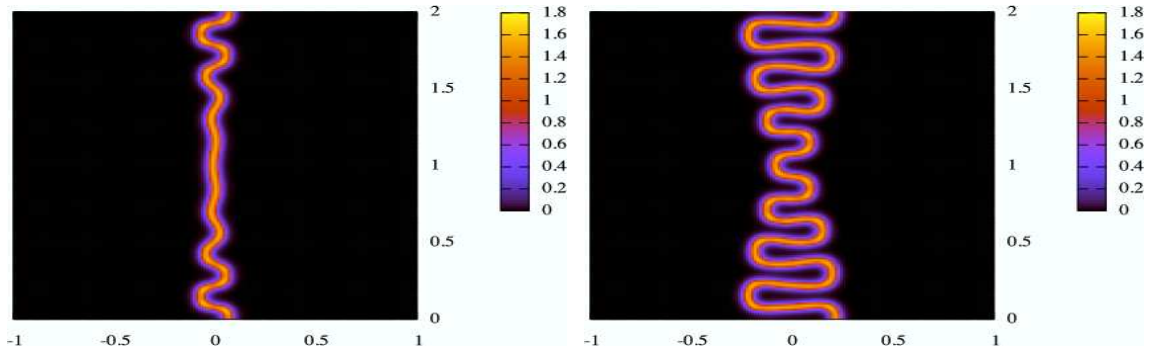

(a) Experiment 5: $t = 1400$

(b) Experiment 5: $t = 1600$

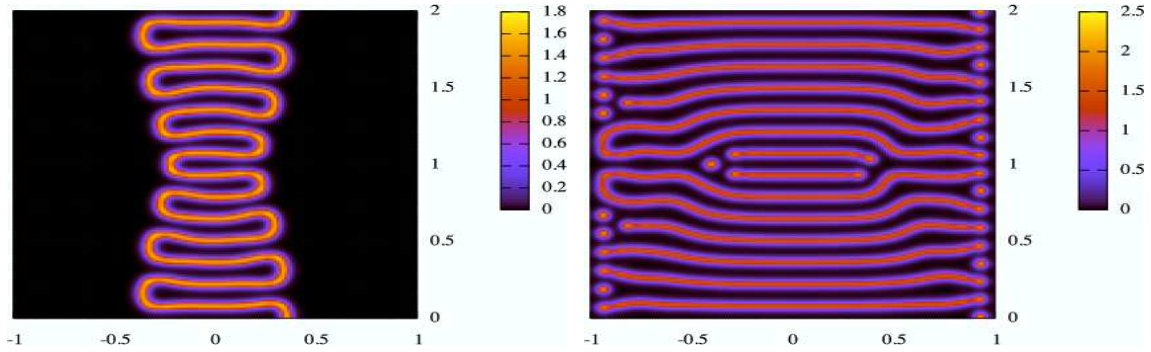

(c) Experiment 5: $t = 1800$

(d) Experiment 5: $t = 4300$

FIGURE 19. **Experiment 5:** The numerical solution to (1.1) for $(p, q, r, s) = (2, 1, 3, 0)$ with $\varepsilon_0 = 0.01$, $D_0 = 14.0$, $\tau = 0.01$, and in a square domain $\Omega = [-1, 1] \times [0, 2]$. There is no breakup instability of the straight stripe and the wriggled stripe is less vulnerable than in Experiment 1 to a breakup instability occurring near local maxima of the curvature. The zigzag instability of the straight stripe is seen to be the precursor to a large-scale deformation of the stripe.

Fig. 19 is less vulnerable than in Experiment 1 (see Fig. 15) to a breakup instability occurring near a local maxima of its curvature. The final pattern in Fig. 19(d) is composed almost exclusively of stripes.

4 The GM Model with Saturation: A Mesa-Stripe Solution in the Near-Shadow Limit

For the modified GM model (1.6) with saturation parameter κ, we now construct a different type of equilibrium stripe solution centered along the mid-line of the rectangular domain $\Omega := [0, 1] \times [0, d_0]$, with $\partial_n a = \partial_n h = 0$ on $\partial\Omega$. In §5 we analyze the stability of this solution. For our analysis of (1.6) we assume that $\varepsilon_0 \ll 1$ and $\kappa > 0$, where κ is independent of ε_0. Recall that the case $\kappa = O(\varepsilon_0^2)$ was considered in §2.3.

Our analysis is limited to a near-shadow limit $D \gg 1$ where $D = \mathcal{D}/\varepsilon_0$ with $\mathcal{D} = O(1)$. A similar restriction was made in [**35**] in their study of interface stability for a generalized Fitzhugh-Nagumo system. The analysis of mesa-stripes in the regime $D = O(1)$ is not a straightforward extension of the analysis for the near-shadow limit $D = O(\varepsilon^{-1})$. For $D = O(1)$ a new phenomenon related to the self-replication of mesa-stripes can occur. This behavior is shown in Experiment 3 below. Since a detailed study of mesa-splitting for the regime $D = O(1)$ is expected to be

rather involved, and is not related to the goal of this paper of characterizing breakup and zigzag instabilities of a stripe, we do not attempt to study the regime $D = O(1)$ here.

In the near-shadow limit, (1.6) admits an equilibrium stripe solution in the form of a front-back transition layer structure, where the layers are connected by an asymptotically flat plateau. We refer to such a solution as a mesa-stripe. This type of solution is distinctly different from the homoclinic stripe solutions of §2 and §3. Since $D \gg O(1)$, then $h \sim \mathcal{H}$ uniformly on $0 \le x_1 \le 1$, where $\mathcal{H}$ is a constant. Therefore, from the inhibitor equation of (1.6), we get

$$\mathcal{H} \sim \int_0^1 a^2 \, dx_1 \, . \tag{4.1}$$

The transition layer solution centered at some $x_1 = \xi_l$ is given by $a \sim \mathcal{H} w(y)$, with $y = \varepsilon_0^{-1}(x_1 - \xi_l)$. From (1.6) we obtain that w satisfies (2.24) with $b = \kappa \mathcal{H}^2$. It was shown in §2.3 that (2.24) has a heteroclinic orbit connecting $w = 0$ and $w = w_+$ when $b = b_0$. Here w_+ and b_0 are given in (2.27). For $b = b_0$, the heteroclinic solution to (2.24) satisfies

$$w'' - w + g_0(w) = 0 \, , \quad -\infty < y < \infty \, ; \quad g_0(w) \equiv \frac{w^2}{1 + b_0 w^2} \, , \quad b_0 = \kappa \mathcal{H}^2 \, , \tag{4.2 a}$$

$$w(y) \sim c_- \exp(y) \, , \quad y \to -\infty \, ; \quad w(y) \sim w_+ - c_+ \exp(-\nu_+ y) \, , \quad y \to +\infty \, , \quad \nu_+ \equiv \sqrt{1 - \frac{2}{w_+}} \, , \tag{4.2 b}$$

for some positive constants $c_\pm$. To break the translation invariance we impose the condition $w(0) = w_+/2$. For the stability analysis in §5, we must evaluate $\beta \equiv \int_{-\infty}^{\infty} (w')^2 \, dy$. A simple calculation gives

$$\beta \equiv \int_{-\infty}^{\infty} (w')^2 \, dy = \int_0^{w_+} \sqrt{2\mathcal{F}(w)} \, dw \approx 1.49882 \, , \qquad \mathcal{F}(w) \equiv \frac{w^2}{2} - \frac{w}{b_0} + \frac{1}{b_0^{3/2}} \tan^{-1}\left(w \sqrt{b_0} \right) \, . \tag{4.3}$$

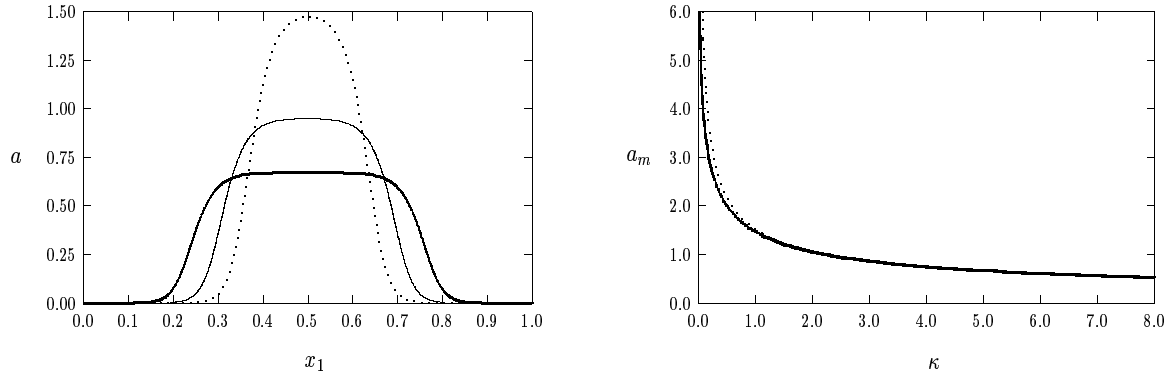

(a) a_e versus x (b) $a_m \equiv a_e\,(1/2)$ versus κ

FIGURE 20. Left figure: the numerically computed equilibrium solution a_e versus x for $\varepsilon_0 = 0.02$ and $D = 10$ when $\kappa = 1$ (dashed curve), $\kappa = 2.5$ (solid curve), and $\kappa = 5.0$ (heavy solid curve). The length L of the plateau increases with increasing κ. Right figure: comparison of the asymptotic plateau value $a_m \equiv a_e\,(1/2) \sim \mathcal{H} w_+$ (dashed curve) versus κ with the corresponding full numerical result for $a_e\,(1/2)$ (heavy solid curve).

For $b = b_0$ and $\varepsilon_0 \ll 1$, a composite expansion for the mesa-stripe solution has the form

$$a \sim \mathcal{H}\left[w_l(y_l) + w_r(y_r) - w_+ \right] \, ; \qquad w_l(y_l) \equiv w\left[\varepsilon_0^{-1}(x_1 - \xi_l) \right] \, , \qquad w_r(y_r) \equiv w\left[\varepsilon_0^{-1}(\xi_r - x_1) \right] \, . \tag{4.4}$$

By using (4.1) and (4.4) , we obtain that $\mathcal{H} \sim \mathcal{H}^2 w_+^2 L + O(\varepsilon_0)$, where $L = \xi_r - \xi_l$. Then, from the relation $b = \mathcal{H}^2\kappa$ of (4.2 *a*), we obtain that

$$\mathcal{H} \sim \frac{1}{w_+^2 L} + O(\varepsilon_0)\,, \qquad L \sim \frac{\sqrt{\kappa}}{\sqrt{b_0}\, w_+^2} < 1\,. \tag{4.5}$$

In Fig. 20(a) we plot the numerically computed equilibrium solution a_e versus x for several values of κ when $\varepsilon_0 = 0.02$ and $D = 10$. This solution was computed using COLSYS [**2**]. Notice that as κ increases the maximum value of a_e decreases while the spatial extent of the plateau also increases. For a range of κ, in Fig. 20(b) we show a very favorable comparison between the numerically computed value for the plateau height $a_e(1/2)$ and the corresponding asymptotic result $a_e(1/2) \sim \mathcal{H} w_+ = (w_+ L)^{-1}$. As a remark, the analysis of homoclinic solutions in §2 showed that $a_e\,(1/2) = O(\varepsilon_0^{-1})$ when $\kappa = 0$. In Fig. 21 we plot the relation (4.5) between the saturation parameter κ and the plateau length L. The condition $L < 1$ ensures that the plateau fits within the unit length of the rectangle. Although ξ_l and ξ_r are undetermined at this stage, we anticipate by symmetry that the plateau is centered in the middle of the interval $[0, 1]$ so that $\xi_l = (1 - L)/2 = (1 - \xi_r)$. This result is derived analytically below.

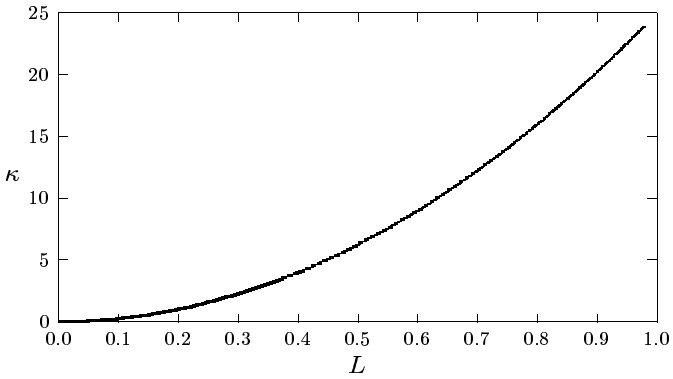

FIGURE 21. The length L of the plateau of the mesa versus the saturation parameter κ of the activator kinetics.

Although (4.4) and (4.5) give the leading-order solution, a higher-order construction of the equilibrium solution is required for the stability analysis of §5. To do so we first consider the outer regions, comprised of the plateau region $\xi_l < x_1 < \xi_r$ together with near-boundary regions $0 < x_1 < \xi_l$ and $\xi_r < x_1 < 1$. In these outer regions we expand

$$h \sim \mathcal{H} + \varepsilon_0 h_1 + \varepsilon_0^2 h_2 + \cdots\,. \tag{4.6}$$

In the near boundary regions a is exponentially small as $\varepsilon_0 \to 0$, while in the plateau region $a \sim \mathcal{H} w_+ + O(\varepsilon_0)$. Therefore, by substituting (4.6) into the inhibitor equation of (1.6) with $D = \mathcal{D}/\varepsilon_0$, we obtain that

$$\mathcal{D} h_{1x_1x_1} = \begin{cases} \mathcal{H}\,, & 0 < x_1 < \xi_l\,, \\ \mathcal{H} - \mathcal{H}^2 w_+^2\,, & \xi_l < x_1 < \xi_r\,, \\ \mathcal{H}\,, & \xi_r < x_1 < 1\,, \end{cases} \tag{4.7}$$

with $h_{1x_1}(0) = h_{1x_1}(1) = 0$. The conditions for h_1 at the transition layers ξ_l and ξ_r are found below upon matching h_1 to appropriate inner solutions. In the plateau region we expand a as

$$a \sim \mathcal{H} w_+ + \varepsilon_0 \mathcal{A}_1 + \cdots\,, \qquad \xi_l < x_1 < \xi_r\,. \tag{4.8}$$

By substituting (4.8) into the activator equation of (1.6), we obtain that $\mathcal{A}_1$ satisfies

$$\mathcal{A}_1 = g_a\left(\mathcal{H}w_+, \mathcal{H}\right)\mathcal{A}_1 + g_h\left(\mathcal{H}w_+, \mathcal{H}\right)h_1\,, \qquad \xi_l < x_1 < \xi_r\,. \tag{4.9}$$

By using $g_a(\mathcal{H}w_+, \mathcal{H}) = 2/w_+$ and $g_h(\mathcal{H}w_+, \mathcal{H}) = -w_+$, we calculate $\mathcal{A}_1$ from (4.9) as

$$\mathcal{A}_1 = \frac{w_+^2 h_1}{2 - w_+}\,. \tag{4.10}$$

In the inner region near $x_1 = \xi_l$, we let $y = \varepsilon_0^{-1}(x_1 - \xi_l)$, and we expand $a(y)$ and $h(y)$ as

$$a = a_0 + \varepsilon_0 a_1 + \varepsilon_0^2 a_2 + \cdots\,, \qquad h = \mathcal{H} + \varepsilon_0\mathcal{H}_1 + \varepsilon_0^2\mathcal{H}_2 + \cdots\,. \tag{4.11}$$

Upon substituting (4.11) into the equilibrium problem for (1.6), and letting $D = \mathcal{D}/\varepsilon_0$, we obtain that $a_0 = \mathcal{H}w$ and that a_1 satisfies

$$La_1 \equiv a_1^{''} - a_1 + g_0^{'}(w)a_1 = g_0(w)\mathcal{H}_1\,, \qquad \mathcal{H}_1^{''} = 0\,, \qquad -\infty < y < \infty\,. \tag{4.12}$$

Here $g_0(w)$ is defined in (4.2 *a*). This yields that $\mathcal{H}_1 = \mathcal{H}_{10} + y\mathcal{H}_{11}$, for some unknown constants $\mathcal{H}_{10}$ and $\mathcal{H}_{11}$. However, since $h = \mathcal{H} + O(\varepsilon_0)$ in the plateau and near-boundary regions, we require that $\mathcal{H}_{11} = 0$ in order to match the inner and outer solutions for h. Therefore, $\mathcal{H}_1 = \mathcal{H}_{10}$. To determine $\mathcal{H}_{10}$ we use a solvability condition. Since $Lw^{'} = 0$, the solvability condition for (4.12) gives $\mathcal{H}_{10}\int_{-\infty}^{\infty} g_0(w)w^{'}\,dy = 0$, which yields $\mathcal{H}_{10} = 0$. Therefore, since $La_1 = 0$ we get $a_1 = c_1 w^{'}$ for some constant c_1. However, since $a(0) = \mathcal{H}w_+/2$ defines the transition layer location, we require that $a_1(0) = 0$. Since $w^{'}(0) \neq 0$, this implies that $c_1 = 0$. Therefore, $a_1 = \mathcal{H}_1 \equiv 0$, and we must proceed to the next order in ε_0 to find the first non-vanishing correction term.

Upon substituting (4.11) into (1.6), we obtain that a_2 and $\mathcal{H}_2$ satisfy

$$La_2 \equiv a_2^{''} - a_2 + g_0^{'}(w)a_2 = g_0(w)\mathcal{H}_2\,, \qquad \mathcal{H}_2^{''} = 0\,, \qquad -\infty < y < \infty\,. \tag{4.13}$$

Therefore, $\mathcal{H}_2 = \mathcal{H}_{20} + \mathcal{H}_{21}y$ for some constants $\mathcal{H}_{20}$ and $\mathcal{H}_{21}$. The solvability condition for (4.13) gives one relation between these two constants in the form

$$\int_{-\infty}^{\infty}\left(\mathcal{H}_{20} + y\mathcal{H}_{21}\right)g_0(w)w^{'}\,dy = 0\,. \tag{4.14}$$

The other relationship between these constants is determined from the matching condition that $h \sim \mathcal{H} + \varepsilon_0^2\mathcal{H}_2 + \cdots$ agrees asymptotically as $y \to \pm\infty$ with the behavior of the outer solution $h \sim \mathcal{H} + \varepsilon_0 h_1(x_1) + \varepsilon_0^2 h_2(x_1) + \cdots$ as $x \to \xi_l^{\pm}$. This matching condition readily yields that

$$h_1(\xi_l^{\pm}) = 0\,, \qquad \mathcal{H}_{21} = h_{1x_1}(\xi_l^{-}) = h_{1x_1}(\xi_l^{+})\,, \tag{4.15}$$

and $h_2(\xi_l^{\pm}) = \mathcal{H}_{20}$. The condition $h_{1x_1}(\xi_l^{-}) = h_{1x_1}(\xi_l^{+})$ is found below to determine the equilibrium transition layer location ξ_l uniquely as $\xi_l = (1 - L)/2$. The conditions (4.15) and (4.14) determine $\mathcal{H}_{20}$ and $\mathcal{H}_{21}$ uniquely.

Finally, we derive a key identity needed in §5. We differentiate (4.13) with respect to y to obtain

$$La_2^{'} = -g_0^{''}(w)w^{'}a_2 + g_0(w)\mathcal{H}_2^{'} + g_0^{'}(w)\mathcal{H}_2 w^{'}\,. \tag{4.16}$$

Since $Lw^{'} = 0$, the solvability condition for (4.16) yields the identity

$$-\mathcal{H}_2^{'}\int_{-\infty}^{\infty} g_0(w)w^{'}\,dy = \int_{-\infty}^{\infty}\left[g_0^{'}(w)\mathcal{H}_2 - g_0^{''}(w)a_2\right](w^{'})^2\,dy\,, \tag{4.17}$$

where $\mathcal{H}_2^{'} = h_{1x_1}(\xi_l^{+})$ by the matching condition (4.15).

A similar analysis can be done near the other transition layer at $x_1 = \xi_r$ to obtain that $h_1(\xi_r^{\pm}) = 0$. By solving (4.7) with $h_{1x_1}(0) = h_{1x_1}(1) = 0$ and $h_1(\xi_l^{\pm}) = h_1(\xi_r^{\pm}) = 0$, we obtain that

$$h_1 = \begin{cases} \frac{1}{2\mathcal{D}w_+^2 L}\left(x_1^2 - \xi_l^2\right), & 0 < x_1 < \xi_l\,, \\ \frac{\mathcal{H}(L-1)}{2\mathcal{D}L}\left[(x_1-\xi_l)^2 - (\xi_r-\xi_l)(x_1-\xi_l)\right], & \xi_l < x_1 < \xi_r\,, \\ \frac{1}{2\mathcal{D}w_+^2 L}\left[(1-x_1)^2 - (1-\xi_r)^2\right], & \xi_r < x_1 < 1\,. \end{cases} \tag{4.18}$$

From this solution, we calculate the following one-sided derivatives, which are also needed in §5 below:

$$h_{1x_1}(\xi_l^+) = \frac{\mathcal{H}(1-L)}{2\mathcal{D}} = -h_{1x_1}(\xi_r^-)\,, \qquad h_{1x_1}(\xi_l^-) = \frac{\mathcal{H}\xi_l}{\mathcal{D}}\,, \qquad h_{1x_1}(\xi_r^+) = -\frac{\mathcal{H}(1-\xi_r)}{\mathcal{D}}\,. \tag{4.19}$$

The condition that h_{1x_1} is continuous across $x_1 = \xi_l$ and $x_1 = \xi_r$ determines the equilibrium layer locations uniquely in terms of the length L of the plateau as $\xi_l = (1-L)/2$ and $1 - \xi_r = (1-L)/2$.

5 The GM Model with Saturation: Stability Analysis in the Near-Shadow Limit

We now study the stability of the mesa-stripe equilibrium solution $a_e(x_1)$, $h_e(x_1)$ constructed in §4. Since there are Neumann boundary conditions on the sides $x_2 = 0, d_0$ of the rectangular domain, the perturbation takes the form

$$a = a_e + e^{\lambda t + imx_2}\phi\,, \qquad h = h_e + e^{\lambda t + imx_2}\psi\,, \qquad m = \frac{k\pi}{d_0}\,, \quad k = 1, 2, \ldots\,, \tag{5.1}$$

where $\phi = \phi(x_1) \ll 1$ and $\psi = \psi(x_1) \ll 1$. The bands of instability with respect to the continuous variable m derived below can be mapped to integer k-bands of instability using (5.1).

Substituting (5.1) into (1.6), and using $D = \mathcal{D}/\varepsilon_0$ we obtain the eigenvalue problem

$$L_\varepsilon\phi + g_h(a_e, h_e)\psi = \bar{\lambda}\phi\,, \quad 0 < x_1 < 1\,; \qquad \phi_{x_1}(0) = \phi_{x_1}(1) = 0\,, \tag{5.2 a}$$

$$\psi_{x_1x_1} - m^2\psi = \frac{\varepsilon_0}{\mathcal{D}}(1+\tau\lambda)\psi - \frac{2\varepsilon_0}{\mathcal{D}}a_e\phi\,, \quad 0 < x_1 < 1\,; \qquad \psi_{x_1}(0) = \psi_{x_1}(1) = 0\,. \tag{5.2 b}$$

Here $\bar{\lambda}$ and the operator L_ε are defined by

$$L_\varepsilon\phi \equiv \varepsilon_0^2\phi_{x_1x_1} - \phi + g_a(a_e, h_e)\phi\,, \qquad \bar{\lambda} \equiv \lambda + \varepsilon_0^2 m^2\,. \tag{5.2 c}$$

In the analysis below we will show that $\lambda = O(\varepsilon_0^2)$ when $m > 0$ and $m = O(1)$. Therefore, for $\varepsilon_0 \ll 1$, the term $\tau\lambda$ in (5.2 *b*) is asymptotically negligible when $\tau = O(1)$ and is consequently neglected.

We first determine the asymptotic form of the eigenfunction ϕ corresponding to $\bar{\lambda} \ll 1$. In the plateau region, where $a_e \sim \mathcal{H}w_+$, $g_a(a_e, h_e) \sim 2w_+^{-1}$ and $g_h(a_e, h_e) \sim -w_+$, we obtain from (5.2 *a*) that

$$\phi \sim \mu\psi\,, \qquad \mu \equiv \frac{w_+^2}{2 - w_+}\,, \qquad \xi_l < x_1 < \xi_r\,. \tag{5.3}$$

In the near-boundary regions ϕ is exponentially small as $\varepsilon_0 \to 0$. Near the transition layers at ξ_l and ξ_r, ϕ is proportional to the derivative w' of the heteroclinic orbit. Therefore, this motivates the asymptotic form

$$\phi \sim \begin{cases} c_l\left(w'(y_l) + O(\varepsilon_0) + \cdots\right), & y_l \equiv \varepsilon_0^{-1}(x_1 - \xi_l) = O(1)\,, \\ \phi_i \equiv \mu\psi\,, & \xi_l < x_1 < \xi_r\,, \\ c_r\left(w'(y_r) + O(\varepsilon_0) + \cdots\right), & y_r \equiv \varepsilon_0^{-1}(\xi_r - x_1) = O(1)\,, \end{cases} \tag{5.4}$$

for some unknown constants c_l and c_r to be found. Here μ is defined in (5.3).

Since ϕ is localized near the transition layers, we use (5.4) to calculate in the sense of distributions that

$$\frac{2\varepsilon_0 a_e \phi}{\mathcal{D}} \sim \frac{\varepsilon_0^2 \mathcal{H} w_+^2}{\mathcal{D}} \left[c_l \delta(x_1 - \xi_l) + c_r \delta(x_1 - \xi_r)\right] + \left(\frac{2\varepsilon_0}{\mathcal{D}}\right) \mathcal{H} w_+ \mu \psi \chi_{[\xi_l, \xi_r]}\,, \tag{5.5}$$

where $\mathcal{H} \sim 1/(w_+^2 L)$. Here $\chi_{[\xi_l,\xi_r]}$ is the indicator function defined to be unity for $\xi_l \le x_1 \le \xi_r$ and zero outside this plateau region. Substituting (5.5) into (5.2 b), we obtain that ψ satisfies

$$\psi_{x_1 x_1} - \theta^2 \psi = -\frac{\varepsilon_0^2 \mathcal{H} w_+^2}{\mathcal{D}} \left[c_r \delta(x_1 - \xi_r) + c_l \delta(x_1 - \xi_l)\right]\,, \quad 0 < x_1 < 1\,; \qquad \psi_{x_1}(0) = \psi_{x_1}(1) = 0\,. \tag{5.6 a}$$

Here θ is the piecewise constant function

$$\theta = \begin{cases} \theta_- \equiv \left[m^2 + \frac{\varepsilon_0}{\mathcal{D}}\right]^{1/2}\,, & 0 < x_1 < \xi_l\,, \quad \xi_r < x_1 < 1\,, \\ \theta_+ \equiv \left[m^2 + \frac{\varepsilon_0}{\mathcal{D}}\left(1 + \frac{2w_+}{L(w_+ - 2)}\right)\right]^{1/2}\,, & \xi_l < x_1 < \xi_r\,. \end{cases} \tag{5.6 b}$$

The jump conditions for (5.6) are that

$$\psi_{x_1}(x_l^+) - \psi_{x_1}(x_l^-) = -\frac{\varepsilon_0^2 \mathcal{H} w_+^2 c_l}{\mathcal{D}}\,, \qquad \psi_{x_1}(x_r^+) - \psi_{x_1}(x_r^-) = -\frac{\varepsilon_0^2 \mathcal{H} w_+^2 c_r}{\mathcal{D}}\,. \tag{5.6 c}$$

Next, we derive a matrix eigenvalue problem for $\bar{\lambda}$. We substitute (5.4) into (5.2 a) and multiply the resulting expression by w_l', where $w_l' \equiv w'(y_l)$. Since w_l' is localized, we then obtain for $\varepsilon_0 \ll 1$ that

$$c_l \left(w_l', L_\varepsilon w_l'\right) + \left(w_l', g_h(a_e, h_e)\psi\right) \sim c_l \bar{\lambda} \left(w_l', w_l'\right)\,. \tag{5.7}$$

Here we have defined $(f, g) \equiv \int_0^1 f g \, dx_1$. We use (4.2) to estimate the second and third terms in (5.7) as

$$\left(w_l', g_h(a_e, h_e)\psi\right) \sim -\varepsilon_0 \psi(\xi_l) \int_{-\infty}^{\infty} w' g_0(w)\, dy = -\varepsilon_0 \psi(\xi_l) \int_{-\infty}^{\infty} (w - w'') w'\, dy = -\varepsilon_0 \psi(\xi_l) \frac{w_+^2}{2}\,, \tag{5.8 a}$$

$$\left(w_l', w_l'\right) \sim \varepsilon_0 \int_{-\infty}^{\infty} (w')^2\, dy = \varepsilon_0 \beta\,, \qquad \beta \equiv \int_{-\infty}^{\infty} (w')^2\, dy\,. \tag{5.8 b}$$

To calculate the first term in (5.7) we first use the inner solution $a_e \sim \mathcal{H} w + \varepsilon_0^2 a_2$ and $h_e \sim \mathcal{H} + \varepsilon_0^2 \mathcal{H}_2$, to obtain

$$g_a(a_e, h_e) \sim g_a\left(\mathcal{H} w, \mathcal{H}\right) + \varepsilon_0^2 \left[g_{aa}\left(\mathcal{H} w, \mathcal{H}\right) a_2 + g_{ah}\left(\mathcal{H} w, \mathcal{H}\right) \mathcal{H}_2\right] + \cdots\,, \tag{5.9 a}$$

$$g_a(a_e, h_e) \sim g_0'(w) + \frac{\varepsilon_0^2}{\mathcal{H}} \left[g_0''(w) a_2 - g_0'(w) \mathcal{H}_2\right] + \cdots\,. \tag{5.9 b}$$

By using (5.9 b), and upon differentiating (4.2) with respect to y, we readily obtain that

$$L_\varepsilon w' \sim \frac{\varepsilon_0^2}{\mathcal{H}} \left[g_0''(w) a_2 - g_0'(w) \mathcal{H}_2\right] w'\,. \tag{5.10}$$

Then, using (5.10) and the identity (4.17), we derive that

$$\left(w_l', L_\varepsilon w_l'\right) \sim \frac{\varepsilon_0^3}{\mathcal{H}} \int_{-\infty}^{\infty} \left[g_0''(w) a_2 - g_0'(w) \mathcal{H}_2\right] (w')^2\, dy = \frac{\varepsilon_0^3 \mathcal{H}_2'}{\mathcal{H}} \int_{-\infty}^{\infty} g_0(w) w'\, dy\,, \tag{5.11 a}$$

$$\sim \frac{\varepsilon_0^3 \mathcal{H}_2'}{\mathcal{H}} \int_{-\infty}^{\infty} (w - w'') w'\, dy = \frac{\varepsilon_0^3 \mathcal{H}_2' w_+^2}{2\mathcal{H}} = \frac{\varepsilon_0^3 h_{1x_1}(\xi_l^+) w_+^2}{2\mathcal{H}}\,. \tag{5.11 b}$$

Finally, upon substituting (5.8) and (5.11 b) into (5.7) we obtain that

$$\bar{\lambda} \varepsilon_0 c_l \beta \sim \frac{\varepsilon_0^3 c_l}{2\mathcal{H}} h_{1x_1}(\xi_l^+) w_+^2 - \frac{\varepsilon_0}{2} \psi(\xi_l) w_+^2\,. \tag{5.12 a}$$

In a similar way, we obtain from the transition layer solution at $x_1 = \xi_r$ that

$$\bar{\lambda}\varepsilon_0 c_r \beta \sim -\frac{\varepsilon_0^3 c_r}{2\mathcal{H}} h_{1x_1}(\xi_r^-) w_+^2 - \frac{\varepsilon_0}{2}\psi(\xi_r) w_+^2 \,. \tag{5.12 b}$$

The next step in the analysis is to reduce (5.12) to an explicit matrix eigenvalue problem. To do so, we first solve (5.6) for ψ in order to calculate $\psi(\xi_l)$ and $\psi(\xi_r)$. A simple calculation shows that

$$\begin{pmatrix} \psi(\xi_l) \\ \psi(\xi_r) \end{pmatrix} = \frac{\varepsilon_0^2 \mathcal{H} w_+^2}{\mathcal{D}} \mathcal{G}\boldsymbol{c}\,, \qquad \boldsymbol{c} \equiv \begin{pmatrix} c_l \\ c_r \end{pmatrix}, \tag{5.13}$$

where $\mathcal{G}$ is the Green's function matrix defined by

$$\mathcal{G} \equiv \frac{1}{d^2 - e^2}\begin{pmatrix} d & e \\ e & d \end{pmatrix}, \qquad d \equiv \theta_+ \coth(\theta_+ L) + \theta_- \tanh\left(\frac{\theta_-(1-L)}{2}\right), \qquad e \equiv \theta_+ \operatorname{csch}(\theta_+ L)\,. \tag{5.14}$$

Substituting (5.13) and (4.19) into (5.12), and recalling that $\bar{\lambda} = \lambda + \varepsilon_0^2 m^2$ and $\mathcal{H} w_+^2 \sim 1/L$ from (5.2 *c*) and (4.5), we obtain that λ is an eigenvalue of the matrix eigenvalue problem

$$\alpha(\lambda + \varepsilon_0^2 m^2)\boldsymbol{c} \sim \varepsilon_0^2 \left[\frac{1}{2}L(1-L)I - \mathcal{G}\right]\boldsymbol{c}\,. \tag{5.15}$$

Here I is the identity matrix, and $\alpha \equiv 2\beta L\mathcal{D}/w_+^2$.

The spectrum $\mathcal{G}\boldsymbol{v} = \sigma\boldsymbol{v}$ is readily calculated as

$$\boldsymbol{v}_+ = \begin{pmatrix} 1 \\ 1 \end{pmatrix}, \qquad \sigma_+ = \frac{1}{d-e} = \left[\theta_+ \tanh\left(\frac{\theta_+ L}{2}\right) + \theta_- \tanh\left(\frac{\theta_-(1-L)}{2}\right)\right]^{-1}, \tag{5.16 a}$$

and

$$\boldsymbol{v}_- = \begin{pmatrix} 1 \\ -1 \end{pmatrix}, \qquad \sigma_- = \frac{1}{d+e} = \left[\theta_+ \coth\left(\frac{\theta_+ L}{2}\right) + \theta_- \tanh\left(\frac{\theta_-(1-L)}{2}\right)\right]^{-1}. \tag{5.16 b}$$

Here $\theta_\pm$ are defined in (5.6 *b*). Combining (5.16) and (5.15), we obtain the explicit eigenvalues

$$\lambda_\pm \sim \frac{\varepsilon_0^2}{\alpha}\left[-\alpha m^2 + \frac{L}{2}(1-L) - \sigma_\pm\right], \quad \boldsymbol{c}_+ = \begin{pmatrix} 1 \\ 1 \end{pmatrix}, \quad \boldsymbol{c}_- = \begin{pmatrix} 1 \\ -1 \end{pmatrix}; \qquad \alpha \equiv \frac{2\beta L\mathcal{D}}{w_+^2}\,. \tag{5.17}$$

The two eigenvectors $\boldsymbol{c}_\pm$ in (5.17), which determine the eigenfunction ϕ in (5.4), lead to two different types of transverse instability of the mesa-stripe. The zigzag mode, where ξ_l and ξ_r are perturbed in the same direction, corresponds to $\boldsymbol{c}_- = (1,-1)^t$ because the signs of x_1 in y_l and y_r in (5.4) are different. . Alternatively, the mode $\boldsymbol{c}_+ = (1,1)^t$ corresponds to a breather-type instability. For α sufficiently large, it is easy to see that $\lambda_\pm < 0$ for any $m \geq 0$. Therefore, a mesa-stripe is stable when $\mathcal{D}$ is above some threshold. However, as $\mathcal{D}$ is decreased (or equivalently as α is decreased), first the zigzag mode and then the breather mode admit a nontrivial band of unstable wave numbers m. The fact that the zigzag mode becomes unstable before the breather mode as $\mathcal{D}$ is decreased arises from the inequality $\sigma_- < \sigma_+$. Since $\lambda_\pm = O(\varepsilon_0^2)$ the time-scale for the development of these instabilities is $O(\varepsilon_0^{-2})$.

We first consider zigzag and breather instabilities for a one-dimensional pulse where $m = 0$. For $\varepsilon_0 \to 0$, a simple calculation using (5.16) for $m = 0$ and $\varepsilon_0 \ll 1$ gives

$$\sigma_- \sim \frac{L}{2} + O(\varepsilon_0)\,, \qquad \sigma_+ \sim \frac{2\mathcal{D}}{\varepsilon_0}\left[1 - \frac{2w_+}{2-w_+}\right]^{-1}. \tag{5.18}$$

Then, from (5.17), we obtain for $m = 0$ and $\varepsilon_0 \ll 1$ that

$$\lambda_- \sim -\frac{\varepsilon_0^2 L^2}{2\alpha} = -1.8112\frac{\varepsilon_0^2 L}{\mathcal{D}} < 0\,, \qquad \lambda_+ \sim -\frac{\varepsilon_0 w_+^2}{\beta L}\left[1 - \frac{2w_+}{2-w_+}\right]^{-1} = -1.1899\frac{\varepsilon_0}{L} < 0\,. \tag{5.19}$$

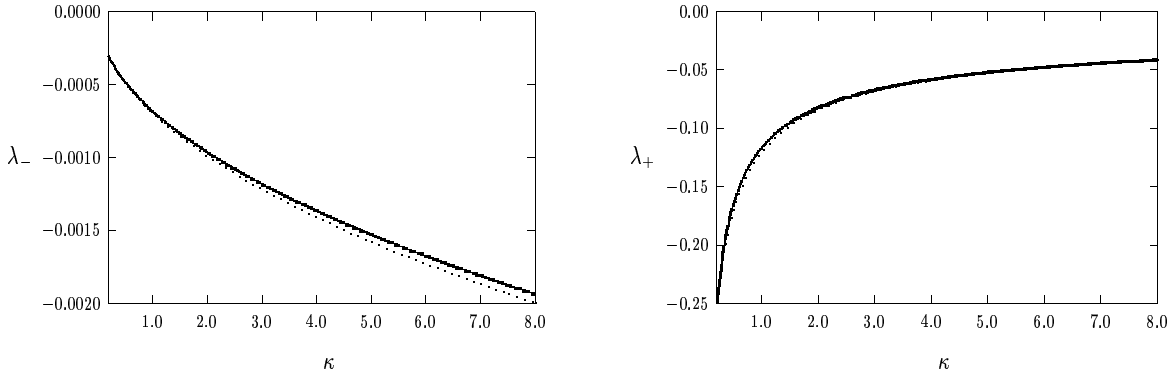

(a) λ_- versus κ for $m = 0$ (b) λ_+ versus κ for $m = 0$

FIGURE 22. Comparison of asymptotic (heavy solid curves) and full numerical results (dashed curves) for $\lambda_\pm$ versus κ for $m = 0$ when $\varepsilon_0 = 0.02$ and $D = 10.0$. Left figure: the zigzag eigenvalue λ_-. Right figure: the breather eigenvalue λ_+.

Therefore, when $L > 0$, we have $\lambda_\pm < 0$ for $m = 0$ and $\varepsilon_0 \ll 1$, with $\lambda_- = O(\varepsilon_0^2)$ and $\lambda_+ = O(\varepsilon_0)$. This shows that a one-dimensional pulse solution is always stable under the effect of activator saturation. For the parameter set $m = 0$, $\varepsilon_0 = 0.02$, and $D = 10$, for which $\mathcal{D} = 0.2$, in Fig. 22(a) we compare the asymptotic result for the zigzag eigenvalue λ_-, given in (5.17), with the corresponding full numerical result computed from (5.2). The numerical result is obtained by first discretizing (5.2) using centered differences and then using LAPACK [1] to compute the relevant eigenvalue of a matrix eigenvalue problem. For the same parameter set $m = 0$, $\varepsilon_0 = 0.02$, and $D = 10$, in Fig. 22(b) we show a similar favorable comparison between the asymptotic result for the breather eigenvalue λ_+ of (5.2) and the corresponding full numerical result for λ_+ computed from (5.2).

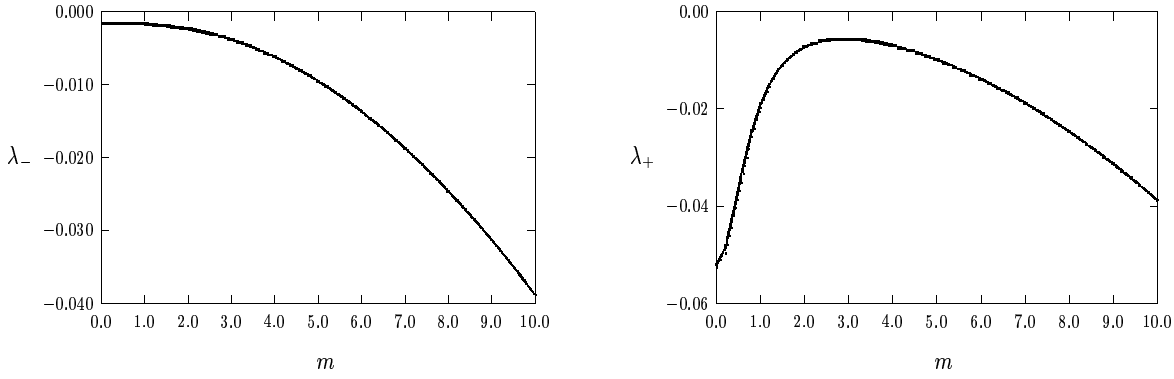

(a) λ_- versus m (b) λ_+ versus m

FIGURE 23. Left figure: Comparison of asymptotic (heavy solid curve) and full numerical results (dashed curve) for λ_- versus m when $\kappa = 5.0$ and $\varepsilon_0 = 0.02$. Right figure: Comparison of asymptotic (heavy solid curve) and full numerical results (dashed curve) for λ_+ versus m when $\kappa = 5.0$ and $\varepsilon_0 = 0.02$.

A similar favorable agreement between the asymptotic and numerical results for $\lambda_\pm$ occur for $m > 0$. As a function of m, in Fig. 23(a) and Fig. 23(b) we show a favorable comparison between the asymptotic result for λ_- and λ_+, respectively, and the corresponding full numerical results computed from (5.2) when $\varepsilon_0 = 0.02$ and $\kappa = 5.0$.

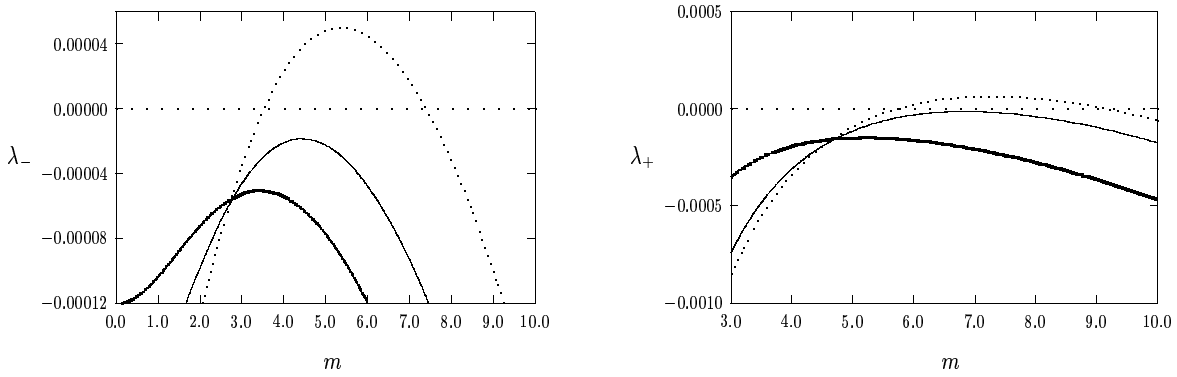

(a) λ_- versus m (b) λ_+ versus m

FIGURE 24. Left figure: the asymptotic result λ_- of (5.17) versus m for $\kappa = 2.0$ and $\varepsilon_0 = 0.0025$ when $D = 10.0$ (heavy solid curve), $D = 6.0$ (solid curve), and $D = 4.0$ (dashed curve). An instability band exists when $D = 4.0$ since $\mathcal{D} = D\varepsilon_0 = 0.010 < \mathcal{D}_z$. Right figure: the asymptotic result λ_+ versus m of (5.17) for $\kappa = 4.0$ and $\varepsilon = 0.0025$ when $D = 10.0$ (heavy solid curve), $D = 3.5$ (solid curve), and $D = 2.8$ (dashed curve). An instability band exists when $D = 2.8$ since $\mathcal{D} = D\varepsilon_0 = 0.007 < \mathcal{D}_b$.

For both λ_- and λ_+ we have $\lambda_\pm < 0$ when $m = 0$ and $\lambda_\pm < 0$ for $m \gg 1$. This latter inequality is readily seen from the estimate $\sigma_\pm = O(m^{-1})$ for $m \gg 1$ obtained from (5.16). For α sufficiently small, or equivalently for $\mathcal{D}$ sufficiently small, it follows from (5.17) that there will be a band of unstable zigzag and breather modes where $m = O(1)$. For three values of $\mathcal{D}$, in Fig. 24(a) we plot λ_- versus m, computed from the asymptotic result (5.17), for $\kappa = 2.0$ and $\varepsilon_0 = 0.0025$. A similar plot is shown in Fig. 24(b) for $\kappa = 4.0$ and $\varepsilon_0 = 0.0025$. For a fixed value of the saturation parameter, these figures show the emergence of $O(1)$ instability bands as $\mathcal{D}$ is decreased.

For the zigzag mode a nontrivial band of unstable modes emerges at the value $\alpha = \alpha_z$ and $m = m_z$ where the tangency conditions $\lambda_- = 0$ and $d\lambda_-/dm = 0$ are satisfied. From these conditions, we obtain that m_z is the root of

$$\frac{m}{2}\frac{d\sigma_-}{dm} = \sigma_- - \frac{L}{2}(1-L)\,. \tag{5.20}$$

Here m_z depends on the plateau length L, which depends on the saturation parameter κ from (4.5). In terms of $m = m_z$, the critical value α_z is $\alpha_z = m_z^{-2}\left[\frac{L}{2}(1-L) - \sigma_-\right]$. Since α is related to $\mathcal{D}$ by (5.17), this latter formula defines a critical value $\mathcal{D}_z$ for the inhibitor diffusivity as a function of either L or κ as

$$\mathcal{D}_z = \frac{w_+^2}{2\beta L m_z^2}\left[\frac{L}{2}(1-L) - \sigma_-\right]\,. \tag{5.21}$$

To compute the curve m_z at each fixed L we use Newton's method coupled to a continuation procedure in L starting from $L \ll 1$. For $L \ll 1$, a simple calculation using (5.16 *b*) for σ_- shows that

$$\sigma_- \sim \frac{L}{2} - \frac{mL^2}{4}\tanh\left(\frac{m}{2}\right) + O(L^3)\,. \tag{5.22}$$

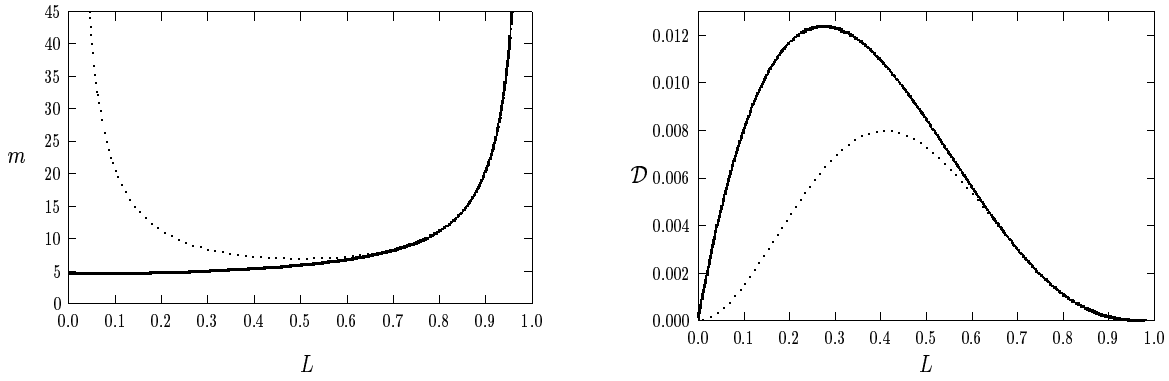

(a) m_z and m_b versus L (b) $\mathcal{D}_z$ and $\mathcal{D}_b$ versus L

FIGURE 25. Left figure: the critical modes m_z and m_b versus L for the emergence of a zigzag (heavy solid curve) and a breather (dashed curve) instability band, respectively. Right figure: the critical diffusivities $\mathcal{D}_z$ (heavy solid curve) and $\mathcal{D}_b$ (dashed curve) at the modes m_z and m_b where an unstable zigzag and breather instability emerge, respectively. The mesa-stripe solution is stable for values of $\mathcal{D}$ that lie above both curves in the right figure.

Therefore, from (5.20) we obtain for $L \ll 1$ that $m_z \approx 4.5298$ is the unique root of

$$-\frac{m}{4}\tanh\left(\frac{m}{2}\right) + \frac{m^2}{8}\mathrm{sech}^2\left(\frac{m}{2}\right) = -1\,. \tag{5.23}$$

In Fig. 25(a) we plot m_z versus L, and in Fig. 25(b) we plot the critical diffusivity $\mathcal{D}_z$ versus L. The relation between L and κ in Fig. 21 then determines these critical values in terms of the saturation parameter. In Fig. 25(b), the maximum value of the curve $\mathcal{D}_z$ versus L occurs at $\mathcal{D}_z \approx 0.0124$ and $m_z = 4.92$ when $L \approx 0.277$, or equivalently $\kappa = 1.92$ from Fig. 21.

A similar calculation can be done for the breather instability corresponding to λ_+. To determine the value $m = m_b$ and $\mathcal{D} = \mathcal{D}_b$ where a nontrivial breather instability band first emerges, we set $\lambda_+ = d\lambda_+/dm = 0$ to obtain

$$\frac{m}{2}\frac{d\sigma_+}{dm} = \sigma_+ - \frac{L}{2}(1-L)\,, \qquad \mathcal{D}_b = \frac{w_+^2}{2\beta L m_z^2}\left[\frac{L}{2}(1-L) - \sigma_+\right]\,. \tag{5.24}$$

In Fig. 25(a) we plot m_b versus L and in Fig. 25(b) we plot the critical diffusivity $\mathcal{D}_b$ versus L. Notice that $\mathcal{D}_z > \mathcal{D}_b$, which implies that a zigzag instability occurs before a breather instability as $\mathcal{D}$ is decreased. From Fig. 25(a) we also observe that $m_b \gg 1$ for $L \ll 1$. This is readily seen by using (5.16 *a*) for σ_+ in the transcendental relation (5.24) for m_b. In Fig. 25(b), the maximum value of the curve $\mathcal{D}_b$ versus L occurs at $\mathcal{D}_b \approx 0.00798$ and $m_b \approx 7.09$ when $L \approx 0.406$, or equivalently $\kappa = 4.11$ from Fig. 21.

Finally, we perform a few full numerical simulations on (1.6) to confirm the asymptotic stability theory.

Experiment 1: Consider (1.6) in the square $[0,1] \times [0,1]$ for the parameter set $\varepsilon_0 = 0.03$, $\kappa = 5.0$, and $D = 10$. For these values, (4.5) yields that $L \approx 0.45$ and $\mathcal{H} \approx 0.2056$. The initial condition for (1.6) is taken to be

$$a = \frac{\mathcal{H} w_+}{2}\left(\tanh\left[\frac{\varepsilon_0^{-1}(x_1 - \xi_l)}{2}\right] + \tanh\left[\frac{\varepsilon_0^{-1}(\xi_r - x_1)}{2}\right]\right)\,, \qquad h = \mathcal{H}\,, \tag{5.25}$$

where $\xi_l = 0.275$ and $x_r = 0.725$. Since $\mathcal{D} = D\varepsilon_0 = 0.3 > \mathcal{D}_z = .0124$, the asymptotic theory predicts that the

mesa-stripe solution is stable to both zigzag and breather instabilities. This is confirmed in Fig. 26 where we plot the numerical solution to (1.6) at time $t = 1000$, showing its convergence to a stable mesa-stripe solution.

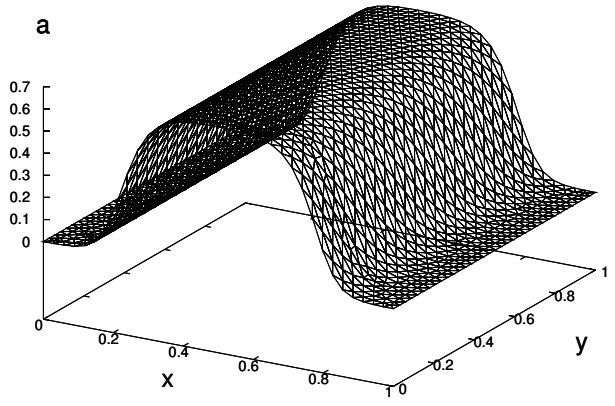

FIGURE 26. **Experiment 1:** The numerical solution to (1.6) in a square domain $[0,1] \times [0,1]$ at time $t = 1000$ for the parameter set $\varepsilon_0 = 0.03$, $\kappa = 5.0$, and $D = 10$ Since $\mathcal{D} = D\varepsilon_0 = 0.3 > \mathcal{D}_z = .0124$, the mesa-stripe solution is stable to both zigzag and breather instabilities.

Experiment 2: Next, we consider (1.6) in the square $[0,1] \times [0,1]$ with $\varepsilon_0 = 0.01$ and $\kappa = 1.92$, and for various values of D. The initial condition for (1.6) is (5.25) with $L \approx 0.28$, $\mathcal{H} = 0.33$, $\xi_l = 0.36$, and $\xi_r = 0.64$. From Fig. 25(b), $\kappa = 1.92$ corresponds to the maximum point $\mathcal{D}_z \approx 0.0124$ of the curve $\mathcal{D}_z$ versus L. Since $\varepsilon_0 = 0.01$ and $D = \mathcal{D}/\varepsilon_0$, the asymptotic theory predicts that a zigzag instability occurs when $D < D_z = 1.24$. Although this asymptotic stability result was derived in the limit $D \gg 1$, we now show that it is in reasonable quantitative agreement with full numerical simulations even when $D \approx 1$. In Fig. 27 we plot the numerical solution to (1.6) for $D = 0.6$, $D = 0.8$, $D = 1.0$, and $D = 1.4$, at the times shown in the figure caption. The mesa-stripe has a pronounced zigzag instability for $D = 0.6$ and $D = 0.8$, but only a very slight instability for $D = 1.0$. For these parameter values and for the domain width $d_0 = 1$, the asymptotic theory predicts that the unstable zigzag mode has exactly one crest. For $D = 1.4$, which is above the zigzag threshold $D = 1.24$, the mesa-stripe is found to be stable. We believe that the saturation of the zigzag instability leading to the apparent steady-state solution in Fig. 27 is a result of the interaction of the global inhibitor field h with the lateral boundaries of the rectangle. We remark that in order to give a more precise test of the instability threshold, one would have to compute numerical solutions of (1.6) with a value of ε_0 that is a decade smaller than $\varepsilon_0 = 0.01$. With such a small value of ε_0, it is challenging to obtain sufficient numerical resolution to resolve the transition layers at the edges of the mesa-stripe.

Experiment 3: Finally, we consider (1.6) in the square $[0,1] \times [0,1]$ with $k = 2.0$. We take ε_0 and D to be slowly decreasing functions of time given by

$$\varepsilon_0(t) = 0.2D(t)\,, \qquad D(t) = 0.2e^{-0.002t}\,. \tag{5.26}$$

The initial condition for (1.6) is (5.25) with $\mathcal{H} = 0.21$, $\xi_l = 0.36$, and $\xi_r = 0.64$. Since D is not asymptotically large, the theory developed in §4 and §5 does not apply for this example. The numerical results in Fig. 28 show a new phenomenon whereby the initial mesa-stripe splits into two, with the two daughter stripes undergoing a further

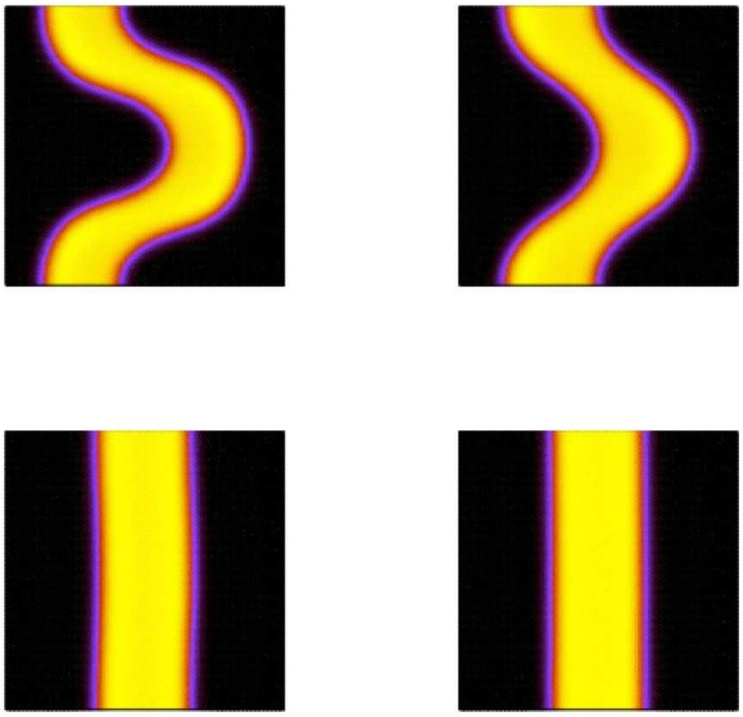

FIGURE 27. **Experiment 2:** The numerical solution to (1.6) in a square domain $[0,1]\times[0,1]$ for $\varepsilon_0 = 0.01$ and $\kappa = 1.92$. Top left: $D = 0.6$ at time $t = 10,000$. Top right: $D = 0.8$ at time $t = 10,000$. Bottom left: $D = 1.0$ at time $t = 20,000$. Bottom right: $D = 1.4$ at time $t = 20,000$. A zigzag instability occurs in each case, except for the value $D = 1.4$ which is above the zigzag instability threshold.

splitting at later times. Since the time-scale for splitting is much less than that for the development of transverse instabilities, there are no zigzag instabilities observed in Fig. 28. This stripe-replication phenomena is significantly more robust than that observed in Experiment 3 of §3 for the unsaturated GM model in the weak interaction regime. An analysis of this mesa self-replication phenomena of Fig. 28 is an open problem.

6 Conclusion

We have analyzed the stability of a stripe for two different forms of the GM activator-inhibitor model in a rectangular domain. For the basic GM model, where saturation effects are neglected, the stability of a homoclinic stripe was analyzed with respect to spot-generating breakup instabilities and transverse zigzag instabilities. The wave-number instability bands for each of these mechanisms was found to depend sensitively on the asymptotic range of the inhibitor diffusivity D. In the semi-strong regime, where $D = O(1)$, the homoclinic stripe typically disintegrates into an array of spots unless the domain width is asymptotically small. In contrast, in the weak interaction regime, where the activator and inhibitor diffusivities have the same asymptotic order, there are certain exponent sets associated with the nonlinear kinetics where the homoclinic stripe can be de-stabilized solely by a transverse zigzag instability. In the semi-strong regime it was also shown that a homoclinic stripe can be stabilized with respect to breakup instabilities upon allowing for an asymptotically small level of activator saturation. For larger levels of the saturation, the homoclinic stripe ceases to exist and is replaced by a mesa-stripe, whose cross-section consists of

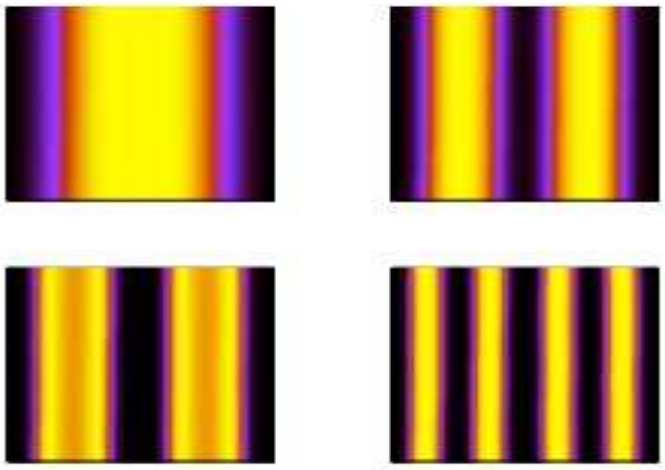

FIGURE 28. **Experiment 3:** The numerical solution to (1.6) in a square domain $[0,1] \times [0,1]$ for $k = 2.0$ when ε_0 and D are slowly decreasing functions of time given in (5.26). The initial condition is given in (5.25) with $\mathcal{H} = 0.21$, $\xi_l = 0.36$, and $\xi_r = 0.64$. The mesa-stripe is found to undergo a self-replication process leading to a multi-stripe pattern. Top left: $t = 100$. Top right: $t = 140$. Bottom left: $t = 160$. Bottom right: $t = 180$.

front-back transition layers joined by an asymptotically flat plateau. For an asymptotically large inhibitor diffusivity, it was shown that such a mesa-stripe can be stable with respect to both zigzag and breakup instabilities.

There are some open problems suggested by this study. For homoclinic stripe solutions of (1.4), a key open problem is to provide an analytical theory that characterizes the intricate nature of the zigzag and breakup instability bands for a homoclinic stripe in the weak interaction regime. For a mesa-stripe solution of (1.6), an interesting open problem is to rigorously study the transition behavior in the stability properties of a stripe as the saturation parameter κ decreases. In particular, for $\kappa = O(\varepsilon_0^2)$ in (2.23), where "fattened" homoclinic stripes occur, it would be interesting to give a rigorous analytical confirmation of the disappearance of the spot-generating breakup instability band shown numerically in §2.3. Additionally, it would be interesting to construct multiple mesa-stripe equilibria to (1.6) when $D = O(1)$ in order to study the global bifurcation properties of these solutions. Such a bifurcation diagram is likely to be crucial for an analysis of the mesa-stripe self-replication behavior observed in Experiment 3 of §5. Other important open problems include providing a weakly nonlinear theory for zigzag and breakup instabilities of homoclinic stripes, and studying the stability of multi-stripe patterns.

Finally, it would be interesting to extend the stability analyzes given here to investigate breakup and zigzag instabilities of stripes in the hybrid chemotaxis reaction-diffusion systems of [**36**], [**45**], [**30**], and [**31**], and in the models of [**9**] and [**19**] for the spatial patterning of vegetation in arid environments.

Acknowledgments. T.K. was supported by a PGS-B graduate scholarship from NSERC Canada. M.J.W. thanks the grant support of NSERC. J.W. is supported by an Earmarked Grant from RGC of Hong Kong.

Appendix A The Nonlocal Eigenvalue Problem: Semi-Strong Regime

We first outline the derivation of the NLEP (2.9). In terms of the inner variable $y = x_1/\varepsilon$, we use (2.1) to calculate $pa_e^{p-1}/h_e^q \sim pw^{p-1}$ and $qa_e^p/h_e^{q+1} \sim q\mathcal{H}^{\gamma p-(q+1)}w^p$. Therefore, from (2.6 a), $\Phi(y)$ satisfies

$$\Phi'' - \Phi + pw^{p-1}\Phi - q\mathcal{H}^{\gamma p-(q+1)}w^p\eta(0) = \left(\lambda + \varepsilon^2 m^2\right)\Phi\,, \quad -\infty < y < \infty\,; \quad \Phi \to 0 \quad \text{as} \quad |y| \to \infty\,. \tag{A.1}$$

In (2.6 b), η is not singularly perturbed, and so we can determine $\eta(0)$ in (A.1) from the outer solution for $\eta(x_1)$. To do so, we use (2.1) and (2.3) to calculate the coefficients in (2.6 b) in terms of Dirac masses. This leads to

$$\eta_{x_1x_1} - \theta_\lambda^2\eta = 0\,, \quad -l < x_1 < l\,; \qquad \eta_{x_1}(\pm l) = 0\,; \qquad \theta_\lambda \equiv \sqrt{1 + m^2 + \tau\lambda}\,, \tag{A.2 a}$$

$$[\eta] = 0\,; \qquad [\eta_{x_1}] = \frac{s\eta(0)}{G_l(0)} - \frac{r\mathcal{H}^{-\gamma+1}}{G_l(0)}\left(\frac{\int_{-\infty}^{\infty} w^{r-1}\Phi\,dy}{\int_{-\infty}^{\infty} w^r\,dy}\right)\,. \tag{A.2 b}$$

Here $[f] \equiv f(0^+) - f(0^-)$. To solve (A.2), we introduce the Green's function $G_\lambda(x_1)$ satisfying

$$G_{\lambda x_1x_1} - \theta_\lambda^2 G_\lambda = -\delta(x_1)\,, \quad |x_1| < l\,; \qquad G_{\lambda x_1}(\pm l) = 0\,; \qquad G_\lambda(x_1) = \frac{\cosh\left[\theta_\lambda\left(l - |x_1|\right)\right]}{2\theta_\lambda \sinh\left(\theta_\lambda l\right)}\,. \tag{A.3}$$

The solution $\eta(x_1)$ can be written in terms of $G_\lambda(x_1)$, and in this way we determine $\eta(0)$ as

$$\eta(0) = r\mathcal{H}^{1-\gamma}\left[s + \frac{\theta_\lambda \tanh(\theta_\lambda l)}{\tanh l}\right]^{-1}\left(\frac{\int_{-\infty}^{\infty} w^{r-1}\Phi\,dy}{\int_{-\infty}^{\infty} w^r\,dy}\right)\,. \tag{A.4}$$

Upon subsitituting (A.4) into (A.1), we obtain the eigenvalue problem (2.9) in Principal Result 2.2.

In the remainder of this appendix we prove Proposition 2.3 for the spectrum of (2.9). We begin with a key Lemma.

Lemma A.1 (From [**39**]): *Let $f(\mu)$ and $C_m(\lambda)$ be as defined in (2.11) and (2.9 b), and let $\nu_0 > 0$ be the unique positive eigenvalue of the local operator L_0 in (2.9). Then, when μ and λ are real, the following properties hold:*

$$\text{(i)} \quad f(0) = \frac{1}{p-1}\,, \qquad f'(0) = \frac{1}{p-1}\left[\frac{1}{p-1} - \frac{1}{2r}\right]\,, \tag{A.5 a}$$

$$\text{(ii)} \quad f'(\mu) > 0 \text{ for } 0 < \mu < \nu_0\,, \quad \text{when either } r = 2\,,\ 1 < p \le 5\,, \quad \text{or} \quad r = p+1\,,\ p > 1\,, \tag{A.5 b}$$

$$\text{(iii)} \quad f''(\mu) > 0 \text{ for } 0 < \mu < \nu_0\,, \quad \text{when either } r = 2\,,\ p = 2\,, \quad \text{or} \quad r = p+1\,,\ 1 < p \le 5\,, \tag{A.5 c}$$

$$\text{(iv)} \quad f(\mu) \to +\infty \text{ as } \mu \to \nu_0^-\,, \qquad f(\mu) < 0 \text{ for } \mu > \nu_0\,. \tag{A.5 d}$$

In addition, $C_m'(\lambda) > 0$, $C_m''(\lambda) < 0$, $\frac{dC_m}{dm}(0) > 0$, and $C_m(\lambda) = O(m)$ for $m \gg 1$, where $C_m(\lambda)$ is given in (2.9 b).

Proof The proof of (A.5) is given in Proposition 3.5 of [**39**]. The positivity of $C_m'(\lambda)$, the concavity of $C_m(\lambda)$, and the positivity of $\frac{dC_m(0)}{dm}$, all follow from a simple direct calculation using the expression for $C_m(\lambda)$ in (2.9 b). ■

The proof of Proposition 2.3 is given in two parts. In Part 1, Lemma A.1 is used to analyze the spectrum of the NLEP (2.9) on the positive real axis. In Part 2 a winding number criterion locates any complex unstable spectrum.

We begin with Part 1. By calculating $C_m(0)$ in (2.9 b), and by using $\frac{dC_m}{dm}(0) > 0$, we obtain that $C_m(0) > 1/(p-1)$ when $m > m_{b-}$, where m_{b-} is the unique root of the transcendental equation (2.12) in Proposition 2.3. Then, with $\varepsilon m \ll 1$, it follows from (A.5) and the conditions $C_m'(\lambda) > 0$ and $C_m''(\lambda) < 0$, that the curves $C_m(\lambda)$ and $f(\lambda + \varepsilon^2 m^2)$ intersect exactly once in $0 < \lambda < \nu_0$ for any $\tau \ge 0$ when the condition (A.5 c) on the exponents r and p are satisfied. Therefore, under this condition, we conclude for $m > m_{b-}$ and $\varepsilon m \ll 1$ that there is a unique real root in $0 < \lambda < \nu_0$ to $g(\lambda) = 0$ defined in (2.11). Under these conditions, we obtain a unique unstable real eigenvalue of (2.9).

Next, we consider real spectrum on the range $0 < m < m_{b-} = O(1)$, for which $C_m(0) < f(\varepsilon^2 m^2) \sim \frac{1}{p-1}$. Since $C_m(\lambda) = O(\tau^{1/2})$ for $\tau \gg 1$, it follows from (A.5) that for $\tau > \tau_m$ there are exactly two real roots to $g(\lambda) = 0$ in $0 < \lambda < \nu_0$ when the condition (A.5 *c*) on the exponents holds. This yields two unstable real eigenvalues. Alternatively, for $\tau < \tau_m$, there are no real roots to $g(\lambda) = 0$, and hence no unstable real eigenvalues. For $m = m_{b-}$ a simple calculation shows that $\lambda = 0$ is a double zero eigenvalue when $C_m'(0) = f'(\varepsilon^2 m^2)$. By using (2.9 *b*) for C_m, (A.5 *a*) for $f'(0)$, and assuming that $p - 1 < 2r$, this condition yields the critical value $\tau_{m-} > 0$ of τ, defined in (2.14) of Proposition 2.3. For $m = m_{b-}$ and $\tau > \tau_{m-}$ there is a unique unstable real eigenvalue of (2.9).

Next, we consider real spectrum when $m > \sqrt{\nu_0}/\varepsilon$. For this range of m, (A.5 *d*) shows that $f(\lambda + \varepsilon^2 m^2) < 0$ for any $\lambda > 0$. Thus, since $C_m(0) > 0$ and $C_m'(\lambda) > 0$, there are no real roots to $g(\lambda) = 0$ in $\lambda > 0$ for any $\tau > 0$, and consequently no unstable real eigenvalues of (2.9). Finally, suppose that $m = \sqrt{\beta}/\varepsilon$ with $0 < \beta < \nu_0$, so that $g(\lambda) = C_m(\lambda) - f(\lambda + \beta)$. Then, since $C_m(0) = O(m)$ for $m \gg 1$, we get $C_m(0) = O(\varepsilon^{-1}) > f(\beta)$ for $0 < \beta < \nu_0$. Therefore, under the condition (A.5 *c*) on the exponents r and p, there is a unique root to $g(\lambda) = 0$ in $0 < \lambda < \nu_0 - \beta$ for any $\tau \geq 0$, and consequently a unique unstable real eigenvalue to (2.9).

In Part 2 of the proof we must count the number N of complex eigenvalues in the right half-plane $\mathrm{Re}(\lambda) > 0$. To do so, we proceed as in §3 of [**39**] by using a winding number criterion that determines N in terms of the change in the argument of $g(i\lambda_I)$ along the positive imaginary axis Γ_I, denoted by $[\arg g]_{\Gamma_I}$, traversed in the downwards direction. For any $\tau > 0$, a slight modification of Proposition 3.3 of [**39**] shows that

$$N = \frac{5}{4} + \frac{1}{\pi}[\arg g]_{\Gamma_I}\,, \quad 0 < m < \frac{\sqrt{\nu_0}}{\varepsilon}\,; \qquad N = \frac{1}{4} + \frac{1}{\pi}[\arg g]_{\Gamma_I}\,, \quad m > \frac{\sqrt{\nu_0}}{\varepsilon}\,. \tag{A.6}$$

Assume that the exponents satisfy $r = 2$ and $p > 1$. Then, by adapting the proof of Proposition 3.4 of [**39**], we conclude that $[\arg g]_{\Gamma_I} = -\pi/4$ when $m > m_{b-}$ and $\tau > 0$. This yields $N = 1$ when $m_{b-} < m < \sqrt{\nu_0}/\varepsilon$ and $N = 0$ when $m > \sqrt{\nu_0}/\varepsilon$. Therefore, the unstable eigenvalue for $m_{b-} < m < \sqrt{\nu_0}/\varepsilon$ is the real positive eigenvalue obtained in Part 1 of the proof. For the range $0 < m < m_{b-}$, Proposition 3.4 of [**39**] can be applied directly, and for $r = 2$ and $p > 1$ we conclude that $[\arg g]_{\Gamma_I} = 3\pi/4$ when τ is sufficiently large and $[\arg g]_{\Gamma_I} = -5\pi/4$ when τ is sufficiently small. For $0 < m < m_{b-}$ with $r = 2$, this shows that $N = 2$ when τ is sufficiently large and $N = 0$ when τ is sufficiently small. Therefore, for this range of the parameters, there is a Hopf bifurcation as τ is increased past some critical value, which generates unstable complex conjugate eigenvalues. Our results above for the positive real axis $\lambda > 0$ show that these unstable complex eigenvalues must merge onto this axis when τ is sufficiently large. This completes the proof of Proposition 3.3. ■

Appendix B Zigzag Eigenvalue: Semi-Strong Regime

In this appendix we outline the derivation of (2.21). We first write (2.6 *a*) in terms of an operator L_ε as

$$L_\varepsilon \phi - \frac{q a_e^p}{h_e^{q+1}}\eta = (\lambda + \varepsilon^2 m^2)\phi\,, \quad -l < x < l\,; \quad \phi_x(\pm l) = 0\,; \qquad L_\varepsilon \phi \equiv \varepsilon^2 \phi_{xx} - \phi + \frac{p a_e^{p-1}}{h_e^q}\phi\,. \tag{B.1}$$

We differentiate the equilibrium problem for a_e in (1.4) with respect to x_1 to get $L_\varepsilon a_{ex_1} = q a_e^p h_{ex_1}/h_e^{q+1}$, where L_ε is defined in (B.1). Therefore, since $a_e \sim \mathcal{H}^\gamma w$, we obtain

$$L_\varepsilon w' \sim \frac{\varepsilon q \mathcal{H}^q w^p}{h_e^{q+1}} h_{ex_1}\,. \tag{B.2}$$

This suggests that we expand ϕ and η as

$$\phi = w^{'} + \varepsilon\phi_1 + \cdots, \qquad \eta(x_1) = \varepsilon\eta_0(x_1) + \cdots. \tag{B.3}$$

We substitute (B.3) into (B.1) and use (B.2) with $\lambda = O(\varepsilon^2)$ and $m = O(1)$. This yields that $\phi_1(y)$ satisfies

$$L_\varepsilon\phi_1 \sim \frac{qw^p\mathcal{H}^q}{h_e^{q+1}} f(\varepsilon y), \qquad f(x_1) \equiv \mathcal{H}^\gamma\eta_0(x_1) - h_{ex_1}(x_1). \tag{B.4}$$

By substituting (B.3) and $\eta = \varepsilon\eta_0$ into (2.6 b), and labeling $\theta_\lambda \equiv \sqrt{1+m^2+\tau\lambda}$, we get that η_0 satisfies

$$\eta_{0x_1x_1} - \theta_\lambda^2\eta_0 = -\frac{ra_e^{r-1}}{\varepsilon^2 h_e^s}\left(w^{'} + \varepsilon\phi_1\right) + \frac{sa_e^r}{\varepsilon h_e^{s+1}}\eta_0, \quad -l < x < l; \qquad \eta_{0x_1}(\pm l) = 0. \tag{B.5}$$

The term proportional to $w^{'}$ on the right hand-side of (B.5) behaves like a dipole as $\varepsilon \to 0$. Therefore, for $\varepsilon \to 0$, it can be represented as a multiple of $\delta^{'}(x_1)$ where $\delta(x_1)$ is the delta function. Thus, η_0 is discontinuous across $x_1 = 0$. However, $f(x_1)$ defined in (B.4) is continuous across $x_1 = 0$. To see this, we differentiate (1.4) for h_e with respect to x_1 and then subtract appropriate multiples of the resulting equation and (B.5) to find that the dipole term cancels exactly. Thus, $f(x_1)$ is continuous across $x_1 = 0$, and so $\langle f\rangle = f(0)$. Since $\langle h_{ex}\rangle = 0$ from (2.1), we get $f(0) = \mathcal{H}^\gamma\langle\eta_0\rangle$. Here and below we have defined $\langle\xi\rangle \equiv (\xi(0^+) + \xi(0^-))/2$ and $[\xi] \equiv \xi(0^+) - \xi(0^-)$, where $\xi(0^\pm)$ are the one-sided limits of $\xi(x_1)$ as $x_1 \to 0^\pm$. Therefore, for $\varepsilon \ll 1$, ϕ_1 in (B.4) satisfies

$$L_\varepsilon\phi_1 \sim qw^p\mathcal{H}^{\gamma-1}\langle\eta_0\rangle. \tag{B.6}$$

Since $L_\varepsilon w = (p-1)w^p + O(\varepsilon)$, the solution to (B.6) is simply

$$\phi_1(y) = \frac{q}{p-1}w(y)\mathcal{H}^{\gamma-1}\langle\eta_0\rangle + O(\varepsilon). \tag{B.7}$$

Next, we use (2.1), (2.3), (B.3), and (B.7), to calculate the coefficients in (B.5) in the sense of distributions. With $\tilde\eta_0$ defined by $\eta_0 = H^{1-\gamma}\tilde\eta_0$, and by using $G_l(0) = \frac{1}{2}\coth l$ as given in (2.3), we obtain that $\tilde\eta_0$ satisfies

$$\tilde\eta_{0x_1x_1} - \theta_\lambda^2\tilde\eta_0 = 0, \quad -l < x_1 < l; \qquad \tilde\eta_{0x_1}(\pm l) = 0; \qquad \theta_\lambda \equiv \sqrt{1+m^2+\tau\lambda}, \tag{B.8 a}$$

$$[\tilde\eta_0] = -\frac{1}{G_l(0)}; \qquad [\tilde\eta_{0x_1}] = \left(s - \frac{qr}{p-1}\right)\frac{\langle\tilde\eta_0\rangle}{G_l(0)}. \tag{B.8 b}$$

The remaining part of the derivation proceeds as in equations (4.16)–(4.23) of [**10**]. This leads to

$$\left(\lambda + \varepsilon^2 m^2\right) \sim \frac{\varepsilon^2 qJ}{p+1}\left(\langle\tilde\eta_{0x_1}\rangle - \frac{h_{ex_1x_1}(0)}{\mathcal{H}}\right), \qquad J \equiv \frac{\int_{-\infty}^{\infty} w^{p+1}\,dy}{\int_{-\infty}^{\infty} w'^{\,2}\,dy}. \tag{B.9}$$

From Appendix A of [**38**] we calculate $J = 2(p+1)/(p-1)$. Then, from (2.1), we obtain $h_{ex_1x_1}(0) = \mathcal{H}$. Finally, by solving (B.8) explicitly, we calculate

$$\langle\tilde\eta_{0x_1}\rangle = \theta_\lambda \tanh l \tanh(\theta_\lambda l). \tag{B.10}$$

Upon substituting these formulae into (B.9), we obtain that the small eigenvalue $\lambda = O(\varepsilon^2)$ satisfies (2.21).

References

[1] E. Anderson et al. *LAPACK User's Guide: Third Edition*, SIAM Publications (1999).

[2] U. Ascher, R. Christiansen, R. Russell, *Collocation Software for Boundary Value ODE's*, Math. Comp., **33**, (1979), pp. 659-679.

[3] A. Doelman, R. A. Gardner, T. Kaper, *Large Stable Pulse Solutions in Reaction-Diffusion Equations*, Indiana U. Math. Journ., Vol. 50, No. 1, (2001), pp. 443-507.
[4] A. Doelman, H. van der Ploeg, *Homoclinic Stripe Patterns*, SIAM J. Appl. Dyn. Systems, **1**, No. 1, (2002), pp. 65-104.
[5] S. Ei, Y. Nishiura, K. Ueda, 2^n *Splitting or Edge Splitting?: A Manner of Splitting in Dissipative Systems*, Japan J. Indust. Appl. Math., **18**, (2001), pp. 181-205.
[6] A. Gierer, H. Meinhardt, *A Theory of Biological Pattern Formation*, Kybernetik, **12**, (1972), pp. 30–39.
[7] R. E. Goldstein, D. J. Muraki, D. M. Petrich, *Interface Proliferation and the Growth of Labyrinths in a Reaction-Diffusion System*, Phys. Rev. E., **53**, (1996), pp. 3933-3957.
[8] P. Hirschberg, E. Knobloch, *Zigzag and Varicose Instabilities of a Localized Stripe Pattern*, Chaos, **3**, (1993), pp. 713-721.
[9] J. von Hardenberg, E. Meron, M. Shachak, Y. Zarmi, *Diversity of Vegetation Patterns and Desertification*, Phys. Rev. Lett., **87**, No. 19, (2001), p. 198101-1.
[10] D. Iron, M. J. Ward, J. Wei, *The Stability of Spike Solutions to the One-Dimensional Gierer-Meinhardt Model*, Physica D, **150**, No. 1-2, (2001), pp. 25-62.
[11] B. S. Kerner, V. V. Osipov, *Autosolitions: A New Approach to Problem of Self-Organization and Turbulence*, Kluwer Academic Publishers, Dordrecht, (1994).
[12] C. A. Klasmeier, *Regular and Irregular Patterns in Semiarid Vegetation*, Science, **284**, (1999), pp. 1826–1828.
[13] A. J. Koch, H. Meinhardt, *Biological Pattern Formation From Basic Mechanisms to Complex Structures*, Rev. Modern Physics, **66**, No. 4, (1994), pp. 1481-1507.
[14] T. Kolokolnikov, M. J. Ward, J. Wei, *Pulse-Splitting for Some Reaction-Diffusion Systems in One-Space Dimension*, Studies in Appl. Math., **114**, No. 2, (2005), pp. 115-165.
[15] T. Kolokolnikov, J. Wei, *On Ring-Like Solutions for the Gray-Scott Model: Existence, Instability, and Self-Replicating Regimes*, **16**, No. 2 (2005), pp. 201–237.
[16] T. Kolokolnikov, M. J. Ward, J. Wei, *Zigzag and Breakup Instabilities of Stripes and Rings for the Two-Dimensional Gray-Scott Model*, Studies in Appl. Math., **116**, No. 1, (2006), pp. 35–95.
[17] T. Kolokolnikov, T. Erneux, J. Wei, *Mesa-Type Patterns in the One-Dimensional Brusselator and their Stability*, submitted, Physica D, (2005).
[18] S. Kondo, R. Asai, *A Viable Reaction-Diffusion Wave on the Skin of Pomacanthus, a Marine Angelfish*, Nature, **376**, (1995), pp. 765–768.
[19] E. Meron, E. Gilad, J. von Hardenberg, M. Shachak, Y. Zarmi, *Vegetation Patterns Along a Rainfall Gradient*, Chaos Solitons and Fractals, **19**, (2004), pp. 367-376.
[20] C. S. Lin, W. M. Ni, I. Takagi, *Large Amplitude Stationary Solutions to a Chemotaxis System*, J. Diff. Eq., **72**, (1988), pp. 1-27.
[21] H. Meinhardt, *Models of Biological Pattern Formation*, Academic Press, London, (1982).
[22] H. Meinhardt, *The Algorithmic Beauty of Sea Shells*, Springer-Verlag, Berlin, (1995).
[23] D. Morgan, T. Kaper, *Axisymmetric Ring Solutions of the Gray-Scott Model and Their Destabilization into Spots*, Physica D, **192**, No. 1-2, (2004), pp. 33–62.
[24] J. D. Murray, *Mathematical Biology II: Spatial Models and Biomedical Applications*, Interdisciplinary Applied Mathematics, Vol. 18, Springer, New York, (2003).
[25] Y. Nishiura, *Far-From-Equilibrium Dynamics*, Translations of Mathematical Monographs, Vol. 209, AMS publications, Providence, Rhode Island, (2002).
[26] Y. Nishiura, D. Ueyama, *A Skeleton Structure of Self-Replicating Dynamics*, Physica D, **130**, No. 1-2, (1999), pp. 73-104.
[27] Y. Nishiura, D. Ueyama, *Spatio-Temporal Chaos for the Gray-Scott Model*, Physica D, **150**, No. 3-4, (2001), pp. 137-162.
[28] Y. Nishiura, H. Fujii, *Stability of Singularly Perturbed Solutions to Systems of Reaction-Diffusion Equations*, SIAM J. Math. Anal., **18**, (1987), pp. 1726-1770.
[29] Y. Nishiura, *Singular Limit Approach to Stability and Bifurcation for Bistable Reaction-Diffusion Systems*, Rocky Mountain J. Math., **21**, No. 2, (1991), pp. 727-767.
[30] K. J. Painter, P. K. Maini, H. G. Othmer, *Complex Patterns in a Hybrid Chemotaxis Reaction-Diffusion Model*, J. Math. Biology, **41**, No. 4, (2000), pp. 285-314.
[31] K. J. Painter, P. K. Maini, H. G. Othmer, *Stripe Formation in Juvenile Pomacanthus Explained by a Generalized Turing Mechanism with Chemotaxis*, Proc. Natl. Acad. Sci. USA, Developmental Biology, **96**, (1999), pp. 5549-5554.
[32] J. E. Pearson, *Complex Patterns in a Simple System*, Science, **216**, (1993), pp. 189-192.
[33] W. Sun, M. J. Ward, R. Russell, *Localized Solutions, Dynamic Bifurcations, and Self-Replication of Spots for the Gierer-Meinhardt Model in Two Spatial Dimensions*, in preparation.
[34] M. Taniguchi, Y. Nishiura, *Instability of Planar Interfaces in Reaction-Diffusion Systems*, SIAM J. Math. Anal., **25**, No. 1, (1994), pp. 99-134.
[35] M. Taniguchi, Y. Nishiura, *Stability and Characteristic Wavelength of Planar Interfaces in the Large Diffusion Limit of the Inhibitor*, Proc. Roy. Soc. Edinburgh Sect. A, **126**, No. 1, (1996), pp. 117-145.

[36] R. C. Tyson, *Pattern Formation by E. Coli; Mathematical and Numerical Investigation of a Biological Phenomenon*, Ph. D. thesis, Dept. of Applied Mathematics, University of Washington, Seatttle, WA, (1996).

[37] XMORPHIA wesbite http://www.cacr.caltech.edu/ismap/image.html, R. Williams, Concurrent Supercomputing Facilities, Caltech, USA.

[38] M. J. Ward, D. McInerney, P. Houston, D. Gavaghan, P. Maini, *The Dynamics and Pinning of a Spike for a Reaction-Diffusion System*, SIAM J. Appl. Math., **62**, No. 4, (2002), pp. 1297–1328.

[39] M. J. Ward, J. Wei, *Hopf Bifurcations and Oscillatory Instabilities of Spike Solutions for the One-Dimensional Gierer-Meinhardt Model*, Journal of Nonlinear Science, **13**, No. 2, (2003), pp. 209–264.

[40] M. J. Ward, J. Wei, *Hopf Bifurcation of Spike Solutions for the Shadow Gierer-Meinhardt Model*, Europ. J. Appl. Math., **14**, No. 6, (2003), pp. 677-711.

[41] J. Wei, *On Single Interior Spike Solutions for the Gierer-Meinhardt System: Uniqueness and Stability Estimates*, Europ. J. Appl. Math., **10**, No. 4, (1999), pp. 353-378.

[42] J. Wei, M. Winter, *On the Gierer-Meinhardt System with Saturation*, Commun. Contemp. Math., **6**, No. 2, (2004), pp. 259-277.

[43] J. Wei, M. Winter, *Spikes for the Two-Dimensional Gierer-Meinhardt System: the Weak Coupling Case*, J. Nonlinear Sci., **11**, No. 6, (2001), pp. 415–458.

[44] J. Wei, M. Winter, *Existence and Stability Analysis of Asymmetric Patterns for the Gierer-Meinhardt System*, J. Math. Pures Appl. (9), **83**, No. 4, (2004), pp. 433-476.

[45] D. E. Woodward, R. C. Tyson, J. D. Murray, E. O. Budrene, H. Berg, *Spatio-Temporal Patterns Generated by Salmonella Typhimurium*, Biophysical J., **68**, (2005), pp. 2181-2189.

[46] F. M. Ytreberg, S. Mckay, *Second Mechanism for Transitions in a Reaction-Diffusion System*, Phys. Rev. E., **59**, No. 3, (1999), pp. 3376-3381.